Thermal kinetics and crystal structure of dapsone polymorphs and solvates

Helanie Lemmer

B.Pharm., M.Sc. (Pharmaceutics)

Thesis submitted in the Department of Pharmaceutics in the School of Pharmacy at the Potchefstroom Campus of the North-West University for the degree **Doctor Philosophiae** in Pharmaceutics.

Supervisor: **Prof. W. Liebenberg**

Co-supervisor: **Dr. N. Stieger**

POTCHEFSTROOM

2012

Acknowledgements

- **Dr. Righard Lemmer**. This would not have been possible without my husband, best friend and colleague.
- **My parents,** Johan & Hela van der Merwe for their love, emotional and financial support through all my ventures.

- **Prof. W. Liebenberg & Dr. N. Stieger** for their support and friendship during my post-graduate years.
- **Prof. M.R. Caira** for his time, insight and work done on the solvates. Many thanks to Cape Town University's chemistry department for their hospitality and use of their apparatus during my study visit in Cape Town.
- **B. Venter** for always being ready to analyse my samples using PXRD.
- **Dr. L. Tiedt** for his endless patience, enthusiasm and my beautiful SEM photos.
- **The NRF** for funding my studies.

- **Potchefstroom Hospital Pharmacy staff** for keeping me sane while completing my Ph.D. and Community Service (at the same time).
- **Dr. D.P. & Dr. A. Otto** for their friendship and also unique, insightful and challenging ideas.
- **For the guys** (Chuck, Jacques and Terence) –you're the best friends anyone could ever have!

Table of Contents

Introduction & Objectives

Dapsone (DDS) is a folic acid synthesis inhibitor. The high degree of chemotherapeutic activity of DDS was first published in 1937. Today this drug is used for the treatment of leprosy and prophylaxis against opportunistic bacterial infections in immune-compromised patients. Despite the age of DDS, not much is known about its polymorphic forms except for the work published by Kuhnert-Brandstätter and Moser in 1979. Reinvestigation of DDS using newly developed techniques and modern equipment will shed light upon the interrelationships of DDS's polymorphs and the formation of solvates.

Recrystallisation of DDS led to the formation of various habit modifications, three solvates and a hydrate. Characterisation and investigation of the recrystallised products were done, using both new and old equipment. The solvates and their respective desolvation processes were extensively investigated to add to the DDS knowledge base.

Objectives:

- Reinvestigate the physical-chemical properties of DDS using modern techniques and equipment such as modulated temperature differential scanning calorimetry, variable temperature X-ray diffraction and single crystal X-ray diffraction.
- Contribute towards the understanding of the interrelationship of DDS's different polymorphic forms.
- Investigate the formation of possible solvates and their properties.
- Evaluate the water solubility of the recrystallised DDS products.

Abstract

Dapsone (DDS) is currently used in the treatment of leprosy and prophylaxis of opportunistic bacterial infections in immune-compromised patients. Despite the age of this drug; not much is known about the interrelationships between its polymorphs. Also, no previous polymorphic screening studies have been done to determine the probability of solvate formation when exposed to various solvents. Re-evaluation of DDS using modern techniques and equipment such as a variable temperature x-ray diffractometer (VTXRD) and modulated temperature differential scanning calorimeter (MTDSC) were crucial to clarify some aspects of DDS's polymorphs that were published in the past.

Recrystallisation of DDS from various neat solvents was done; the products that formed from recrystallisation included some habit modifications, a hydrate and three solvates.

The solid-solid phase transition of DDS form III to form II was observed at ~82°C for most recrystallised products. Most of the recrystallised products melted at ~177.6°C which is the melting point of DDS form II. Some of the recrystallised products melted at ~179.5°C (DDS form I).

DDS•(0.33)H_2O has been described before by several research groups. A hydrate would be even less water soluble than the anhydrated DDS and was therefore not pursued further. DDS solvates have not been reported before in any literature. Solvates recrystallised from dichloromethane (DCM), 1,4-dioxane (DXN) and tetrahydrofuran (THF) in stoichiometric relationships of DDS•0.5(DCM), DDS•DXN and DDS•THF. The crystal structures of the solvates were elucidated using single-crystal X-ray diffraction. The results were deposited into the Cambridge structural database (CSD) for future reference regarding DDS.

The desolvation of these solvates was extensively studied. The activation energy (E_a) and kinetic model that each solvate followed during desolvation was calculated by isothermal thermogravimetric analysis (TGA) and verified by micrographs obtained by using a thermal microscope (TM). The nucleation and growth model (***A***2) was statistically chosen to explain the desolvation process for DDS•0.5(DCM) although the involvement of the geometric contracting area (***R***2) model cannot be neglected. Model-fitting results for the desolvation of DDS•DXN and DDS•THF concluded that they respectively followed the ***A***2 and ***R***2-model; the micrographs confirmed these model-fitting results. The order of thermal stability between the solvates is as follows: DDS•0.5(DCM) >> DDS•THF > DDS•DXN. The calculated E_a values followed the opposite trend but unfortunately accurate assumptions

about E_a may not be reliable since these three solvates are not isostructural. After desolvation of the solvates they completely converted back to the crystal structure of DDS form III at room temperature.

A full polymorphic study was done. This knowledge is absolutely important for manufacturing, storage and use of DDS.

Uittreksel

Dapsoon (DDS) word tans vir die behandeling van melaatsheid en voorkoming van opportunistiese bakteriële infeksies in pasiënte met swak immuunstelsels gebruik. Nie veel is bekend oor die verwantskappe tussen DDS se polimorf vorme nie, ten spyte daarvan dat hierdie geneesmiddel reeds oud is, is nie veel oor die onderlinge verwantskap tussen die polimorfe vorme van DDS bekend nie. Geen studies is gedoen om die moontlikheid van solvaatvorming in verskeie oplosmiddels te ondersoek nie. Herondersoek van DDS se polimorfe vorme deur gebruik van moderne tegnieke en toerusting soos 'n x-straaldiffraktometer (VTXRD) met wisselende temperatuur en 'n modulêre temperatuur differensiële skandeerkalorimeter (MTDSC) is noodsaaklik om sekere aspekte van DDS se polimorfe wat voorheen gepubliseer is, op te klaar.

Rekristallisasie van DDS vanuit verskeie oplosmiddels is gedoen en dit het verskeie kristalvorme, 'n hidraat en drie solvate opgelewer.

Die vastestof-vastestof fase-oorgang van DDS-vorm III na vorm II is by ~82°C waargeneem. Die meeste van die rekristallisasieprodukte het by ~177.6°C gesmelt wat ooreenstem met die smeltpunt van DDS-vorm II; sommige rekristallisasie produkte het by ~179.5°C gesmelt (DDS-vorm I).

DDS•(0.33)H_2O is al voorheen deur ander navorsingsgroepe beskryf. 'n Hidraat sal swakker wateroplosbaarheid toon as die anhidraat van DDS. As gevolg hiervan is hierdie vorm nie verder ondersoek nie. DDS-solvaat is nog nooit vantevore gepubliseer nie. Solvaatvorming vanuit dichloormetaan (DCM), 1,4-dioksaan (DXN) en tetrahidrofuraan (THF) het in stoichiometriese verhoudings van DDS•0.5(DCM), DDS•DXN en DDS•THF gevorm. Die kristalvorme van die solvaat is met enkelkristal x-straaldiffraktometrie (SCXRD) bepaal en die resultate is in die Cambridge strukturele databasis gedeponeer.

Die desolvering van die solvaat is breedvoerig bestudeer. Die aktiveringsenergie (E_a) en kinetiese model van elke solvaat is met isotermiese termogravimetriese analise (TGA) bepaal. Die resultate is bevestig deur 'n termiese mikroskoop (TM) te gebruik. Kernvorming en groeimodel (***A***2) is statisties gekies om die desolveringsproses van DDS•0.5(DCM) te beskryf, hoewel die betrokkenheid van die geometries vernouende area-model (***R***2) nie geïgnoreer kan word nie. Die resultate van die model-passing van DDS•DXN en DDS•THF het getoon dat die ***A***2 en ***R***2-modelle statisties die meeste verteenwoordigend van die tipe desolvering is en hierdie resultate is met TM mikrograwe bevestig. Die volgorde van die

termiese stabiliteit van die solvate is DDS•0.5(DCM) >> DDS•THF > DDS•DXN. Die bepaalde E_a-waardes volg die teenoorgestelde tendens, maar akkurate aannames rakende die E_a kan nie gemaak word nie omdat die solvaat nie iso-struktureel is nie. Die solvaat keer heeltemal terug na die kristalstruktuur van DDS-vorm III nadat desolvering volledig verloop het.

'n Volledige polimorfiese studie is gedoen. Hierdie verworwe kennis is belangrik vir die vervaardiging, stoor en gebruik van DDS.

List of Equations:

Nr.	Equation	Name/description	page
(1)	Gibbs function	$\Delta G = \Delta H - T\Delta S$	4
(2)	Desolvation reaction process	$A_{(solid)} \rightarrow B_{(solid)} + C_{(gas)}$	14
(3)	Conversion fraction (α)	$\alpha = \frac{(m_0 - m_t)}{(m_0 - m_\infty)}$	14
(4)	Arrhenius equation	$k = A\, e^{-\left(\frac{E_a}{RT}\right)}$	14
(5)	Rate of a solid-state reaction	$\frac{d\alpha}{dt} = kf(\alpha)$	15
(6)	Integral rate law	$g(\alpha) = kt$	15
(7)	Power law (***P***2*)*	$kt = \alpha^{1/2}$	17
(8)	Power law (***P***3)	$kt = \alpha^{1/3}$	17
(9)	Power law (***P***4)	$kt = \alpha^{1/4}$	17
(10)	Avrami-Erofeev (***A***2)	$kt = [-\ln(1-\alpha)]^{1/2}$	17
(11)	Avrami-Erofeev (***A***3)	$kt = [-\ln(1-\alpha)]^{1/3}$	17
(12)	Avrami-Erofeev (***A***4)	$kt = [-\ln(1-\alpha)]^{1/4}$	17
(13)	Prout-Tompkins (***B***1)	$kt = \mathrm{Ln}[\alpha/(1-\alpha)] + c^a$	17
(14)	Contracting area / cylinder (***R***2)	$1 - (1-\alpha)^{1/2}$	17
(15)	Contracting volume / sphere (***R***3)	$1 - (1-\alpha)^{1/3}$	17
(16)	1-D Diffusion (***D***1)	α^2	17
(17)	2-D Diffusion (***D***2)	$[(1-\alpha)\ln(1-\alpha)] + \alpha$	17

(18)	3-D Diffusion – Jander (***D***3)	$[1-(1-\alpha)^{1/3}]^2$	17
(19)	Ginstling-Brounshtein (***D***4)	$1-(2/3)\alpha-(1-\alpha)^{2/3}$	18
(20)	Zero-order (***F***0/***R***1)	α	18
(21)	First-order (***F***1)	$-\ln(1-\alpha)$	18
(22)	Second-order (***F***2)	$[1/(1-\alpha)]-1$	18
(23)	Third-order (***F***3)	$(1/2)[(1-\alpha)^{-2}-1]$	18
(24)	General power law equation	$(\alpha)^{1/n} = kt$	18
(25)	Total number of nuclei sites	$N_1(t) = N - N(t) - N_2(t)$	18
(26)	General ***A*** model equation	$[-\ln(1-\alpha)]^{1/n} = kt$	19
(27)	General ***B*** model equation	$ln\frac{\alpha}{1-\alpha} = k\ t + c$	20
(28)	Reaction rate for cylindrical/spherical crystals	$r = r - kt$	20
(29)	Standard model-free method	$-\ln t = \ln\left(\frac{A}{g(\alpha)}\right) - \frac{E}{RT}$	22
(30)	Friedman's model-free method	$\ln\left(\frac{d\alpha}{dt}\right)_\alpha = \left(lnAf(\alpha)\right)_\alpha - \frac{Ea_\alpha}{RT_\alpha}$	22
(31)	Solvate thermal reactivity	$\Delta T = T_{on} - T_b$	24
(32)	TGA weight loss	$TGA\ loss\ 1{:}1\ (\%){:}\ \frac{MW_S}{MW_S + MW_{API}}\ \text{x}\ 100 = x\ \%$	34
(33)	MTDSC	$\frac{dQ}{dt} = Cp\,.\frac{dT}{dt} + f(t,T)$	35

List of Figures

List of Tables

List of Abbreviations

1BT	1-Butanol
1D	One dimensional
1PR	1-Propanol
2BT	2-Butanol
2D	Two dimensional
2PR	2-Propanol
3D	Three dimensional
α	Conversion fraction
α'	Extended conversion fraction
A	Avrami-Erove'ef models
A	Frequency factor
ACE	Acetone
ACL	Acetonitrile
ASCII	American standard code for information interchange 2
$A_{(solid)}$	Solvated solid product
API	Active pharmaceutical ingredient
Au	Gold
B	Prout-Tompkins model
BCS	Biopharmaceutical classification system
BP	British Pharmacopoeia

$B_{(solid)}$	Desolvated solid product
c	Cisoid-shaped flexible molecules
c	Integration constant
°C	Temperature in degrees Celsius
C	Side centred lattice
CDS	Cambridge Structural Database
$C_{(gas)}$	Gaseous by-product from desolvation
C_p	Heat capacity at constant pressure
D	Diffusion models
DCM	Dichloromethane
DDS	Dapsone
DMF	*N,N*-Dimethylformamide
DMSO	Dimethyl sulfoxide
DSC	Differential scanning calorimeter / calorimetry
DXN	1,4-Dioxane
E_a	Activation energy
Exo	Exothermic
F	Face centered lattice
F	Flexible molecules
F	Reaction-order models
$f(\alpha)$	Reaction model
FT-IR	Fourier transformation infrared

G	Gibbs free energy
$g(\alpha)$	Integral of the reaction model
H	Enthalpy
H_f	Enthalpy of fusion
I	Body centred lattice
IR	Infrared
k	Rate constant
K	Kelvin
KBr	Potassium bromide
k_B	Rate of branching
m_0	Initial weight of the sample
m_t	Weight of sample at time t
m_∞	Final weigh of desolvated sample
min	Minutes
MOH	Methanol
MTDSC	Modulated temperature differential scanning calorimeter / calorimetry
MW	Molecular weight
MW_{API}	Molecular weight of the API
MW_S	Molecular weight of the solvent
mW	Milliwatt for heat flow measurements
N_0	Total number of possible nuclei-forming sites
N_1	Actual number of nuclei

N_2	Number of ingested nuclei
N(t)	Number of nuclei that developed into growth nuclei
O_2	Oxygen
P	Primitive lattice point
Pd	Palladium
PXRD	Powder X-ray diffractometer / diffraction
r	Radius
R	Gas constant (8.314 $J.K^{-1}.mol^{-1}$)
R	Geometric contraction models
R	Rigid molecules
R	Rhombohedral lattice
R^2	Regression value
S	Entropy
S	Solvent
SD	Standard deviation
S_f	Entropy of fusion
SEM	Scanning electron microscope / microscopy
SCXRD	Single crystal X-ray diffractometer / diffraction
SS-EB2HCL	[*S*,*S*]-ethambutol dihydrochloride
t	Time (in minutes)
t	Transoid-shaped flexible molecules
T	Temperature (in Kelvin (K) or Celsius (°C))

ΔT	Difference in temperature
T_b	Boiling point of solvent
T_{on}	Temperature of desolvation onset
TGA	Thermogravimetric analyser / analysis
THF	Tetrahydrofuran
TM	Thermal microscope / microscopy
TOL	Toluene
UV	Ultraviolet
VTXRD	Variable temperature powder X-ray diffractometer / diffraction

Chapter 1

Solid-State Compounds

An Introduction

1.1 THE SOLID-STATE

Active pharmaceutical ingredients (APIs) are preferably formulated as solid pharmaceutical dosage forms because of the ease of handling and stability during the various stages of drug development compared to its fluid and gaseous counterparts.

The solid-state of API's can be subdivided into two sub-phases, namely crystalline- and amorphous, which are characterised by differences in molecular packing. The crystalline form contains both short- and long-range order while the amorphous form only exhibits short-range order. Short-range order refers to the specific way each molecule is situated next to its neighbouring molecule. Long-range order is depicted in the crystalline form by the regular and periodic packing of molecules grouped together in the short-range order which then repeats throughout the phase. Because of the amorphous form's lack of long-range order this phase exhibits longer intermolecular distances, higher molecular mobility and higher free energy levels compared to the crystalline form. The amorphous state of an API can be induced by quenching (super cooling) the melt of such an API. It can also be obtained by fast evaporation of solvents, lyophilisation, vapour deposition and mechanical stress. What these various methods have in common is that by following these routes, crystallisation would be kinetically avoided and the molecules would remain as they were in the liquid state (Vippagunta *et al.*, 2001; Cui, 2007).

1.1.1 The single unit cell

The short range packing of the crystalline form is termed a ***unit cell***. This refers to the smallest three-dimensional volume element from which the crystalline solid can be constructed. A unit cell can be seen as a box defined by the lengths of its axes (a, b and c) and the angles between these axes (α, β and γ). A ***single crystal*** is made up of a continuous repetition of unit cells in all three dimensions (Vippagunta *et al.*, 2001). Seven classes of unit cells exist although only three of these are commonly found, namely triclinic, monoclinic and orthorhombic. Table 1.1 provides the properties of the different unit cells defined by their axes and angles and the allowed lattices. Symmetry within each crystal system can be defined by its lattices. A primitive unit cell (P) contains just one lattice point and is the smallest unit cell possible. A triclinic and a hexagonal crystal system can only be primitive. A body centred unit cell (I) may have a lattice point at each corner and one at the centre of the unit cell. A face centred unit cell (F) has lattice points in the middle of each face whereas a unit cell that only has one of its faces centred can be called an A-face

centred or a B-face centred or a C-face centred unit cell. A trigonal unit cell contains both a primitive lattice as well as a rhombohedral (R) lattice (Tilley, 2006).

According to the Cambridge Structural Database (CSD) the space group that is most common among organic molecules is $P2_1/c$ which is part of the monoclinic crystal system while the most common space group among hydrates is $P2_12_12_1$ which is orthorhombic (Brittain *et al.*, 2009). More information regarding the 230 space groups can be found in Tilley (2006).

Table 1.1: The seven crystal systems; the cell parameters and allowed lattices (Tilley, 2006; Brittain *et al.*, 2009).

Crystal system	Cell parameters	Allowed lattices
Cubic	$a = b = c$, $\alpha = \beta = \gamma = 90°$	P, F, I
Tetragonal	$a = b \neq c$, $\alpha = \beta = \gamma = 90°$	P, I
Orthorhombic	$a \neq b \neq c$, $\alpha = \beta = \gamma = 90°$	P,C,F, I,
Hexagonal	$a = b \neq c$, $\alpha = \beta = \gamma = 120°$	P
Trigonal (a)	$a = b = c$, $\alpha = \beta = \gamma = 120°$	P
(b)	$a = b \neq c$, $\alpha = \beta = \gamma \neq 90°$	*R*
Monoclinic	$a \neq b \neq c$, $\alpha = \gamma$, $\beta \neq 90°$	P, C
Triclinic	$a \neq b \neq c$, $\alpha \neq \beta \neq \gamma \neq 90°$	P

1.2 POLYMORPHISM

Most API's exist in one or more crystalline forms, namely polymorphs or solvates. These different crystalline forms have different physicochemical characteristics which include melting and sublimation temperatures, heat capacity, conductivity, volume, density, viscosity,

crystal hardness, crystal shape, colour, refractive index, solubility, dissolution rate, stability, hygroscopicity and solid-state reactions (Giron, 1995).

Polymorphs are different arrangements and/or conformations of the same molecule or molecules resulting in different free energy states (Cui, 2007). As stated by Haleblian & McCrone (1969), Mitscherlich was the first person in 1822 to use the term "polymorphism" to describe his observations on various metal sulphates. Since then polymorphism trends were observed in a great variety of organic and inorganic compounds. Giron (1995) published a comprehensive collection of APIs and excipients showing polymorphic or solvate behaviour.

Process-induced transformation from one polymorph into another can take place during storage or processing when the temperature and/or pressure are elevated (Morris *et al.*, 2001). If the phase transition takes place prior to melting it are termed reversible and the two polymorphs are then enantiotropes; although not all solid-solid transitions are reversible. If the phase transition is irreversible, the two polymorphs are monotropes (Giron, 1995).

1.2.1 Enantiotropy and monotropy

The difference between enantiotropy and monotropy was first defined by Ostwald in 1885. He used vapour pressure versus temperature diagrams to point out the differences by using the positions of the polymorphs' vapour pressure curves. The crystal form with the lowest vapour pressure at a specific temperature is the thermodynamically most stable form, but this is only true for a system under constant (or atmospheric) pressure (Henck & Kuhnert-Brandstätter, 1999).

The semi schematic energy versus temperature diagrams based on the Gibbs function is more informative than the vapour pressure versus temperature curves. The Gibbs function can be defined by the following equation:

$$\Delta G = \Delta H - T\Delta S \qquad (1)$$

It relates the Gibbs free energy (G) and enthalpy (H) to the absolute temperature (T) and entropy (S). The polymorphs with the lowest amount of Gibbs free energy at a certain temperature will always be the most stable form at that specific temperature. The stable form at the lower temperatures will often have a higher density, and the form that is more stable close to the melting temperature will melt at a higher temperature and will have a lower solubility and a lower vapour pressure at that temperature (Haleblian & McCrone, 1969).

Burger and Ramburger (1979) have developed four rules to qualitatively evaluate the enantiotropic or monotropic nature of a polymorph. These rules include the heat of transition

rule, heat of fusion rule, infrared rule and density rule. Simplified explanations of these rules are:

(1) **The heat of transition rule:** If an endothermic phase change is observed at a given temperature, then the phase transition point lies below this temperature and the polymorph forms are enantiotropic in nature. Two polymorphs are monotropically related where an exothermic transition is observed.

(2) **The heat of fusion rule:** The higher melting polymorph will have a lower heat of fusion (H_f) in an enantiotropic system; otherwise the modifications are monotropic.

(3) **Infrared rule:** This rule is applicable to hydrogen-bonded molecular crystals; if the first absorption band in the infrared spectrum is higher for one form than for the other then that form will have a higher entropy value and will be less stable at 0 K.

(4) **Density rule:** The polymorph form with the highest density at room temperature will be the thermodynamically stable form at absolute zero. The more stable polymorph will have energetically more favourable packaging with the strongest bonds between the molecules and thus the greatest density. The stable polymorph form will require more energy than the metastable form for the bonds between these tightly packed molecules to break or weaken such as in the case of melting or dissolution.

Excellent examples of real-life enantiotropic/monotropic polymorphs are given by Rubin-Preminger *et al*. (2004) and Kuhnert-Brandstätter & Moser (1979) regarding ethambutol dihydrochloride. Two pairs of enantiotropically related polymorphs were observed for [*S*,*S*]-ethambutol dihydrochloride (SS-EB2HCl) of which the unit cells are all orthorhombic. A vapour pressure versus temperature plot was provided by Kuhnert-Brandstätter & Moser (1979) for SS-EB2HCl while Rubin-Preminger *et al*. (2004) provided well constructed energy versus temperature plots to further illustrate the enantiotropic nature of the [S,S]-polymorphs (figure 1.1).

Rubin-Preminger and co-workers improved the knowledge regarding SS-EB2HCl and corrected some misconceptions published in previous papers by using modern techniques to analyse the transitions and crystal structures of the different polymorphs. A polymorph transition took place at 70°C, following a single-crystal-to-single-crystal mechanism from form II to form I which was seen as a front moving from the one end of the crystal to the other. The phase transition was caused by a rotation of ± 7° at the midpoint of the long molecular axis of ethambutol's molecular structure (see figure 1.2). From the phase diagrams it can be seen that an enantiotropic relationship exists between form II and form I (figure 1.1). Form III recrystallised from the melt which then changes to form IV at 36°C upon further cooling. The relationship between form III and form I is monotropic since the

phase transition is irreversible and the intersection point of the polymorphs takes (virtually) place after the melting of SS-EB2HCl as can be seen from figure 1.1 (a & b). The transition between form IV and II is reversible; conversion of form IV back to form II takes place upon standing of the sample at room temperature (this relationship is not indicated in fig. 1.1). The conversion of form IV back to form II is again an indication that form II is the thermodynamically most stable form at room temperature.

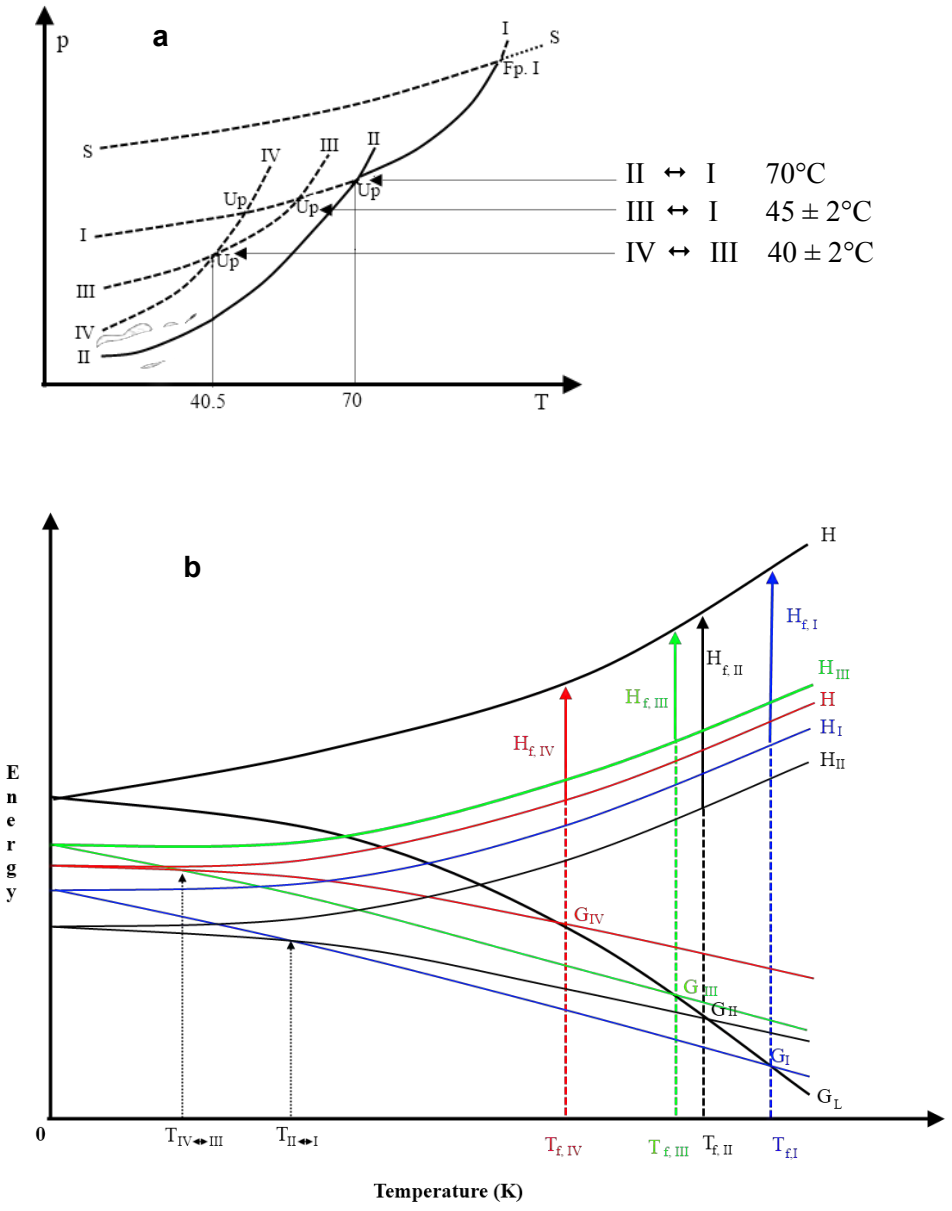

Figure 1.1: Enantiotropic relationship between the polymorphs of SS-EB2HCl (**a**) Pressure (p) versus temperature (T) phase diagram of the four modifications of SS-EB2HCl; where S indicates the melt, Fp is the melting point and Up indicates the phase transitions (Kuhnert-Brandstätter & Moser, 1979; Rubin-Preminger *et al.*, 2004). **(b)** The enantiotropic relationship between the four polymorphs of SS-

EB2HCl. L indicates the melt, $T_{II} \leftrightarrow T_I$ indicates the reversible phase transformation from form II to form I at 74°C; $T_{f,I}$ indicates the melting point of form I observed at 200°C. Virtual melting points for forms II, III and IV are indicated as $T_{f,II}$, $T_{f,III}$ and $T_{f,IV}$ respectively (Rubin-Preminger *et al.*, 2004).

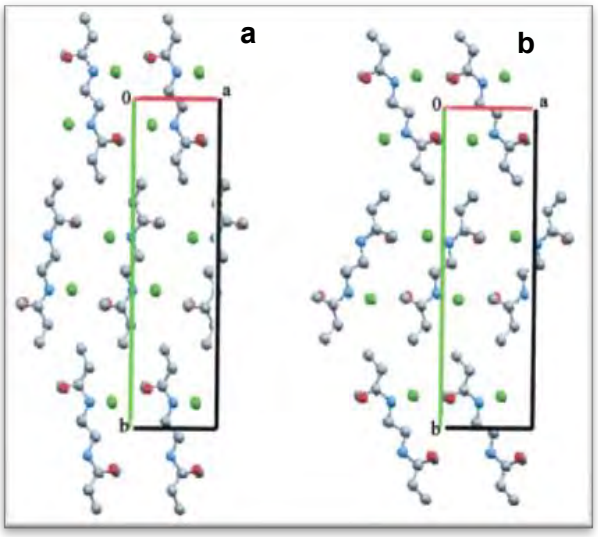

Figure 1.2: Unit cells of two enantiotropically related polymorphs of SS-EB2HCl as viewed down the c axis (a axis is seen as a red line while the b axis is green). (**a**) The packing of form II and (**b**) the packing of form I of SS-EB2HCl after phase transition has taken place (Rubin-Preminger *et al.*, 2004).

1.2.2 Conformational polymorphism

Conformationally flexible molecules have more degrees of freedom than rigid molecules thus increasing polymorphic possibilities. Polymorphs may be the consequence of molecules being packed into different arrangements or packing diverse conformations of this molecule into the same or different packing motifs (Buttar *et al.*, 1998). This might be better explained by figure 1.3. SS-EB2HCl's polymorphs (as mentioned above) are also examples of conformational polymorphism.

Oxitropium bromide, an anticholinergic drug, provides us with another example of conformational polymorphism. Upon heating of a prismatic single-crystal of oxitropium bromide the crystal undergoes a highly anisotropic change in the cell-unit volume which causes it to jump a couple of centimetres high from the heating stage resulting in disaggregation of the crystal. This phase transformation takes place at 45°C and appears to be reversible under slower heating rates of 5°C.min^{-1} (Skoko *et al.*, 2010).

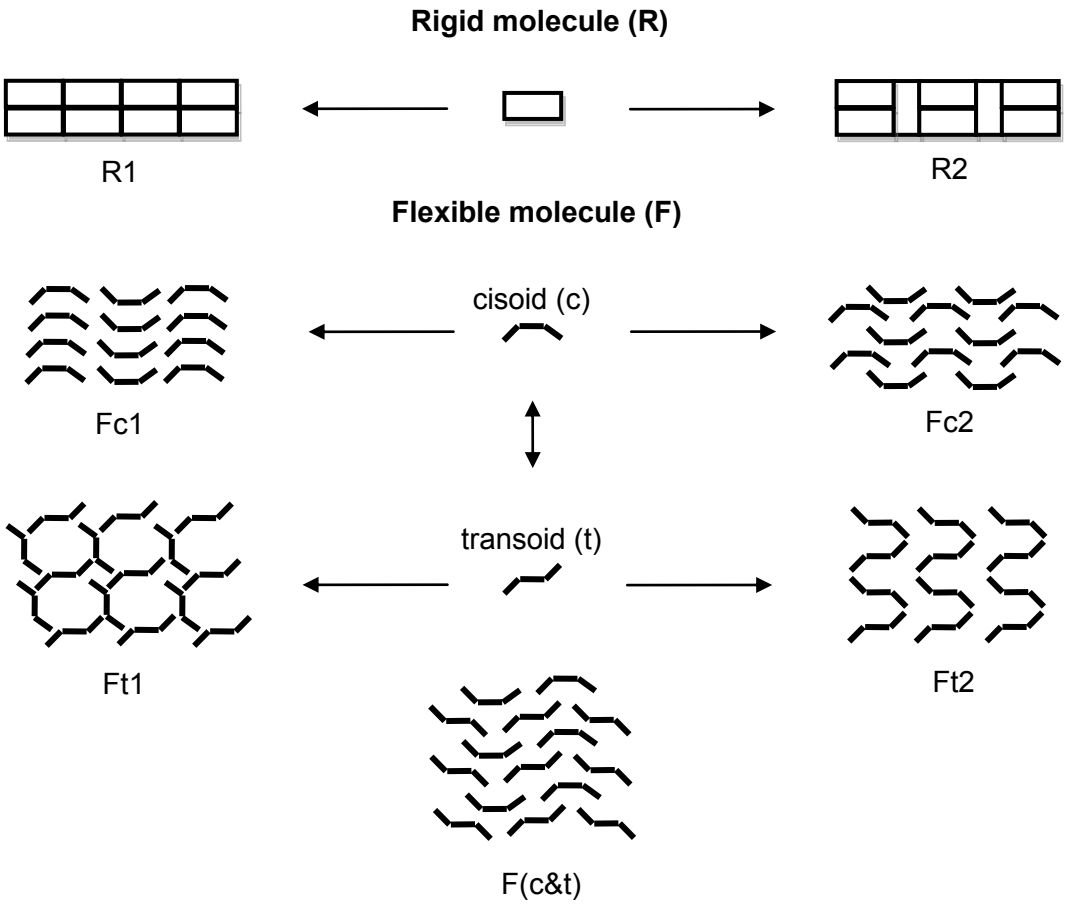

Figure 1.3: Schematic presentations of the possible polymorphs for a rigid (R) and a flexible (F) molecule; polymorphs F(c&t) are known as conformational isomorphs which consist of flexible molecules in both the cisoid and transoid positions (Nangia, 2008).

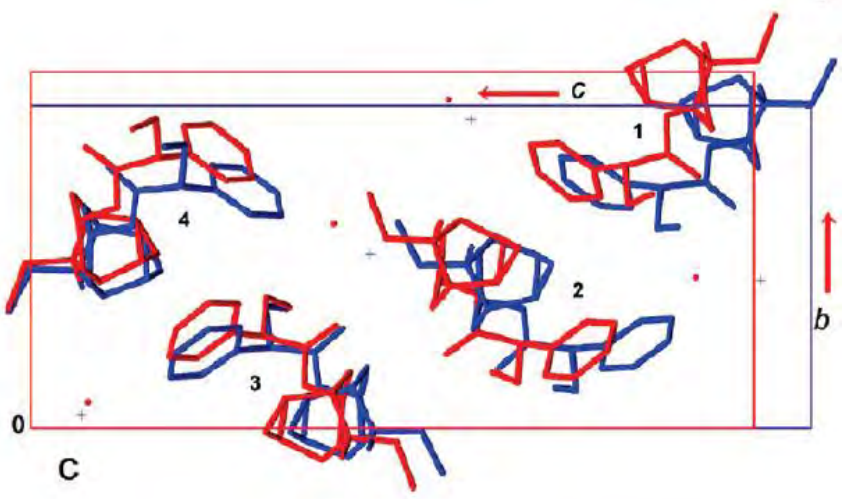

Figure 1.4: Stick-type representation of the unit cell and structures of phase A (blue) and phase B (red) as caused by the phase transition in oxitropium bromide (Skoko *et al.*, 2010).

1.2.3 Host-guest inclusions and solvates

When one species (guest molecule) is spatially confined within another species (host); this system is called an inclusion compound (figure 1.5). Inclusion compounds can be subdivided into two classes, namely (a) moieties within molecules, where the host is a molecule with a cavity that can enclose a guest molecule, and (b) moieties within crystals, where the guest is enclosed within the crystal structure formed by the host (Harris, 1993). Examples of molecules with cavities capable of inclusion include the crown ethers (Herbstein, 2005) and cyclodextrins (Singh *et al.*, 2010).

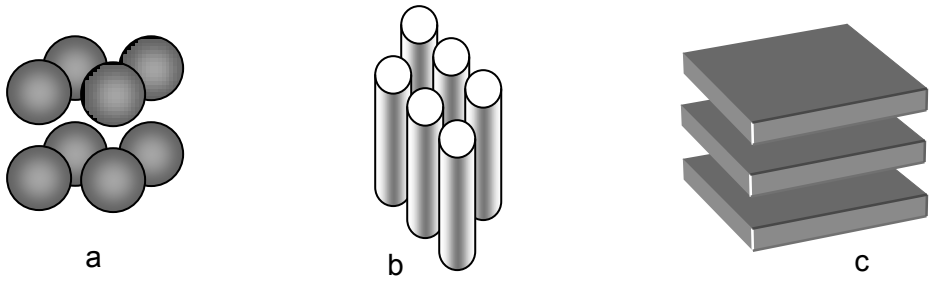

Figure 1.5: Some topologies of inclusion cavities in crystalline solids; (a) cage, (b) tunnel/channel and (c) layer-type inclusion (Adapted from Harris, 1993).

Should a solvent molecule be included as a guest molecule into the architecture of the API's (host) crystalline structure it is called a solvate; when the solvent is water the compound is termed a hydrate (Khankari & Grant, 1995). Solvates have also been called "pseudo-polymorphs" in the past but the use of this term should be avoided due to its ambiguous nature (Seddon, 2005). Byrn (1982) provided a list of some organic drugs that form solvates. Incorporation of a water or solvent molecule into the crystalline structure of an API may change the dimensions, shape, symmetry and capacity of the unit cell of the API. This may lead to changes in the API's stability, solubility, dissolution rate, bioavailability and product performance (Khankari & Grant, 1995). Solvates are not always a practical or acceptable choice when developing an API because of the toxicity of the incorporated solvent and instability during storage (Blagden *et al.*, 2007).

Different stable and metastable polymorphic modifications can be obtained after desolvation depending on different parameters like the kinetics of the reaction, the thermodynamic relationship between all solvent-free forms, the nature of the solvate, or the actual condition for the removal of the solvent. This was masterfully explained by Suitchmezian *et al*. (2009) evaluating the polymorphic and solvated forms of hydrocortisone. Hydrocortisone exists as

stable form I, and metastable forms II and III, with form I and II having comparable structures. It was reported that hydrocortisone form solvates with 5 different solvents; namely 2-propanol, methanol, pyridine, chloroform and *N,N*'-dimethylformamide (DMF). Desolvation of the chloroform- and methanol solvates results in the thermodynamically stable form I and desolvation of the 2-propanol solvate resulted in the formation of meta-stable form III. The methanol, pyridine and DMF solvates are isostructural and therefore the formation of form III after desolvation would be expected; unfortunately this did not happen so further investigation was done by Suitchmezian and co-workers. The desolvation of the DMF-solvate by heating the sample led to the thermodynamically most stable form I, but by desolvating the sample under reduced pressure at room temperature the sample smoothly transformed into the meta-stable form III as expected. The thermodynamically stable form I was always obtained after the desolvation of the pyridine solvate independent of the desolvation method used by this specific research group.

1.2.4 Mesophases

Mesophases are the fourth type of phase which shares various properties of both the liquid and solid phases. Mesophases are rare but exist as liquid crystals, plastic crystals and condis crystals (Cui, 2007).

Liquid crystals present positional and dynamic disorder with some long-range orientation order in its structure. A plastic crystal is a molecular solid with long-range positional order but with rotational disorder between the molecules (Wunderlich, 1989). Condis crystals (also known as conformational disordered crystals) illustrate dynamic conformational disorder but with long-range positional and orientational order (Chen *et al.*, 1999). The degree of solidity of mesophases is in the following order: liquid crystals < plastic crystals < condis crystals (Wunderlich, 1989).

1.3 CONCLUDING REMARKS

Development of an API into a pharmaceutical product is a lengthy and expensive process and thus it is immensely important to thoroughly investigate possible polymorphic changes that may occur. Conformationally flexible molecules may form a great variety of polymorphs upon exposure to heat, pressure, light and moisture during manufacturing and storage. Exposing APIs to solvents may lead to solvate/hydrate formation which may negatively alter the pharmaceutical product's properties.

1.4 REFERENCES

BLAGDEN, N., DE MATAS, M., GAVAN, P.T. & YORK, P. 2007. Crystal engineering of active pharmaceutical ingredients to improve solubility and dissolution rates. *Advanced Drug Delivery Reviews*, 59(7):613-630.

BRITTAIN, H.G., MORRIS, K.R. & BOERRIGTER, S.X.M. 2009. 192 vols. Structural aspects of solvatomorphic systems. (*In*: BRITTAIN, H.G., ed. *Polymorphism in pharmaceutical solids*, 2nd ed. New York: Informa Healthcare. 233-281 p).

BURGER, A & RAMBURGER, R. 1979. On the polymorphism of pharmaceuticals and other molecular crystals. I. *Microchimica Acta*, 72(4):259-271.

BUTTAR, D., CARLTON, M.H., DOCHERTY, R. & STARBUCK, J. 1998. Theoretical investigations of conformational aspects of polymorphism. Part 1: *0*-acetamidobenzamide. *Journal of the Chemical Society, Perkin Trans 2*, 4:763-772.

BYRN, S.R. 1982. Solid-state chemistry of drugs. New York: Academic Press. 574p.

CHEN, W, TODA, A, MOON, I-K. & WUNDERLICH, B. 1999. Analysis of transitions of liquid crystals and conformationally disordered crystals by temperature-modulated calorimetry. *Journal of Polymer Science: Part B: Polymer Physics*, 37(13):1539-1544.

CUI, Y. 2007. A material science perspective of pharmaceutical solids. *International Journal of Pharmaceutics*, 339(1-2):3-18.

GIRON, D. 1995. Thermal analysis and calorimetric methods in the characterisation of polymorphs and solvates. *Thermochimica Acta*, 248:1-59.

HALEBLIAN, J & McCRONE, W. 1969. Pharmaceutical applications of polymorphism. *Journal of Pharmaceutical Sciences*, 58(8):911-929.

HARRIS, K.D.M. 1993. Molecular confinement. *Chemistry in Britain*, 29(2):132-136.

HENCK, J-O & KUHNERT-BRANDSTÄTTER, M. 1999. Demonstration of the terms enantiotropy and monotropy in polymorphism research exemplified by flurbiprofen. *Journal of Pharmaceutical Sciences*, 88(1):103-108.

HERBSTEIN, F.H. 2005. Crystalline molecular complexes and compounds: structures and principles. New York: Oxford University Press. 678

KHANKARI, R.K. & GRANT, D.J.W. 1995. Pharmaceutical hydrates. *Thermochimica Acta*, 248:61-79.

KUHNERT-BRANDSTÄTTER, M & MOSER, I. 1979. Zur Polymorphie von dapson und ethambutoldihydrochlorid. *Microchimica Acta*, 71(1):125-136.

MORRIS, K.R., GRIESSER, U.J., ECKHARDT, G.J. & STOWELL, J.G. 2001. Theoretical approaches to physical transformations of active pharmaceutical ingredients during manufacturing processes. *Advanced drug delivery reviews*, 48(1):91-114.

NANGIA, A. 2008. Conformational polymorphism in organic crystals. *Accounts of chemical research*, 41(5):595-604.

RUBIN-PREMINGER, J.M., BERNSTEIN, J, HARRIS, R.K., EVANS, I.R. & GHI, P.Y. 2004. Variable temperature studies of a polymorphic system comprising two pairs of enentiotropically related forms: [*S*,*S*]-ethambutol dihydrochloride. *Crystal growth & Design*, 4(3):431-439.

SEDDON, K.R. 2005. Pseudopolymorph: a polemic. *Crystal Growth & Design*, 6(4):1087.

SINGH, R., BHARTI, N., MADAN, J. & HIREMATH, S.N. 2010. Characterization of cyclodextrin inclusion complexes -a review. *Journal of Pharmaceutical Science and Technology*, 2(3):171-183.

SKOKO, Z, ZAMIR, S, NAUMOV, P & BERNSTEIN, J. 2010. The thermosalient phenomenon. "Jumping crystals" and crystal chemistry of the anticholinergic agent oxitropium broimide. *Journal of the American Chemical Society*, 132(40):14191-14202.

SUITCHMEZIAN, V, JESS, I & NATHER, C. 2009. Investigations of desolvation reaction of pseudopolymorphic forms of hydrocortisone. *Crystal growth & Design*, 9(2):774-782.

TILLEY, R. 2006. Crystals and crystal structures. Hoboken: John Wiley. 255p.

VIPPAGUNTA, S.R., BRITTAIN, H.G. & GRANT, D.J.W. 2001. Crystalline solids. *Advanced Drug Delivery Reviews*, 48(1):3-26.

WUNDERLICH, B. 1989. The detection of conformational disorder by thermal analysis. *Pure & Applied Chemistry*, 61(8):1347-1351.

Chapter 2

Solid-State Kinetics

"When one attempts to read the intimidating and rather indigestible literature of kinetics of solid state processes and, in particular, the papers on non-isothermal kinetics, one cannot help noticing the similarities between Science and Religion. Those who believe that they have found the 'true way' promote their points-of-view with evangelistic fervour and often mention with contempt, or even attack, the practice of the 'heathen'. The field is full of dogma: 'Thou shalt do this... and thou shalt not do the other'! An agnostic in the field (defined as a person who is uncertain or noncommittal) searches, perhaps in vain, for what is useful and what is not." - Brown (1997).

2.1 SOLID-STATE KINETICS

Ninan (1989) explained the kinetic aspect of solid-state reactions as being concerned with the rate of transformation of the reactants into products and the mechanism of the transformation.

Solid-state kinetic studies regarding APIs are mostly done on single-solid- (such as decomposition), solid-solid- (e.g. polymorphic transitions) and solid-gas (desolvation) reactions (Brown *et al.*, 1980). This discussion will focus mainly on desolvation reactions under isothermal conditions for simplicity reasons. A common desolvation reaction in solid-state kinetics follows the scheme where a solid ($A_{(\text{solid})}$) desolvates, producing a solid product ($B_{(\text{solid})}$) and a gaseous ($C_{(\text{gas})}$) by-product (Khawam & Flanagan, 2006a):

$$A_{(\text{solid})} \rightarrow B_{(\text{solid})} + C_{(\text{gas})} \tag{2}$$

The conversion fraction (α) is obtained from gravimetric measurements during desolvation reactions using this equation:

$$\alpha = \frac{(m - m_t)}{(m - m_\infty)} \tag{3}$$

Where, m_0 is the initial weight of the sample, m_t being the weight at time t, and m_∞ is the final weight of the desolvated sample.

As stated by Vyazovkin (2000); Arrhenius related the rate constant (k) of a simple homogenous one-step reaction to the temperature (T in Kelvin [K]) and gas constant (R) through the activation energy (E_a) and the pre-exponential frequency factor (A) using the following equation:

$$k = A\, e^{-\left(\frac{E}{RT}\right)} \tag{4}$$

Arrhenius also described E_a as the heat absorbed by an inactive molecule in the process of transformation into active molecules or, in other words, the heat (or energy) necessary for

activation. A constant E_a is the anticipated outcome of kinetic evaluations, although the phenomenon of variable E_a exists in the solid-state due to its heterogeneous composition (this phenomenon will be described in detail later in the chapter). The rate of a solid-state reaction can be described as

$$\frac{d\alpha}{dt} = kf(\alpha) \tag{5}$$

Where, the reaction model *f*(α) is defined as the change of the conversion fraction (α) over change in time (t). This equation can be integrated to give the integral rate law where *g*(α) is the integral reaction model

$$g(\alpha) = kt \tag{6}$$

Computational methods for analysis of solid-state kinetic data can be grouped in two categories, namely ***model-fitting*** and ***model-free*** methods. A complementary approach of using both model-fitting and model-free methods leads to more reliable evaluation of reaction kinetics and E_a (Vyazovkin & Wight, 1997; Khawam & Flanagan, 2005; Koradia *et al.*, 2010).

2.1.1 Model-fitting analysis

A model is a theoretical, mathematical description of what occurs physically during a reaction (Khawam & Flanagan, 2006a). The model-fitting method generates the kinetic triplet (k, A and E_a) by two subsequent model fittings. The first model fitting obtains the reaction rate constant (k) by drawing a graph of $g(\alpha)$ versus t (in minutes) for each kinetic model and substituting the slope of this graph into equation (6). The $g(\alpha)$-value for each α-point is obtained by using the equations given in table 2.1. The regression (R^2) value is an indication of how well the experimental data fit the generated data of the kinetic model: the graph illustrating a regression value closest to one will be the model that best describes the experimental reaction. The calculated k-value for each corresponding kinetic model will then be used for obtaining the A and E_a. The slope of the graph k versus 1/T can be substituted into equation (4) to give E_a; by substituting the y-intercept of the graph into the Arrhenius equation the value of A can be calculated (Khawam & Flanagan, 2006a).

Solid-state kinetics can be classified according to the characteristic shape the isothermal α-t curves represent (figure 2.1), namely acceleratory, sigmoid, deceleratory and linear. Mechanistically the solid-state kinetic models can be classified as nucleation, geometrical contraction, diffusion and reaction-order models (Khawam & Flanagan, 2006a).

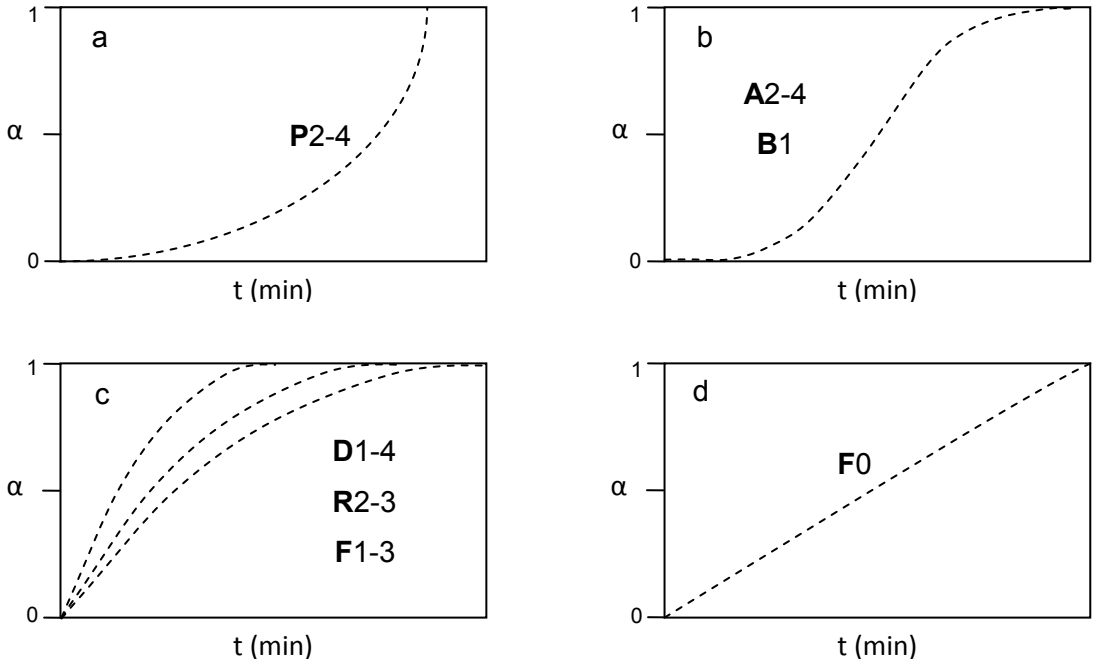

Figure 2.1: Simple graphical illustration of the different solid-state kinetic models for the conversion factor (α) against time (t) in minutes; (a) an acceleratory curve describing the power-models (P2-4), (b) a sigmoidal nucleation curve illustrating the application of Avarami-Erofeev (A2-4) and Prout-Tompkins (B1) models, (c) deceleratory curves for models such as diffusion- (D1-4), geometric contraction (R2-3) and reaction order models (F1-3) and (d) describes the constant reaction rate for a zero-order reaction (F0) (adapted from Khawam & Flanagan, 2006a).

2.1.1.1 Nucleation and growth models

Crystal structures may have built-in imperfection (nucleation) sites with variable local energies caused by impurities, surfaces, edges, dislocations, cracks and point defects. These reaction sites initiate exclusively at reactant surfaces with locally enhanced reactivity (e.g. imperfections). Nucleation can take place during a single step (giving either the exponential or linear law) or multiple steps (describing the power law). For a single step nucleation it is assumed that when nuclei are formed growth takes place in a single first-order process.

Table 2.1: Rate equations for solid-state kinetic models according to the integral equation form (modified from Khawam & Flanagan, 2006b and Koradia *et al*., 2010).

MODEL	Abbre-viation	$g(\alpha) = kt$	Equation number
Nucleation models			
Acceleratory rate equations			
Power law	***P***2	$\alpha^{1/2}$	(7)
Power law	***P***3	$\alpha^{1/3}$	(8)
Power law	***P***4	$\alpha^{1/4}$	(9)
Sigmoid rate equations			
Avrami-Erofeev (1D nuclei growth)	***A***2	$[-\ln(1-\alpha)]^{1/2}$	(10)
Avrami-Erofeev (2D nuclei growth)	***A***3	$[-\ln(1-\alpha)]^{1/3}$	(11)
Avrami-Erofeev (3D nuclei growth)	***A***4	$[-\ln(1-\alpha)]^{1/4}$	(12)
Prout-Tompkins	***B***1	$\mathrm{Ln}[\alpha/(1-\alpha)] + c^a$	(13)
Geometric contraction models			
Contracting area / cylinder (*2D* phase boundary reaction)	***R2***	$1-(1-\alpha)^{1/2}$	(14)
Contracting volume / sphere (*3D* nuclei growth)	***R3***	$1-(1-\alpha)^{1/3}$	(15)
Diffusion models			
***1D* Diffusion**	***D***1	α^2	(16)
***2D* Diffusion**	***D***2	$[(1-\alpha)\ln(1-\alpha)] + \alpha$	(17)
***3D* Diffusion - Jander**	***D***3	$[1-(1-\alpha)^{1/3}]^2$	(18)

Ginstling-Brounshtein	***D***4	$1 - (2/3)\alpha - (1-\alpha)^{2/3}$	(19)
Reaction-order models			
Zero-order	(***F***0/***R***1)	α	(20)
First-order	***F***1	$-\ln(1-\alpha)$	(21)
Second-order	***F***2	$[1/(1-\alpha)] - 1$	(22)
Third-order	***F***3	$(1/2)[(1-\alpha)^{-2} - 1]$	(23)

In the case of a multiple step nucleation process; several distinct steps are necessary for nucleus formation and growth. The formation of product $B_{(solid)}$ within $A_{(solid)}$ will cause strain which will cause $B_{(solid)}$ to convert back to $A_{(solid)}$; this process will continuously take place until a critical number of $B_{(solid)}$ has nucleated. *Germ* nuclei are made up of product $B_{(solid)}$ below the critical number necessary to convert to stable *growth* nuclei. It is a common assumption that the nucleus growth rate exceeds the rate of nucleus formation (Brown *et al.*, 1980; Khawam & Flanagan, 2006b). The power and Avrami-Erofey'ev models are both examples of nucleation mechanistic models.

The ***Power models*** (***P***) assume constant nuclei growth without any growth restrictions. They also follow an accelerator trend for α versus t curves; this implies that the rate of the reaction increases over time as described by equation (7) which governs the various power models:

$$(\alpha) \quad = kt \tag{24}$$

The **Avrami-Erofey'ev** (***A***) models take nucleation growth restrictions into consideration. Nucleus growth may be constricted by way of two processes, as illustrated in figure 2.2. Coalescence (a) takes place when the active reaction zones of two growing nuclei meet which leads to loss of interface and can also be described as an overlap of nuclei. The growth limit on these nuclei is set by their spacing. Ingestion (b) refers to the total elimination of a possible nucleus site by the growth of an existing nucleus; these ingested sites are often called phantom nuclei (Brown *et al.*, 1980).

The total number of nuclei sites can be given by the following expression:

$$N\ (t) = N\ - N(t) - \ N\ (t) \tag{25}$$

Where N_0 is the total of possible nuclei-forming sites, $N_1(t)$ relates to the actual number of nuclei at time t, $N_2(t)$ is the number of ingested nuclei and $N(t)$ is the number of nuclei that developed into growth nuclei. Avrami proposed using an extended conversion fraction (α') which neglects both ingestion and nuclei coalescence processes; this leads to the assumption that $\alpha' \geq \alpha$. By taking this into account and rearranging the equation; the base equation for the ***A*** models can be given as

$$[-\ln(1-\alpha)] \quad = kt \tag{26}$$

Erofeev was able to derive equation (9) for circumstances where n = 3. Since both men contributed to the development of this equation, the ***A*** models are known as the Avrami-Erofeev models or even the JMAEK models should you also take all the other contributing researchers into account (Khawam & Flanagan, 2006b).

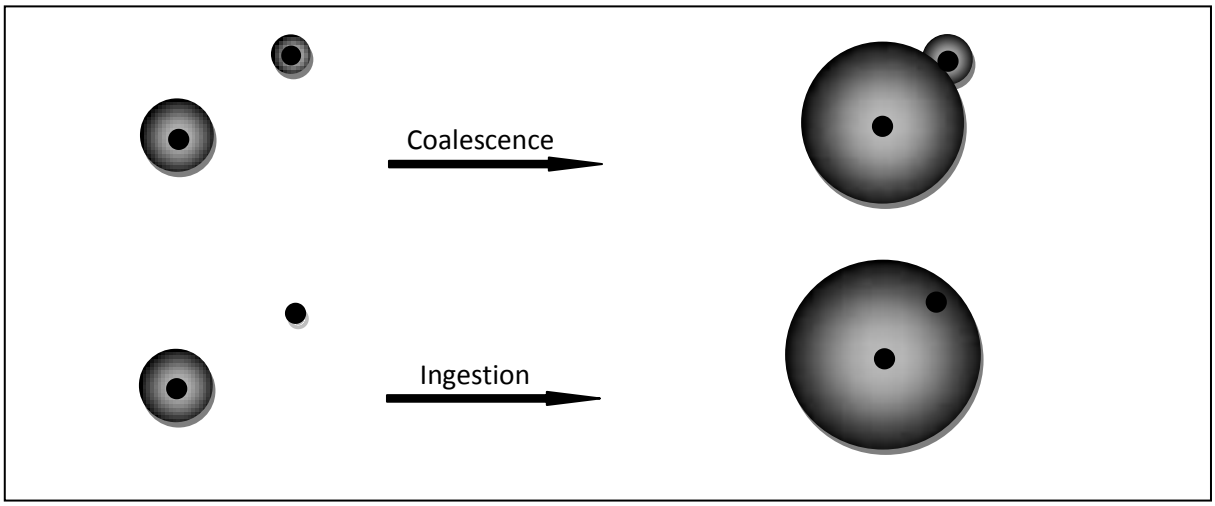

Figure 2.2: Growth restriction of nuclei by way of coalescence and ingestion; the black dots are nucleation sites and the grey areas are nuclei growth regions (adapted from Khawam & Flanagan, 2006b).

The **Prout-Tompkins** (***B***1) model describes the process of autocatalysis in the crystal which assumes a chain reaction-like progress also called “branching”. This takes place when the nuclei growth promotes (catalyses) continued reaction due to the formation of imperfections such as dislocations or cracks at the reaction surface. This reaction is terminated when the reaction spreads into material that has decomposed (Khawam & Flanagan, 2006b). Prout and Tompkins (1944) found that a crystal of potassium permanganate produced considerable cracking during decomposition. The decomposition kinetics obtained did not

comply with any existing model at that time; they therefore postulated a theory and provided an applicable equation for this reaction:

$$ln\frac{\alpha}{1-\alpha} = k\ t + c \tag{27}$$

When plotting α versus time for a reaction following the ***B***1 model it will illustrate a sigmoid curve, with the rate of branching (k_B) and termination being equal at the inflection point of this sigmoid curve. The integration constant (c) was entered into the equation to prevent the obtainment of negative values for α < .5 ; it thus shifts the curve towards positive time values.

2.1.1.2 Geometric contracting models

The solid-state reaction for this model is controlled by the advancement of phase boundaries rather than nucleation-and-growth. The reaction initiates on the surface of the crystal and proceeds inward. The reaction rate is controlled by the movement of the reaction front towards the inside of the crystal (Khawam & Flanagan, 2006b). Different mathematical models exist depending on the crystal shape (Byrn, 1982). The following equation is applicable to these crystals where r is the radius at time *t*, r_0 is the radius at t_0, and *k* is the reaction constant as illustrated in figure 2.3:

$$r = r\ - kt \tag{28}$$

The ***contracting cylinder/rectangle*** or **contracting area *model*** (***R****2)* is a two-dimensional process where nucleation rapidly takes place on the outside surfaces (neglecting the ends) of the crystal moving towards the inside. Equation (14) was derived for this model by taking the volume and weight of a cylindrical particle into consideration and substituting it into equation (3) (Khawam & Flanagan, 2006b).

The ***contracting sphere/cube*** or **contracting volume *model*** (***R***3) is a three-dimensional process. Taking the volume and weight of a spherical/cubic particle into consideration and substituting it into equation (3) it is possible to derive equation (15) (Brown *et al.*, 1980).

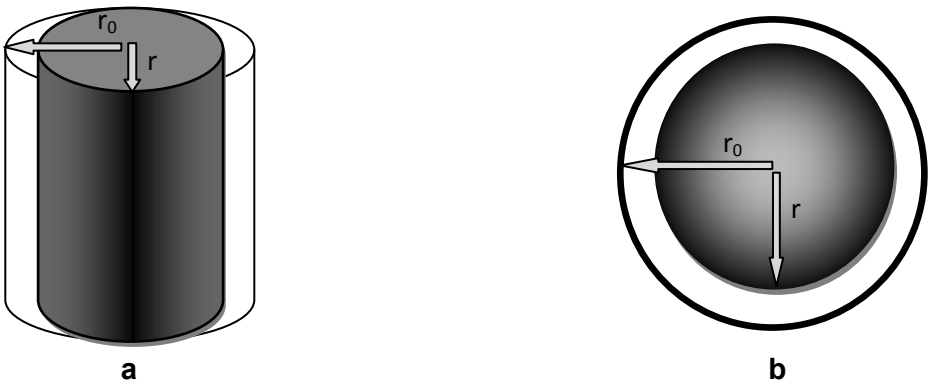

Figure 2.3: Geometric crystal shapes illustrating contraction mechanism: (a) cylinder and (b) sphere (adapted from Khawam & Flanagan, 2006b).

2.1.1.3 Diffusion models

The diffusion model has a characteristic deceleratory *α/t*-curve since the rate of product formation decreases proportionally with the thickness of the product barrier layer (Khawam & Flanagan, 2006b).

One dimensional diffusion model (***D***1) takes no shape factor into consideration, but assume the particle to be an infinite flat plane where the conversion fraction (α) is directly proportional to the thickness of the product layer formed. Equation (29) therefore represents the ***D***1 model.

The **two dimensional diffusion model** (***D***2) describes the process taking place in a cylindrical particle assuming that diffusion occurs radially through a cylindrical shell with an increasing reaction zone. The equation that represents the ***D***2 process is given as (17).

The **three dimensional diffusion model – Jander** (***D***3) and the **Ginstling-Brounshtein** (***D4***) equations assume the diffusion process taking place for a spherical particle and are respectively given as equation (18) and (19).

2.1.1.4 Order models

A constant reaction rate is characteristic of zero-order (***F***0) kinetic behaviour which can be seen from equation (20). The reaction rate (k) of order-based reactions raised to a particular power is proportional to the fraction of remaining reactants. A first-order (***F***1) reaction rate increases at a constant rate throughout the reaction (equation 21), whereas second- (***F***2) and third-order (***F***3) reactions' rates increase by the given power as described by their respective equations (22) and (23) (Brown *et al.*, 1980).

2.1.2 Model-free analysis

The terms “model-free” and “isoconversional” can in certain cases be used interchangeably although not all model-free methods are isoconversional. Isoconversional methods can be used for both isothermal and non-isothermal data analysis (Khawam & Flanagan, 2006a).

The model-free methods generate E_a for each progressive α value without modelistic assumptions. The model-free kinetic models involve the use of isoconversional plots, which enables the calculation of activation energy at each conversion value. There are two model-free methods for isothermal data analysis which can be used to determine the activation energy at progressive conversion values, namely the standard isoconversional method (a), and Friedman’s isoconversional method (b).

The **standard isothermal isoconversional method** was chosen as the model-free method for this study for simplicity reasons. E_a can be obtained by drawing a plot of *–ln t* versus 1000/T for each *α*-value and then substituting the value of the slope into equation (29):

$$-\ln t = \ln\left(\frac{A}{g(\alpha)}\right) - \frac{E_a}{RT} \qquad (29)$$

The **Friedman’s isoconversional method** (Khawam & Flanagan, 2006a) derives E_a by substituting the slope from the plot of *ln(dα/dt)* versus / T at each α value into equation (3).

$$\ln\left(\frac{d\alpha}{dt}\right)_\alpha = \left(lnAf(\alpha)\right)_\alpha - \frac{Ea_\alpha}{RT_\alpha} \qquad (30)$$

2.2 EXPERIMENTAL CONSIDERATIONS

Churchill (1979) said that “Our ability and inclination to postulate and construct models appear to exceed our ability and inclination to obtain good rate data. Improvement in rate correlations will come primarily from more and better measurements rather than from improvements in modelling or mathematical procedures.”

Khawam & Flanagan (2006a) explained that varying activation energy can be divided into two groups: true variation and artifactual variation. True variation is influenced by product or defect formation during the reaction in the solid-state as well as by experimental variables such as temperature changes or purge gas flow-rate. Artifactual variation in activation energy may be caused by variable experimental conditions such as variable sample mass and sample packing especially when using isoconversional methods for analysis.

The shapes of α/t curves are significantly influenced by changes in the distributions of sizes and shapes of the crystals. This is due to the variation in geometry of the surface production of nuclei and the subsequent interface advance in particles of different dimensions. Ideally,

kinetic studies should be done using a single crystal of simple and constant geometry, but in practice this is not always possible since crystals grow in different shapes and sizes (Brown *et al.*, 1980). Many authors have proposed that crystal sizes should be fractioned by grinding and sieving the crystals to limit the particle size and the influence of the crystal symmetry on the desolvation mechanism. Agbada & York (1994) studied the influence of sample weight (17 mg vs. 6 mg) and particle sizes (unfractionated, < 500 μm, < 150 μm) for the dehydration reaction of theophylline monohydrate on the kinetic models and the consequential kinetic results. They found that different models were attained for fractionated and unfractionated particles in large mass samples; however, there was no difference in the mechanism observed between the fractionated and unfractionated particles analysed in lower mass samples.

Brown *et al*. (1980) urged that special care should be taken when preparing a sample for kinetic analysis since the formation of desolvation nuclei are very sensitive to superficial imperfections in the crystal and reaction often initiates within these damaged regions. In recent kinetic studies, researchers are refraining from crushing (Khawam & Flanagan, 2008) and even from sieving (Koradia *et al.*, 2010) crystals since this would lead to the formation of crystal defects which may conceal the actual desolvation/dehydration mechanism and rate of the reaction. The dehydration for a single-crystal 5-nitrouracil monohydrate sample occurs as a random nucleation process at room temperature (see figure 2.4). Should both ends of another single-crystal 5-nitrouracil monohydrate sample be cut off then the dehydration process will progress as a front moving along the long axis of the crystal starting at the new artificial faces (Perrier & Byrn, 1982).

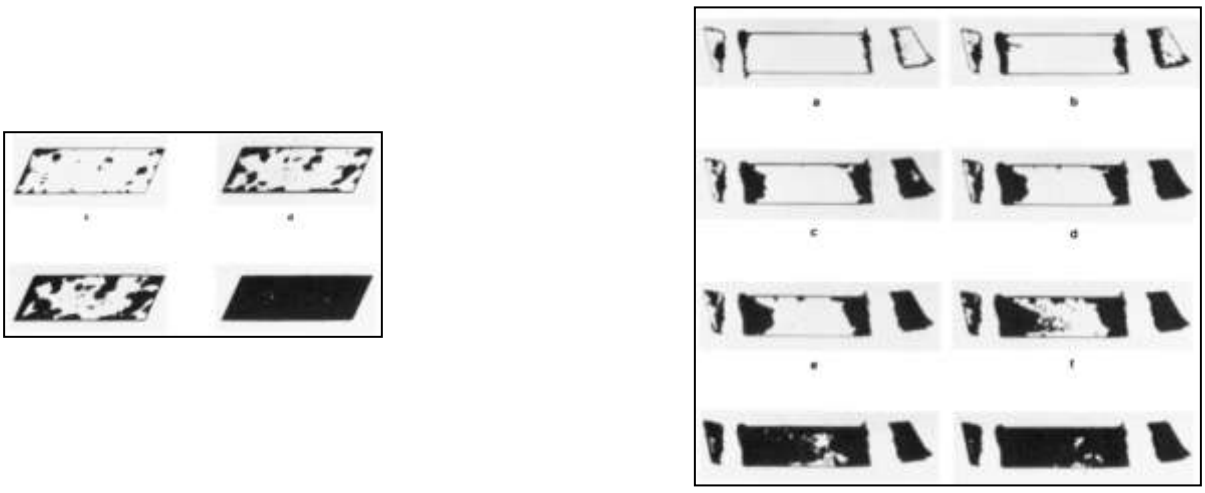

Figure 2.4 : Desolvation of 5-nitrouracil monohydrate at room temperature over anhydrous CaSO4; (a) intact single crystals and (b) a single crystal which was cut using a scalpel to create artificial ends (Perrier & Byrn, 1982).

2.3 EXAMPLES OF RECENT SOLID-STATE KINETIC STUDIES

Laidler (1972) presented a paper in which he described a number of peculiar events which followed an Arrhenius-type of temperature dependence. He explains the findings of various authors who measured the frequency of the flashing of fireflies, the chirping of tree crickets and the creeping of ants. The calculated activation energy for each of these processes was 51 kJ.mol^{-1}. This entertaining piece of evidence reminds us that it is possible to apply the Arrhenius equation even to every-day biological events that involve chemical processes.

Khawam & Flanagan (2008) studied the solid-state stability of five structurally related solvates of sulfameter regarding the kinetics of their desolvation. Sulfameter formed solvates in a one to one relationship with tetrahydrofuran, dioxolane, oxane, dioxane and oxepane. Studies were performed with a thermogravimetric analyser, both isothermally and non-isothermally. Model-fitting analysis of the desolvation reactions under isothermal conditions showed that all the solvates followed the ***A***2 model, except for the oxane solvate which followed the ***R***3 model. Analysis of the desolvation reactions under non-isothermal conditions led to either ***A***2 or ***A***3 model (oxane solvate = ***R***3). This indicates that the reaction takes place in one dimension following the isothermal method, but occurs in one or two dimensions for desolvation under non-isothermal conditions.

The ***A*** model results were verified by the fact that the solvents were accommodated in cavities as described by the crystal structure obtained with single crystal x-ray diffraction. The ***R***3 model was also verified since the morphology of the oxane solvate crystals are roughly cubic. The authors concluded that due to the variations regarding the kinetic parameters for isothermal and non-isothermal studies it is not possible to extend kinetic results from an isothermal method to non-isothermal results.

2.3.1 Correlations between the reactivity of the solvent, E_a and host-guest bonding

Various authors (Coetzee *et al.*, 1999; Caira, 2004; Alkhamis *et al.*, 2006) have studied the kinetics and mechanisms of dehydration and/or desolvation reactions of pharmaceutical compounds. Equation 31 presents a simple method used by these authors to evaluate the thermal reactivity of their solvates/hydrates.

$$\Delta T = T_{\mathrm{on}} - T_{\mathrm{b}} \tag{31}$$

The relative stability of the solvate (ΔT) is described by subtracting the neat solvent's boiling point (T_{b}) from the onset temperature of desolvation/dehydration (T_{on}). The solvate/hydrate will be deemed "stable" should the obtained value be positive and unstable/reactive should the ratio be negative.

Alkhamis *et al*. (2006) analysed the dehydration and desolvation kinetics of fluconazole monohydrate and fluconazole ethyl acetate solvate. They did this by using three different methods of analysis (the results are summarised in table 2.2). They concluded that the model that best describes the dehydration process of fluconazole monohydrate is the three-dimensional phase boundary (***R***3) model; implicating that the hydrogen bonding dissociation had a larger E_a barrier than the diffusion process since the H_2O molecules were confined in isolated cages. Each ethyl acetate -molecule was held in a constricted channel; the chosen model for desolvation was the three-dimensional diffusion model (***D***3). The constricted channels in this structure were the cause for the larger energy barrier for desolvation compared to the E_a of the dehydration processes. The calculated relative stability values gave a good indication of the expected E_a values and the order of stability between these two products.

Table 2.2: Correlations between the dehydration and desolvation kinetics of fluconazole monohydrate and fluconazole ethyl acetate solvate and their respective structures (Alkhamis *et al.*, 2006).

	Water (H_2O)	**Ethyl acetate ($C_4H_8O_2$)**
Stoichiometric relationship	1 fluconazole : 1 H_2O	4 fluconazole : 1 $C_4H_8O_2$
Onset of desolvation (°C)	90	120
Boiling point of solvent (°C)	100	77
Relative stability according to equation 31	-10	43
E_a (kJ.mol^{-1})	90	177
Kinetic model	***R***3	***D***3
Inclusion type	Isolated cages	Constricted channels

2.4 CONCLUDING REMARKS

The E_a, A and kinetic model can be calculated from solid-state kinetic studies. It can be used to verify the mechanism which is followed for a specific process such as desolvation.

Kinetic results should not be used alone to explain the mechanism of action of an event. Other techniques such as observations from TM micrographs should be incorporated into the final conclusion. It is very important to minimise variable experimental conditions and not to harm the single crystals before analysis since this will lead to incorrect analysis results.

The E_a can be used with some certainty to confirm the thermal stability of one solvate over another.

2.5 REFERENCES

AGBADA, C.O. & YORK, P. 1994. Dehydration of theophylline monohydrate powder - effects of particle size and sample weight. *International Journal of Pharmaceutics*, 106(1):33-40.

ALKHAMIS, K.A., SALEM, M.S. & OBAIDAT, R.M. 2006. Comparison between dehydration and desolvation kinetics of fluconazole monohydrate and fluconazole ethylacetate solvate using three different methods. *Journal of Pharmaceutical Sciences*, 95(4):859-870.

BROWN, M.E. 1997. Steps in a minefield: some kinetic aspects of thermal analysis. *Journal of Thermal Analysis*, 49(1):17-32.

BROWN, M.E., DOLLIMORE, D & GALWEY, A.K. 1980. 22 vols. Reactions in the solid state. (*In*: BAMFORD, C.H. & TIPPER, C.F.H, eds. *Comprehensive chemical kinetics*, Amsterdam: Elsevier. 340 p).

BYRN, S.R. 1982. Solid state chemistry of drugs. New York: Academic Press. 574p.

CAIRA, M.R. 2004. Isostructurality of inclusion compounds. (*In*: *Encyclopaedia of supramolecular chemistry*, New York: Marcel Dekker Inc. 767-775 p).

CHURCHILL, S.W. 1979. The interpretation and use of rate data: the rate concept. Washington: Hemisphere. 510p.

COETZEE, A., NASSIMBENI, L.R. & SU, H. 1999. Thermal stabilities and kinetics of desolvation of related inclusion compounds of trans-9,10-dihydroxy-9,10-diphenyl-9,10-dihydroanthracene. *Journal of Chemical Research (S)*, 7:436-437.

KHAWAM, A & FLANAGAN, D.R. 2005. Complementary use of model-free and modelistic methods in the analysis of solid-state kinetics. *Journal of Physical Chemistry B*, 109(20):10073-10080.

KHAWAM, A & FLANAGAN, D.R. 2006a. Basics and applications of solid-state kinetics: a pharmaceutical perspective. *Journal of Pharmaceutical Sciences*, 95(3):472-498.

KHAWAM, A & FLANAGAN, D.R. 2006b. Solid-state Kinetic models: basic and mathematical fundamentals. *Journal of Physical Chemistry B*, 110(35):17315-17328.

KHAWAM, A. & FLANAGAN, D.R. 2008. Desolvation kinetics of sulfameter solvates. *Journal of Pharmaceutical Sciences*, 97(6):2160-2175.

KORADIA, V, LOPEZ DE DIEGO, H, ELEMA, M.R. & RANTANEN, J. 2010. Integrated approach to study the dehydration kinetics of nitrofurantoin monohydrate. *Journal of Pharmaceutical Sciences*, 99(9):3966-3976.

LAIDLER, K.J. 1972. Unconventional applications of the Arrhenius law. *Journal of Chemical Education*, 49(5):343.

NINAN, K.N. 1989. Kinetics of solid state thermal decomposition reactions. *Journal of Thermal Analysis*, 35(4):1267.

PERRIER, P.R. & BYRN, S.R. 1982. Influence of crystal packing on the solid-state desolvation of purine and pyrimidine hydrates: loss of water of crystallization from thymine monohydrate, cytosine monohydrate, 5-nitrouracil monohydrate, and ’-deoxyadenosine monohydrate. *Journal of Organic Chemistry*, 47(24):4677-4680.

PROUT, E.G. & TOMPKINS, F.C. 1944. The thermal decomposition of potassium permanganate. *Transactions of the Faraday Society*, 40(0):488-498.

VYAZOVKIN, S. 2000. Kinetic concepts of thermally stimulated reaction in solids: a view from a histrorical perspective. *International Reviews in Physical Chemistry*, 19(1):45-60.

VYAZOVKIN, S. & WIGHT, C.A. 1997. Kinetics in solids. *Annual Review of Physical Chemistry*, 48(1):125-149.

Chapter 3

Methods

Identification, characterisation and analysis

3.1 VISUAL INSPECTION

Crystallisation may occur through regular packing of unit cells in all three different directions, although growth in a certain direction may be preferred which leads to a certain morphology (habit). Differences in the morphological appearance of a substance do not necessarily mean that it is a different polymorph (Giron, 1995). Experimental conditions that influence the habit a crystal takes on during crystallisation include the extent of supersaturation, rate of cooling, degree of solution agitation, the presence of co-solutes and co-solvents and absorbable foreign bodies/ions in the solution (Mullin, 1961; Byrn, 1982). The shape and size of crystals play an important role in the possible pharmaceutical application of the API. The shape affects the flow and packing properties of a powder, and it also influences the available surface area. The surface area per weight or volume influences surface adsorption and dissolution rate. Asymmetric particles have a greater surface area per unit volume compared to that of a sphere which has the least surface area per unit volume (Martin, 1993). Figure 3.1 shows the classification of different crystal habits.

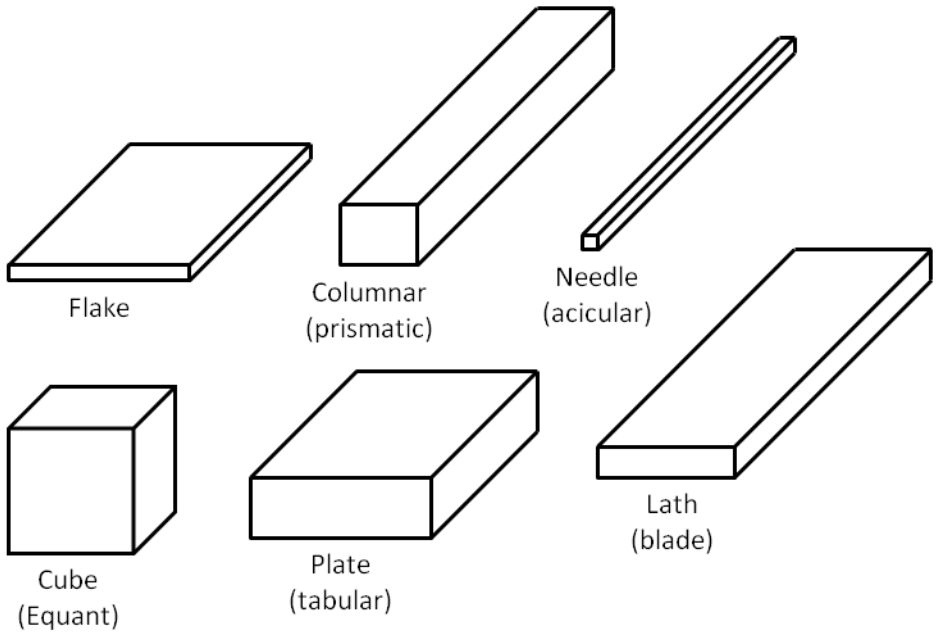

Figure 3.1: Diagram of the six common crystal shapes adapted from Nicols (2006).

Acicular crystals (or needles) are slender and/or tapered needle-like structures. They are thinner than prismatic crystals, but thicker than a flake. ***Bladed*** crystals (laths) are blade-like, slender and flattened. These crystals are more elongated than flaky crystals and thinner than tabular crystals. ***Equant*** crystals have three perpendicular axes that are equal in size. They can also be described as rounded or angular crystals. ***Flaky*** crystals are flattened and thin since they are wider than bladed and thinner than tabular crystals. ***Prismatic*** (columnar) crystals are pencil-like, with elongated sides, and are thicker than acicular crystals. A ***tabular*** crystal (plate) is thicker than flaky crystals but not as long as bladed crystals (Nicols, 2006; Nichols *et al.*, 2011).

3.1.1 **Scanning electron microscopy (SEM)**

The SEM is used for evaluating surface characteristics, identifying the morphology of a crystal and to observe details in the sub-optical to macro-molecular size range.

Samples were analysed by covering the carbon tape on the SEM pin with sample, and it was then covered with a gold-palladium film (Eiko engineering ion coater IB-2, Japan) in a vacuum. The samples were placed in the microscope sample holder and analysed using a FEI Quanta 200 ESEM & Oxford INCA 400 EDS microscope system (FEI Corporation, USA) and operated at 10 kV under high vacuum modes while heating the sample at 10°C.min^{-1} where applicable.

3.1.2 **Thermal Microscopy (TM)**

Examples of thermally-induced events that can be observed using a thermal microscope include a change in the birefringence in the absence of melting, change in transparency or outward appearance, signs of gas evolution, crystallisation from a melt, melting behaviour and sublimation (Byrn, 1982).

Changes in the birefringence and variation in the colours observed in the crystal because of the polarised light indicates a change in the crystal structure. Rubin-Preminger *et al*. (2004) identified the enantiotropic phase transition of form II to form I of ethambutol (SS-EB2HCl) heated above 74°C. The phase transition can be seen under polarised light as a front moving from the one side of the crystal to the other (previously described in chapter 1).

A change in the transparency or outward appearance of the crystal and/or the evolution of gas when submerged in mineral/silicon oil may be an indication of a dehydration, desolvation or decomposition reaction taking place.

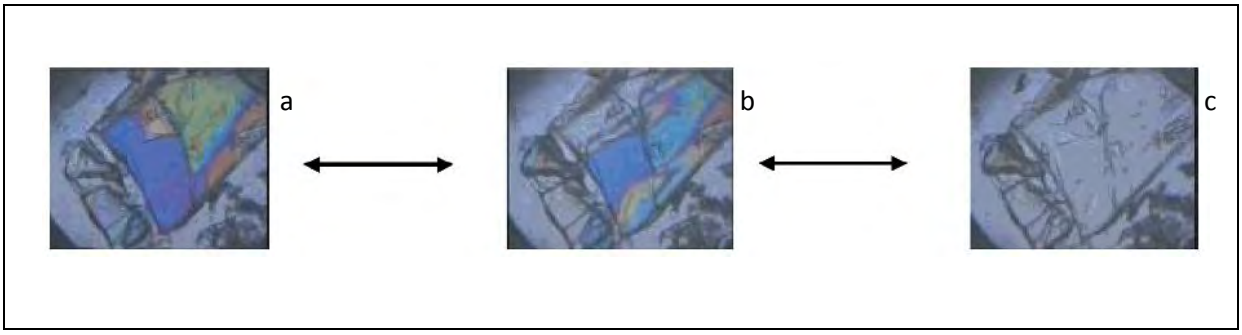

Figure 3.2: The phase transition of SS-EB2HCl from form II (a) at room temperature to form I above 74°C (c) can be seen as a front moving (b) through the crystal as captured by Rubin-Preminger *et al*. (2004).

The samples were placed on glass microscope slides with/without the addition of silicone oil and covered with glass cover slips. The samples were then placed on a hot stage (Leitz Wetzlar hotstage with a Goertz Metrawatt BBC Metratherm 1200d thermometer) for heating. Any changes in the solid sample in relation to the temperature change were observed through a Nikon Eclipse E400 (Nikon, Japan) microscope at a ten time magnification with crossed polarised light. Images were captured using a Nikon DS-Fil camera with NIS-Elements F 2.30 (Nikon, Japan) image capturing software.

3.2 THERMAL ANALYSIS

Thermal analysis means the analysis of change in a property of a sample which relates to heating the sample.

As the solid sample is heated, the amplitudes of the vibrations of the lattice constituents are increased. When a certain amount of energy has been added; one of the following changes will occur in the sample:

(a) ***Phase transition*** - a new arrangement of the molecules may be more stable than the original configuration at the higher temperature.

(b) ***Melting*** - this happens when the forces of attraction between the molecules become insufficient to hold the ordered lattice together and the sample relaxes to the non-ordered state of a liquid. In *liquid crystals* the transition from the solid-state to the liquid state takes place in steps rather than instantaneously.

(c) ***Sublimation*** - when direct transformation from the solid-state to the gas-state takes place without the formation of a liquid phase.

(d) ***Thermal decomposition*** - this happens when the bonding forces between the molecules of the sample become weaker than the forces between the atoms of

which these molecules were made of. Increasing the temperature to this point may lead to bond redistributions which then lead to the formation of chemically different molecules (Brown, 2001).

Some of these events can be described by once again using SS-EB2HCl as an example (Rubin-Preminger *et al.*, 2004). SS-EB2HCl is commercially available as form II. Upon heating (at 10°C.min^{-1}) past 72°C it converts to form I *via* a solid-solid phase transition which can be seen as an endothermic peak. Form I melts (green endothermic peak) at ± 200°C. Upon cooling of the melt, form III re-crystallises at 124 ± 5°C (seen as an exothermic peak). Reheating form III does not render an endothermic phase-transition peak which means that it does not convert back to form II regardless of how many times the temperature cycling is repeated. The phase transition, melting and re-crystallisation can all be confirmed using a thermal microscope.

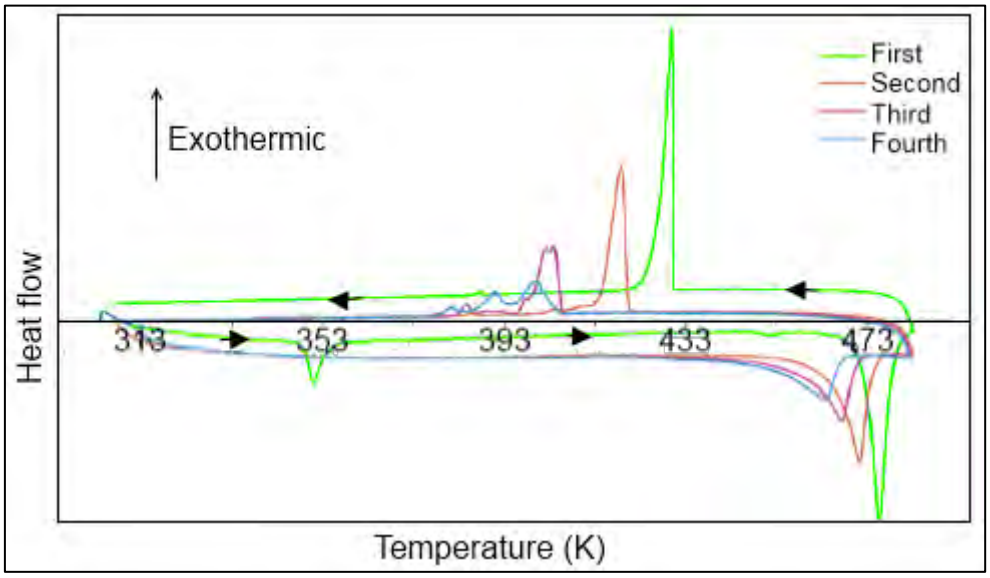

Figure 3.3: DSC thermogram of SS-EB2HCl being heated and cooled during four cycles (Rubin-Preminger *et al.*, 2004).

Thermal studies on the solid-state samples are usually performed using three modes of heating, namely isothermal, non-isothermal or a modulated temperature mode. The temperature is kept at a constant for the isothermal mode while the heating rate is kept constant for the non-isothermal mode of analysis. A modulated temperature programme can

be induced when a sample is heated using a sinusoidal heating/cooling programme with an underlying constant heating rate.

3.2.1 **Thermogravimetric analysis (TGA)**

Thermogravimetric analysis is based on measuring the difference in sample mass over a variation in temperature. This technique is especially handy for evaluating desolvation, dehydration or decomposition reactions, since the original solid sample would progress into a solid and/or a gas (Byrn, 1982; Brown, 2001). Thermogravimetric analysis further helps with resolving the stoichiometric relationship of two molecules captured in the same single unit cell (e.g. hydrate/solvate). The following equation is used for measuring the hypothetical percentage mass loss necessary for a one-to-one API to solvent molecule relationship:

$$TGA\ loss\ 1{:}1\ (\%){:}\quad \frac{MW}{MW\ +MW}\ \mathrm{x}\ 100\ = x\ \% \tag{32}$$

In this equation $\mathrm{MW_S}$ is the molecular weight of the solvent and $\mathrm{MW_{API}}$ is the molecular weight of the unsolvated API. If the experimental analysis gives the same result as x % then the two molecules are in a 1:1 relationship and will be called a hydrate or solvate. Should the obtained value be ½ x % then this crystal will be called a hemi-hydrate or hemi-solvate and this would indicate that there are two API molecules for each S molecule in the unit cell.

3.2.1.1 **Non-isothermal TGA analysis**

Non-isothermal analysis is routinely used for estimation of mass loss. Mass losses were recorded with a Shimadzu DTG-60 (Shimadzu, Japan), using TA60 software version 2.11. Samples (3-10 mg) were heated from 25°C to 200°C at 10°C.min^{-1} in an open aluminium crucible purged with nitrogen (35 mL.min^{-1}). The instrument was calibrated with high purity indium and tin standards according to first principles.

3.2.1.2 **Isothermal TGA analysis**

Isothermal TGA runs were done using duplicate samples at three different temperatures to obtain data for solid-state kinetic fittings.

Crystals (weighing ± 3 mg) were broken into identical pieces (dimensions 3 mm x 1 mm x 1 mm for DDS•(0.5)DCM & DDS•THF and 1 mm x 1 mm x 1 mm flakes in the case of DDS•DXN) under solvent two days before analysis to allow for crystal healing. A Stainless

steel adjustable measurement tool was used for measurement of the crystals under solvent. The crystals were not crushed or sieved to prevent unnecessary superficial imperfections. The temperature was slowly increased (3°C.min^{-1}) to the desired temperature to prevent overshooting. The isothermal temperatures ranged from 50–60°C for DDS•(0.5)DCM, 60-70°C for DDS•DXN and 40-50°C for DDS•THF.

The obtained binary data was ASCII converted into text tables and manipulated using Microsoft Excel 2007. The principles and procedure for isothermal solid-state kinetic evaluation were discussed in chapter 2.

3.2.2 **Differential scanning calorimetry**

DSC is the most popular thermoanalytical technique to date. Two crucibles, one containing the sample and the other being the reference, are both heated/cooled with identical sensors measuring the difference in heat response between these two crucibles. A DSC thermogram may provide us with information such as the melting point, heat of fusion, the purity of the sample, possible polymorphs or solvates, glass and phase transitions, interaction or compatibility of multiple components, thermal stability and decomposition (Brown, 2001; Roy *et al.*, 2002).

3.2.2.1 **Differential scanning calorimetry (DSC)**

Temperature and enthalpy values were measured with a Shimadzu DSC-60A (Shimadzu, Japan) with TA60 version 2.11 software. Approximately 4-10 mg of each sample was weighed and heated in an aluminium crucible with a pierced lid. Samples were heated at 10°C.min^{-1} in an inert nitrogen atmosphere (35 mL.min^{-1}). The instrument was calibrated with high purity indium and tin standards according to first principles.

3.2.2.2 **Modulated temperature differential scanning calorimetry (MTDSC)**

MTDSC allows one to separate the total heat flow signal into the reversing and non-reversing signals. These two signals are related to the heat capacity and kinetically hindered components of the response according to

$$\frac{dQ}{dt} = Cp\,.\frac{dT}{dt} + f(t,T) \qquad (33)$$

Where the **total heat flow** (dQ/dt) results from average heating rate, the **reversing signal** heat flow (Cp.dT/dt) results from sinusoidal temperature modulation (heat capacity

component) and the **non-reversing signal** (kinetic component) where $f(t, T)$ is a function of time and temperature representing kinetically controlled thermal events (Craig *et al.*, 2000).

MTDSC work was done at UCT's Chemistry Department using a TA Q200 MDSC™ and analysis of the results was done using TA Universal Analysis software (TA Instruments, USA). The aluminium TZero™ reference and sample pans were all weighed to ensure that no difference in weight greater than 0.1 mg existed between the pans to minimise any possible discrepancies. The sample weight was meticulously controlled (1 ± 0.07 mg) to ensure reproducibility. The parameters for the MTDSC were chosen after great consideration and experimentation. All samples were heated after being held at 25°C for one minute at an underlying heating rate of 2°C.min^{-1} to 200°C. Amplitude of 0.7°C was added to produce proper heating-and-cooling modulation to the underlying heating rate and the period of such a full modulation lasted 40 seconds.

3.3 WATER CONTENT OF A SAMPLE

The amount of water present in each sample was measured according to a Karl Fischer titration method using a Metrohm 870 KF Titrino Plus (Metrohm, Switzerland). Accurately weighed samples of 100mg were dissolved in methanol and the water content was titrated using hydranal.

3.4 SPECTRAL ANALYSIS

Visible light (3.8 - 7.8 x 10^{-7} m), the colours humans can see, is only a small portion of the total electromagnetic spectrum. X-rays (± 10^{-10} - 10^{-8} m) and ultraviolet (± 10^{-8} - 10^{-7} m) light have shorter wavelengths than visible light. Infrared (± 10^{-6} - 10^{-4} m) light's wavelength is much longer than that of visible light.

When irradiating an organic compound with electromagnetic radiation it will absorb certain wavelengths while transmitting others. This can be seen as an absorption spectrum.

3.4.1 Fourier transform infrared spectroscopy (FT-IR)

In the case of a FT-IR a transmittance of 100 % means that the light is passing through the sample while a lower transmittance will mean that the energy of that wavelength is absorbed by the compound. The molecules that absorb the infrared energy are in an excited vibrational state. These vibrations can give us information about the specific molecular

motion that is possible within the structure which ultimately leads us to the specific type of bonds (or functional groups) that may exist in the compound (McMurry, 2000).

A potassium bromide (KBr) spectrum was obtained as the background. Each sample was dispersed in a matrix of powdered KBr by gently grinding the sample and KBr together with a mortar and pestle. Spectra were recorded over a wavenumber of 4000 - 500 cm^{-1} (can also be stated as 2.5-20 x 10^{-6} m in wavelength) using a Shimadzu IRPrestige-21 (Shimadzu, Japan) with Shimadzu IRsolution software version 1.40. The FT-IR signal was validated on a weekly basis to confirm that it met with the requirements set by the European Pharmacopoeia.

3.4.2 **Solubility studies**

The solubility determination in this study was conducted according to a modified saturation shake-flask method. This method is based on the technique that was developed by Higuchi and Connors (1965). The apparatus used in this study consists of a solubility bath with a horizontal rotating axis (54 rpm) submerged in water. The temperature of the water bath was maintained at 37 ± 2°C. A surplus of sample powder was added to each test tube, and the solvent then added. Each test tube was sealed with Parafilm®, Pechiney, USA, inside the screw cap to prevent leaking. The test tubes were placed in the solubility bath for a period of 24 hours. The sample was collected and the content of each test tube was filtered using a PVDF 0.45 µm disposable filter.

The analysis of the solubility samples was done using a Shimadzu UV-1800 (Shimadzu, Japan). A calibration curve was set up using DDS raw material at several known concentrations (5.05 – 35.35 $\mu g.ml^{-1}$) in water at 37 ± 2°C, by following the Beer-Lambert law. All the determinations were done manually with quartz cuvettes. The British Pharmacopeia states that DDS can be identified in solution using ultraviolet spectroscopy between 230 nm and 350 nm since it renders two distinctive absorption maxima at 260 nm and 295 nm (British Pharmacopoeia, 2011).

3.4.3 **X-ray diffractometry (XRD)**

Von Laue was responsible for the discovery of X-ray diffraction by bombarding a crystal with x-rays and allowing the transmitted beams to be captured onto a photographic plate. The intensities of the diffracted x-rays are nowadays automatically recorded and analysed using computers (James, 1950; Byrn, 1982).

XRD data is particularly useful since it can verify whether two crystals are polymorphs or only different crystal habits in a quick and easy fashion without destroying the crystals (Byrn, 1982).

The unit cell and atomic positions of a compound may be determined using its x-ray diffraction data. Figure 3.4 provides us with an example of a complete X-ray diffraction study. Isostructural inclusion compounds can easily be identified by observing their respective XRD patterns. Diffraction peak positions might be very similar for such compounds because of the small differences in their lattice constants (Caira, 2004).

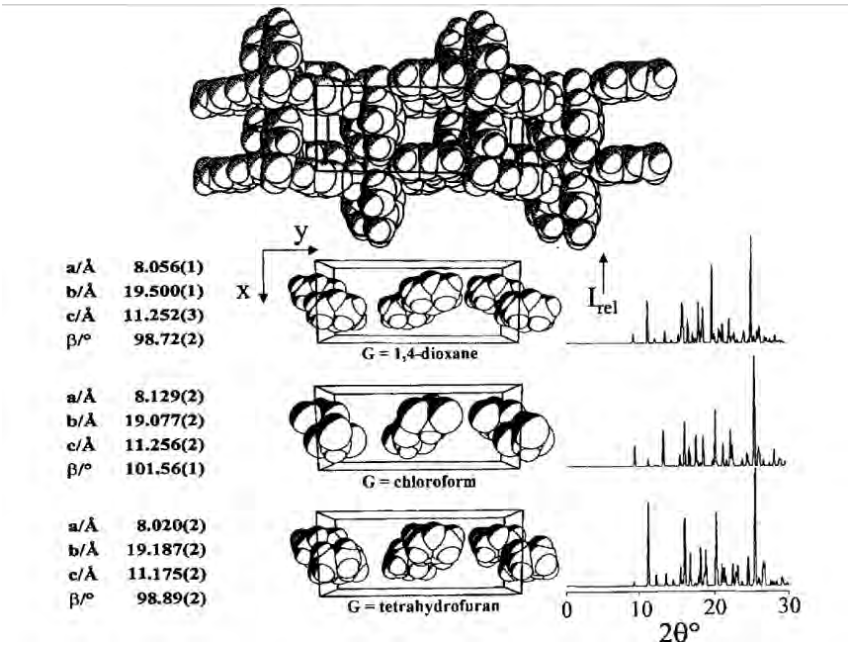

Figure 3.4: Representation of three isostructural channel-type solvates of 5-methoxysulfadiazine. Unit cell data, PXRD patterns and space-filling representation of the cavity occupation are shown (Caira, 2004).

3.4.3.1 Ambient powder X-ray diffraction (PXRD)

Samples for PXRD were lightly ground to improve particle size distribution. Solvates were ground under mother liquor to prevent desolvation. Data was generated on a PANalytical X'Pert-PRO diffractometer (PANalytical, Netherland) at 25°C using CuKα-radiation with a minimum step size of 0.0001 °θ and generator settings at 45 mA, 40 kV.

3.4.3.2 Variable temperature X-ray diffraction (VTXRD)

VTXRD data were generated using a PANaytical EMPYREAN (PANalytical, Netherland) with CuKα-radiation at a minimum step size of 0.0001 °θ, using a PIXcel3D detector. Generator settings were at 45 mA, 40 kV. An Anton Paar Cryo and humidity chamber (Anton Paar, Germany) was used for the heating of the samples. The samples were heated at 10°C/min to a predetermined temperature where a 5 minute scan was done. Longer scans could improve resolution but would cause unnecessary temperature exposure leading to desolvation.

3.4.3.3 Single crystal X-ray diffraction (SCXRD)

The crystal structure of DDS has already been deposited into the Cambridge Structural Database (CSD). Reports of DDS solvates, however, have not been made before, except for a (1:3) hydrate form. The crystal structures of the three solvates were solved using different SCXRD apparatus and analysis software. For more information regarding the apparatus, software and techniques used, please see the attached paper (Annexure A) titled "Solvatomorphism of the antibacterial dapsone: X-ray structures and thermal desolvation kinetics" published in the March 2012 edition of *Crystal Growth & Design*.

3.5 CONCLUDING REMARKS

New methods offer new opportunities to revisit and solve old problems. New methods can also add to existing knowledge of an API regarding its polymorphic forms and solvate/hydrate formation.

Different physical forms of an API can exhibit pronounced differences in physiochemical properties. Identification and characterisation of these manifestations with the widest variety of techniques are of the utmost importance.

3.6 REFERENCES

BRITISH PHARMACOPOEIA. 2011. London: The Stationary Office. 639-640 p.

BROWN, M.E. 2001. Introduction to thermal analysis: techniques and applications. 2nd ed. Dordrecht: Kluwer academic publishers. 264 p.

BYRN, S.R. 1982. Solid-state chemistry of drugs. 2nd ed. New York: Academic press. 574 p.

CAIRA, M.R. 2004. Isostructurality of inclusion compounds. (*In Encyclopaedia of supramolecular chemistry*, New York: Marcel Dekker Inc. 767-775 p).

CRAIG, D.Q.M., BARSNES, M., ROYALL, P.G. & KETT, V.L. 2000. An evaluation of the use of modeluated temperature DSC as a means of assessing the relaxation behaviour of amorphous lactose. *Pharmaceutical Research*, 17(6):696-700.

GIRON, D. 1995. Thermal analysis and calorimetric methods in the characterisation of polymorphs and solvates. *Thermochimica Acta*, 248:1-59.

HIGUCHI, T. & CONNORS, K.A. 1965. Phase solubility techniques. *Advances in Analytical Chemistry and Instrumentation*, 4:177-212.

JAMES, M.A. 1950. X-Ray crystallography. London: Methuen & Co. LTD. 88p.

MARTIN, A. 1993. Physical pharmacy: physical chemical principles in the pharmaceutical sciences. Philadelphia: Lippincott Williams & Wilkins. 622p.

MCMURRY, J. 2000. Organic chemistry. Pacific Grove: Brooks/Cole. 1284p.

MULLIN, J.W. 1961. Crystallization. London: Butterworths. 268p.

NICHOLS, G., LUK, S. & ROBERTS, C. 2011. Microscopy. (*In*: STOREY, R.A. & YMÈN, I, *eds*. *Solid-state characterization of pharmaceuticals*, Chichester: John Wiley. 288-355 p).

NICOLS, G. 2006. Light Microscopy. (*In* HILFIKER, R., *ed*. *Polymorphism*, Wiley-VCH: Weinheim. 167-209 p).

ROY, S., RIGA, A.T. & ALEXANDER, K.S. 2002. Experimental design aids the development of a differential scanning calorimetry standard test procedure for pharmaceuticals. *Thermochimica Acta*, 392-393:399-404.

RUBIN-PREMINGER, J.M., BERNSTEIN, J, HARRIS, R.K., EVANS, I.R. & GHI, P.Y. 2004. Variable temperature studies of a polymorphic system comprising two pairs of enantiotropically related forms: [S,S]-ethambutol dihydrochloride. *Crystal growth & Design*, 4(3):431-439.

Chapter 4

Dapsone

4.1 GENERAL PROPERTIES AND INDICATIONS

Dapsone (4-[4-aminophenyl]sulfonylaniline) is also known as p,p'-sulfonyldianiline or bis(4-aminophenyl) sulfone 4,4'-sulfonyldianiline or DDS. Dapsone will be referred to as DDS from here on.

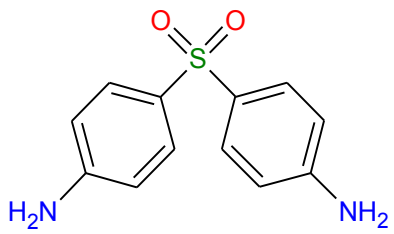

$C_{12}H_{12}N_2O_2S$ MM = 248.3

Figure 4.1: Chemical structure of DDS (British Pharmacopoeia, 2011).

DDS (figure 4.1) is a folic acid synthesis inhibitor. The high degree of chemotherapeutic activity of DDS was first published in 1937 by Buttle and also by Fourneau and their co-workers (Roblin *et al.*, 1941). Today, DDS is used for the treatment of leprosy and in combination with other drugs to avoid the development of bacterial resistance. It is furthermore used in immune-compromised patients as secondary prophylaxis to *Pneumocystis jirovecii* pneumonia (formerly known as *P. carinii* pneumonia) and toxoplasmosis. For toxoplasmosis prophylaxis DDS may be given as primary prophylaxis as a daily dose or as secondary prophylaxis together with pyrimethamine and folic acid as a weekly dose. DDS is also used as treatment for dermatitis herpetiformis (Rositter, 2012).

DDS may be used for the treatment of rheumatoid arthritis not responsive to NSAIDs and should chloroquine be contraindicated for use (Fowler *et al.*, 1984). This drug can also be used in combination with other drugs to combat malaria (Amukoye *et al.*, 1997).

4.2 PHYSICOCHEMICAL AND PHARMACOKINETIC PROPERTIES

DDS is a light-sensitive API characterised as a white or creamy white powder with no odour. DDS is very slightly soluble in water, sparingly soluble in ethanol and methanol but freely soluble in acetone and diluted mineral acids (O'Neil *et al.*, 2001; British Pharmacopoeia,

2011). The solubility of DDS in water at 37°C is 38 mg/100g (Roblin *et al.*, 1941) whereas the solubility in blood plasma at the same temperature was calculated by Linderstrøm-Lang and Naylor (1962) to be 68 mg/100 g. DDS was classified as a class II drug according to the Biopharmaceutical Classification System (BCS) because of its poor solubility but high membrane permeability (Lindenberg *et al.*, 2004).

4.3 IDENTIFICATION AND ANALYSIS

Various techniques can be employed to identify DDS and also to verify differences in the crystal structure.

4.3.1 Thermal properties

The current British Pharmacopeia (2011) provides the melting temperature of anhydrous DDS as 175 – 181°C. The Merck Index (O'Neil *et al.*, 2001) states that DDS melts at 175 – 176°C but also says a higher melting form exists which melts at 180.5°C. Butt (1953) was the first person to mention that DDS exists in more than one form; one that melts at 180°C and another form that melts at 180.5°C.

4.3.1.1 *DDS polymorphs*

Not much is known about the solid-solid phase transformations or the interrelationships between the DDS polymorphs, except for the work published by Kuhnert-Brandstätter and Moser (1979).

According to the above mentioned article; anhydrous dapsone that exists at room temperature is called DDS form III. DDS form III can change *via* an enantiotropically based mechanism to DDS form II at ~82°C and revert back to form III at ~70°C; for this reason the melting point of DDS form III cannot be obtained. DDS form II melts at 177°C. Form I is said to melt at 179°C but is recrystallised from the melt of form II and an enantiotropic relationship exists between form I and form II and additionally between form I and III. The hydrated form of DDS was named DDS form IV and its dehydrated form melts at 170°C.

The thermal behaviour mentioned above is inconsistent with the pressure versus temperature phase diagram (figure 4.2) and also some discrepancies exist according to the four rules provided by Burger and Ramburger (1979). The enantiotropic and monotropic nature of polymorphs have been explained in section 1.2.1 using pressure versus temperature and energy versus temperature plots (figure 1.1).

- The first discrepancy can be observed from the pressure versus vapour plot: DDS form III is the most stable form at room temperature and should therefore have the lowest vapour pressure at that temperature, but according to the plot (figure 4.2 (a)) it is DDS form IV and not III. This discrepancy can easily be fixed by switching the titles of DDS form III and IV as was done in figure 4.2 (b). DDS form IV has no interrelationship with any other DDS polymoph; the exact nature of form IV still has to be investigated.
- The second discrepancy is that of the statement that DDS form I crystallises from the melt of DDS form II and that there exists an enantiotropic relationship between DDS forms I and II; this statement does not match that of the provided plot (figure 4.2 (a)) and also since two polymorphs can only be enantiotropic in nature if the transition takes place prior to melting. Reinvestigation of the interrelationships between the DDS polymorphs using modern techniques will be necessary to evaluate and reconstruct a possible truth about the interrelationship of DDS polymorphs especially with regard to DDS form I.

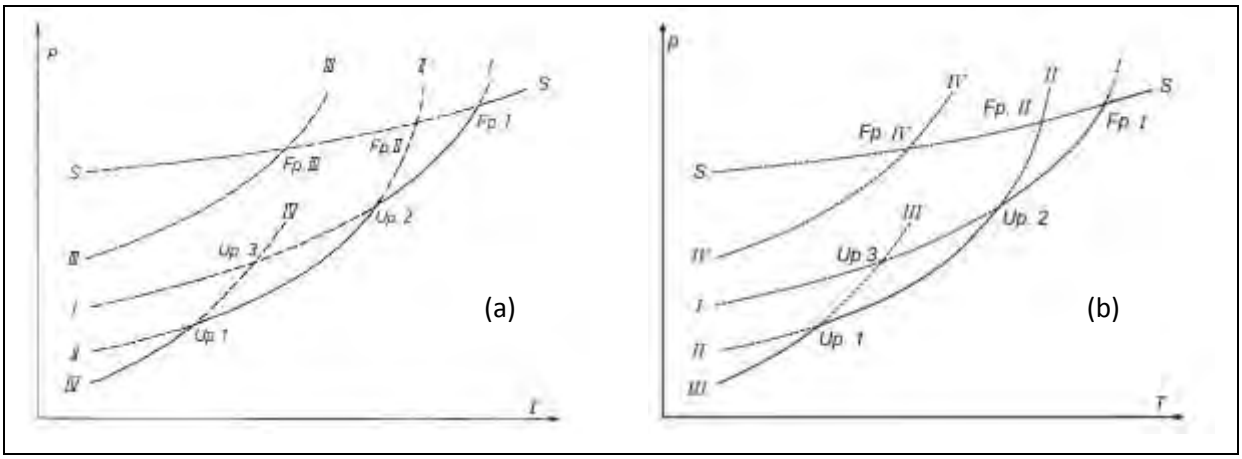

Figure 4.2: Relationship between the polymorphs of DDS (**a**) Pressure versus temperature phase diagram of the four modifications of DDS according to the article published by Kuhnert-Brandstätter and Moser in 1979; where S indicates the melt, Fp is the melting point and Up indicates the phase transitions. Proposed corrected pressure versus temperature phase diagram (**b**) of the four modifications of DDS.

4.3.2 **UV spectroscopy**

The British Pharmacopeia states that DDS can be identified in solution using ultraviolet spectroscopy between 230 nm and 350 nm since it renders two distinctive absorption maxima at 260 nm and 295 nm (British Pharmacopoeia, 2011).

4.3.3 **IR analysis**

Orzech *et al*. (1976) have provided us with the necessary information (table 4.1) for interpretation of DDS's spectra while Kuhnert-Brandstätter and Moser (1979) investigated the slight variations between the different modifications of DDS and concluded that the differences between form III and II should be subtle based on their respective transitional states.

Table 4.1: Interpretation of DDS's IR-spectrum as provided by Orzech *et al*. (1976).

Band frequency (cm^{-1})	**Assignment**
3200-3500	N-H stretch
3000-3100	Aromatic C-H stretch
1635	N-H deformation
1590, 1500, 1440	Aromatic C=C stretch
1300 region	Asymmetric $-SO_2^-$ stretch
1150	Symmetric $-SO_2^-$ stretch
830-840	2 Adjacent H on aromatic ring
550	$-SO_2^-$ scissoring

4.3.4 **PXRD**

Orzech *et al*. (1976) have also provided us with the X-ray diffraction data (table 4.2) for three known forms of DDS, namely form III, form II and a hydrate.

Table 4.2: X-ray diffraction data for the different dapsone forms (Orzech *et al.*, 1976).

Form III		**Form II**		**1:3 Hydrate**	
d-spacing (Å)	**Relative intensity (%)**	**d-spacing (Å)**	**Relative intensity (%)**	**d-spacing (Å)**	**Relative intensity (%)**
12.79	4	13.07	5	12.25	4
7.74	8	7.41	7	11.13	3
6.69	32	6.85	8	8.54	16
6.42	53	6.66	89	7.73	29
5.88	4	6.57	18	7.62	13
5.66	9	6.40	18	7.54	47
5.28	60	5.80	3	7.45	28
5.03	34	5.68	3	6.39	7
4.71	17	5.45	27	6.25	7
4.64	100	5.35	54	5.98	4
4.42	49	5.01	23	5.74	28
4.30	62	4.66	97	5.68	35
4.00	48	4.57	20	5.62	19
3.84	22	4.37	96	5.53	17
3.78	44	4.27	9	5.45	11
3.42	10	3.99	8	5.32	4
3.32	2	3.86	21	5.12	3
3.21	10	3.82	100	5.00	21
3.16	4	3.52	23	4.93	58
3.09	46	3.50	25	4.86	9
2.94	9	3.42	8	4.68	100
2.88	4	3.37	9	4.59	39
2.80	6	3.33	17	4.55	75
2.78	4	3.28	2	4.45	6
2.74	4	3.20	8	4.39	27
2.64	7	3.13	22	4.31	13
2.56	3	3.09	14	4.27	54
2.44	5	3.02	26	4.22	31
2.40	5	2.89	9	4.18	12
2.35	3	2.86	17	4.09	87
2.25	5	2.73	3	4.05	19
2.20	3	2.68	3	4.01	13
2.17	4	2.52	6	3.95	4
2.13	8	2.34	5	3.86	15
2.08	5	2.17	3	3.83	19

	2.10	7	3.77	4
			3.72	3
			3.58	14
			3.46	11
			3.42	9
			3.37	13
			3.35	6
			3.30	15
			3.28	8
			3.23	30
			3.20	10
			3.14	21
			3.09	14
			3.02	8
			2.96	6
			2.87	5
			2.84	3
			2.82	3
			2.79	6
			2.72	6
			2.69	5
			2.65	7
			2.62	7
			2.50	3
			2.45	3
			2.27	6
			2.15	5
			2.07	3
			1.96	3

4.3.5 **SCXRD**

It is interesting to note that DDS has already been submitted into the Cambridge Structural Database (CSD) several times but only two different forms stand out, namely DDS (form III since it was analysed at 22°C) and a hydrate (table 4.3). The crystal system for DDS form III is orthorhombic while DDS•0.33(H_2O) is monoclinic and there seems to be no major difference in the density between the two forms.

Table 4.3: Published crystal and molecular structure of DDS (Cambridge Structural Database and Cambridge Structural Database System, Version 5.32, 2011).

DAPSUO01	**C. Dickinson, J.M. Steward & H.L. Ammon**						
Formula	$C_{12}H_{12}N_2O_2S_1$	**Name**	4,4,-Diaminodiphenyl sulfone				
Space group	P212121	**Cell:**	**a**	8.065(5)	**b**	25.570(20)	**c** 5.760(1)
Space group number	19	**Å,°**	**α**	90.00	**β**	90.00	**γ** 90.00
R-factor (%)	12	**Temp. (K)**	295	**Density (g/cm^3)**		1.388	
DAPSUO02	**N. Deo**						
Formula	$C_{12}H_{12}N_2O_2S_1$	**Name**	4,4,-Diaminodiphenyl sulfone				
Space group	P21212	**Cell:**	**a**	25.740(20)	**b**	8.240(40)	**c** 5.790(10)
Space group number	18	**Å,°**	**α**	90.00	**β**	90.00	**γ** 90.00
R-factor (%)	0.00	**Temp. (K)**	295	**Density (g/cm^3)**		1.343	
DAPSUO03	**G. Bocelli and A. Cantoni**						
Formula	$C_{12}H_{12}N_2O_2S_1$	**Name**	4,4,-Diaminodiphenyl sulfone				
Space group	P212121	**Cell:**	**a**	8.078(2)	**b**	25.589(3)	**c** 5.772(1)
Space group number	19	**Å,°**	**α**	90.00	**β**	90.00	**γ** 90.00
R-factor (%)	4.60	**Temp. (K)**	295	**Density (g/cm^3)**		1.382	
DAPSUO04	**G.-B. Su, F. Pan, Y.-P. He and S.-W. Guo**						
Formula	$C_{12}H_{12}N_2O_2S_1$	**Name**	4,4,-Diaminodiphenyl sulfone				
Space group	P212121	**Cell:**	**a**	8.057(2)	**b**	25.554(6)	**c** 5.759(2)
Space group	19	**Å,°**	**α**	90.00	**β**	90.00	**γ** 90.00

number							
R-factor (%)	4.40	**Temp. (K)**	295	**Density (g/cm^3)**			1.391
DAPSUO05	**V. Bertolasi, V. Ferretti and P. Gilli**						
Formula	$C_{12}H_{12}N_2O_2S_1$	**Name**	4,4,-Diaminodiphenyl sulfone				
Space group	P212121	**Cell:**	**a** 5.758(1)	**b**	8.058(1)	**c**	25.529(3)
Space group number	19	**Å,°**	**α** 90.00	**β**	90.00	**γ**	90.00
R-factor (%)	3.20	**Temp. (K)**	295	**Density (g/cm^3)**			1.392
DAPSUO10	**M. Alleaume**						
Formula	$C_{12}H_{12}N_2O_2S_1$	**Name**	4,4,-Diaminodiphenyl sulfone				
Space group	P212121	**Cell:**	**a** 25.570(10)	**b**	8.070(10)	**c**	5.770(10)
Space group number	19	**Å,°**	**α** 90.0	**β**	90.00	**γ**	90.00
R-factor (%)	13.20	**Temp. (K)**	295	**Density (g/cm^3)**			1.385
ANSFON	**L.G. Kuz'mina**						
Formula	$C_{12}H_{12}N_2O_2S_1$, $0.33(H_2O_1)$	**Name**	Dianiline-sulfone hydrate				
Space group	C2/c	**Cell:**	**a** 48.971 (7)	**b**	11.432(2)	**c**	13.094(0)
Space group number	15	**Å,°**	**α** 90	**β**	92.65(1)	**γ**	90
R-factor (%)	11.92	**Temp. (K)**	295	**Density (g/cm^3)**			1.384
ANSFON01	**V.K. Bel'skii**						
Formula	$C_{12}H_{12}N_2O_2S_1$, $0.33(H_2O_1)$	**Name**	4,4;-Diaminodiphenylsulfone hydrate				

Space group	A112/a	**Cell:**	**a**	13.123(3)	**b** 49.048 (10)	**c**	11.445(3)
Space group number	15	**Å,°**	**α**	90	**β** 90	γ	87.42
R-factor (%)	3.80	**Temp. (K)**		295	**Density (g/cm^3)**		1.377
ANSFON02	**H.S. Yathirajan**						
Formula	$C_{12}H_{12}N_2O_2S_1$, $0.33(H_2O_1)$	**Name**		4,4;-Diaminodiphenylsulfone hydrate			
Space group	C2/c	**Cell:**	**a**	48.583(0)	**b** 11.418(0)	**c**	13.004(0)
Space group number	15	**Å,°**	**α**	90	**β** 92.28(0)	γ	90.00
R-factor (%)	4.89	**Temp. (K)**		120	**Density (g/cm^3)**		1.406

4.4 CONCLUDING REMARKS

This drug has great potential for future use in immune-compromised individuals to combat opportunistic infections. Despite the age of DDS, prior knowledge about its polymorphic profile was still incomplete, hazy and fraught with misconceptions. No investigation has previously been done regarding possible solvate formation of DDS. Reinvestigation of DDS using modern techniques such as MTDSC and VTXRD might significantly add to the existing knowledge of this clinically useful drug.

4.5 REFERENCES

AMUKOYE, E., WINSTANLEY, P.A., WATKINS, W.M., SNOW, R.W., HATCHER, J., MOSOBO, M., NGUMBAO, E., LOWE, B., TON, M., MINYIRI, G. & MARSH, K. 1997. Chlorproguanil-dapsone: effective treatment for uncomplicated falciparum malaria. *Antimicrobial Agents and Chemotherapy*, 41(10):2261-2264.

BRITISH PHARMACOPOEIA. 2011. London: The Stationary Office. 639-640 p.

BUTT, L.T. 1953. The melting point of 4:4'-diaminodiphenyl sulphone (dapsone). *Journal of Pharmacy and Pharmacology*, 5(1):568.

CAMBRIDGE STRUCTURAL DATABASE AND CAMBRIDGE STRUCTURAL DATABASE SYSTEM, VERSION 5.32. 2011. Cambridge Crystallographic Data Centre. Cambridge.

FOWLER, P.D., SHADFORTH, M.F., CROOK, P.R. & LAWTON, A. 1984. Report on chloroquine and dapsone in the treatment of rheumatoid arthritis: a 6-month comparative study. *Annals of the Rheumatic Diseases*, 43(2):200-204.

KUHNERT-BRANDSTÄTTER, M. & MOSER, I. 1979. Zur Polymorphie von dapson und ethambutoldihydrochlorid. *Microchimica Acta*, 71(1):125-136.

LINDENBERG, M., KOPP, S & DRESSMAN, J.B. 2004. Classification of orally administered drugs on the World Health Organization Model list of essential medicines according to the biopharmaceutics classification system. *European Journal of Pharmaceutics and Biopharmaceutics*, 58(2):265-278.

LINDERSTRØM-LANG, C.U. & NAYLOR, R.F. 1962. 4,4'-Diaminodiphenyl sulphone: solubility and distrubution in blood. *Biochemical Journal*, 83(3):417-420.

O'NEIL, M.J., SMITH, A. & HECKELMAN, P.E., 2001. Dapsone. (*In The Merck Index: an encyclopedia of chemicals, drugs, and biologicals*, 13th ed. Whitehouse Station: Merck. 2851 p).

ORZECH, C.E., NASH, N.G. & DALEY, R.D. 1976. Dapsone. (*In*: FLOREY, K, *ed. Analytical profiles of drug substances*, vol 5. New York: Academic Press. 87-114 p).

ROBLIN, R.O., WILLIAMS, J.H. & ANDERSON, G.W. 1941. Studies in chemotherapy. III. Sulfones. *Journal of the Americal Chemical Society*, 63(7):1930-1934.

ROSITTER, D., 2012. South African Medicines Formulary. 10th ed. Rondebosch: Health and Medical Publishing Group. 326 p.

Chapter 5

Dapsone Recrystallisation Study

5.1 INTRODUCTION

Amidon and co-workers recognised that most oral drugs can be organised into four groups according to the Biopharmaceutical Classification System (BCS) which is based on the correlation between the drug product's *in vitro* dissolution and *in vivo* bioavailability with regards to its gastrointestinal membrane permeability (Amidon *et al.*, 1995).

Class I drugs are highly soluble and highly permeable through biological membranes, thus having good bioavailability. BCS class II drugs show low solubility but high membrane permeability. Class III drugs exhibit good solubility but poor permeability. Class IV drugs are known for their poor solubility combined with poor membrane permeability (Amidon *et al.*, 1995).

Dapsone is classified as a class II drug since it is poorly water soluble and highly permeable through gastrointestinal membranes (Lindenberg *et al.*, 2004). Dissolution is the rate-limiting step for bioavailability of class II drugs (Löbenberg & Amidon, 2000) since this would influence the amount of drug available at the gastrointestinal membrane surface.

Several methods have been proposed and tested in the past to improve the dissolution of such drugs by micronisation of the drug particles (Douroumis & Fahr, 2006), formulation of salt-forms (Serajuddin, 2007), solubilisation of drugs in co-solvents (Miller *et al.*, 2012), formulation of micellar solutions (Seedher & Kanojia, 2008), formation of cyclodextrin-complexes (Loftsson, 2002) and using lipid-based delivery systems for the delivery of lipophilic drugs (Porter *et al.*, 2007).

Blagden and co-workers (2007) discussed crystal-engineering as an alternative to these processes to improve the solubility, dissolution and subsequently the bioavailability of BCS class II and IV drugs by habit modification, polymorphism, solvate formation, co-crystal formation and modification of the particle surface.

5.2 RECRYSTALLISATION

Crystallisation is a dynamic process where different polymorphs may compete for nucleation and crystal growth in order to transform from meta-stable to stable forms.

Recrystallisation samples were prepared by adding a requisite amount of the anhydrous dapsone form III (Ria International LLC, East Hanover, USA, batch 20100128) to the neat solvents and heating the mixture to the respective boiling point. The hot, saturated solution was lightly covered with Parafilm® (Pechiney, USA) and allowed to recrystallise by spontaneously cooling to room temperature. The solvents used for this study are listed in

table 5.1 along with their assigned codes, general properties such as molecular weight and boiling points.

Table 5.1: Solvents used for recrystallisation, their respective assigned code, molecular weight and boiling point.

Name of solvent	**Assigned Code**	**Molecular weight ($g.mol^{-1}$)**	**Boiling point (°C)**
Acetone	ACE	58.08	56.2
Acetonitrile	ACL	41.05	81.6
1-Butanol	1BT	74.12	117.6
2-Butanol	2BT	74.12	98
Chloroform	CLF	119.38	61.7
Dichloromethane	DCM	98.96	41
N,N-Dimethylformamide	DMF	73.09	153
Dimethyl sulfoxide	DMSO	78.13	189
1,4-Dioxane	DXN	88.11	101
Ethanol	EOH	46.07	78.5
Methanol	MOH	32.04	64.6
1-Propanol	1PR	88.15	97
2-Propanol	2PR	88.15	82.4
Tetrahydrofuran	THF	72.11	66
Water	H2O	18.02	100

Figure 5.1 shows the concentration of DDS necessary to create a saturated solution with each respective solvent compared to the solvent's polarity. The general trend seen on this graph indicates that DDS's intrinsic solubility increases in accordance with the solvent's polarity, except in the case of water. The solvents used for this study can be divided into three categories:

(1) Dipolar protic solvents such as H_2O, EOH, and MOH which are polar and able to donate a proton (H^+);

(2) Dipolar aprotic solvents are also polar but are not able to donate a proton (H^+) for bonding; namely ACE, ACL, DCM, DMF, DMSO and THF; and

(3) Non-polar solvents e.g. CLF, DXN and TOL (Mirmehrabi & Rohani, 2005).

A possible explanation for the low water solubility might be that the hydrogen bonds formed between the water molecules are stronger than the possible hydrogen bonds formed with DDS.

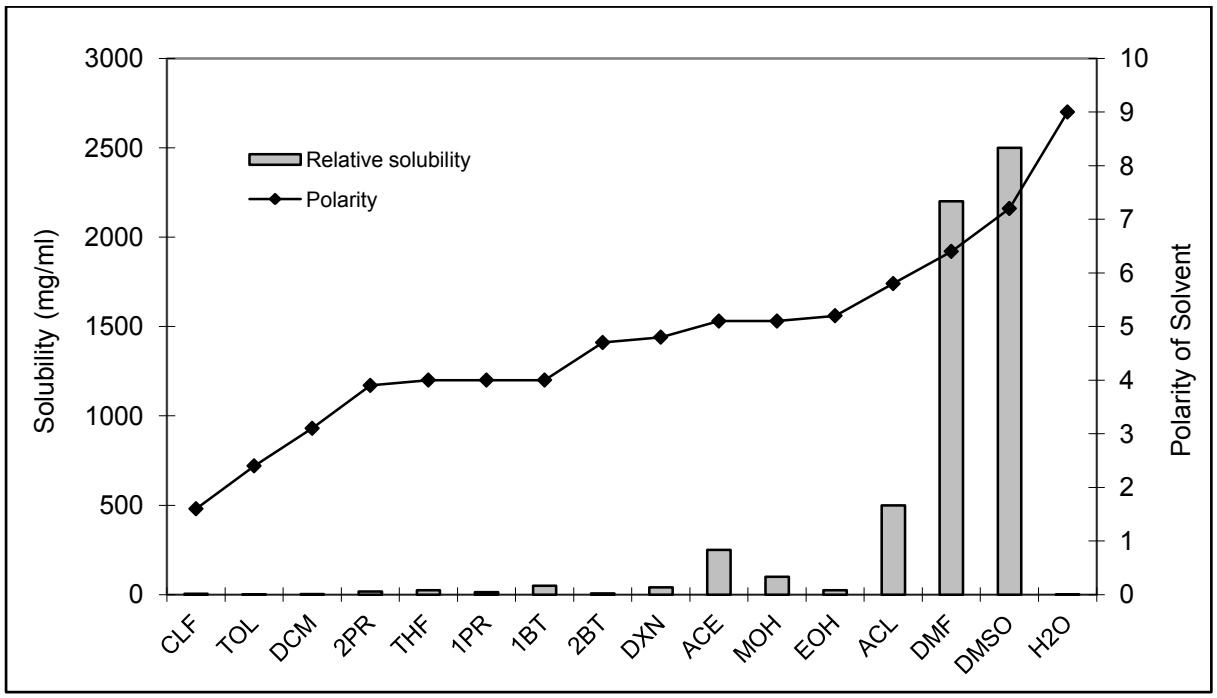

Figure 5.1: Experimental concentration (relative solubility) of DDS in each solvent (near boiling point) versus the polarity of the specific solvent.

5.3 THE PHASE TRANSITION AT 82°C

A solid-solid phase transition was easily observed at ± 82°C upon heating a recrystallised DDS sample (recrystallised from toluene, figure 5.2) on the TM. Using polarised light; the phase transition was seen as a front moving from one side of the crystal to the other. In thicker or chunkier crystals it was noticed as cracks appearing in the crystals or a minor twist/turn of the crystal in the immersion oil. A slight extension of the long side and a further

contraction of the short side may be visible after the phase transition. Please see included CD for more examples.

The samples melted at about 178°C. Crystallisation of the melt can be seen upon cooling the sample back to ambient temperature; this event did not always take place at the same temperature since the rate of cooling could not be controlled. Crystallisation of the melt upon cooling can also be seen as a front moving from one side to the other. A change in colour or cracks appeared in the crystallised melt at ± 70°C.

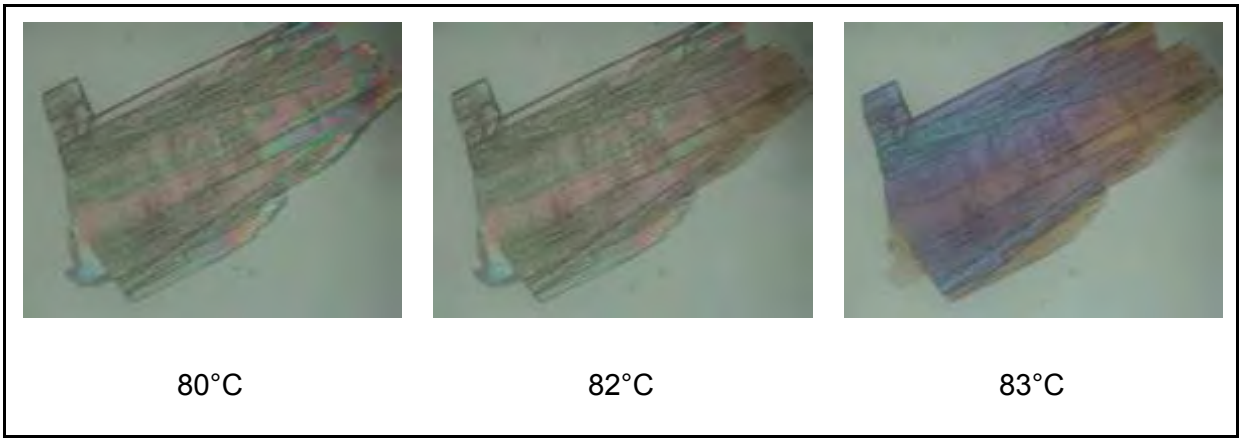

Figure 5.2: Solid-solid phase transition seen as a front moving from one side of a crystal to the other in this product recrystallised from toluene.

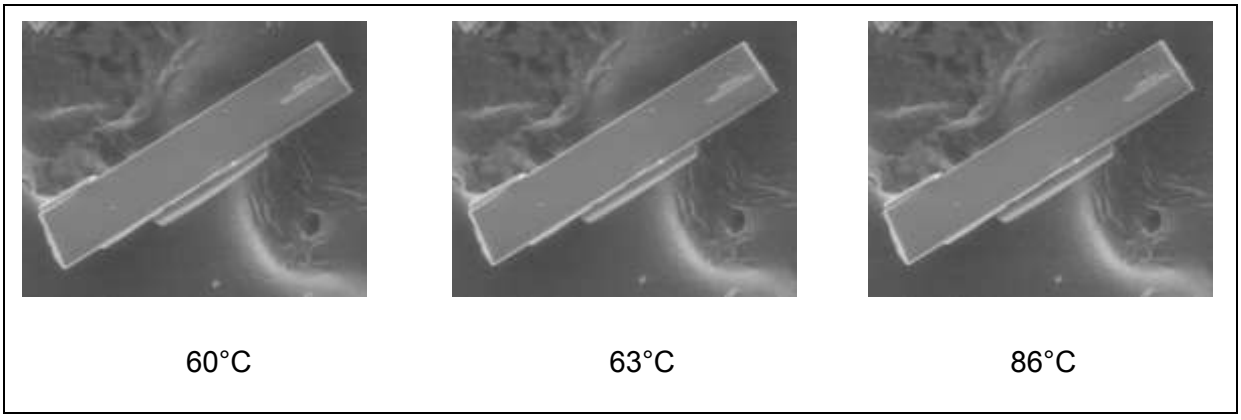

Figure 5.3 SEM micrographs of DDS recrystallised from 2-propranol.

The solid-solid phase transition could also be seen by utilising the heating stage of the SEM (figure 5.3). DDS was crystallised in 2-propanol to provide us with a well-defined

recrystallised crystal of DDS since the original powder form was composed of pieces of various shapes and sizes. The blade-shaped crystal was mounted onto the carbon tape and heated under vacuum. The phase transition can be seen as a wave moving through the crystal. This slight change in the crystal's dimensions takes place at 63°C, a temperature lower than the normal ~82°C as recorded by the DSC but it should be taken into account that this event took place under vacuum. [Please see the file "SEM micrographs of phase transition" on the included CD for more detail].

5.4 CHARACTERISATION OF DDS AND ITS RECRYSTALLISED PRODUCTS

DDS was characterised, by using most of the techniques described in chapter 3, and will be used as reference to compare the re-crystallisation products with. The first step was visual inspection of the colour and morphology of the newly formed crystals. A crystal with different habit/morphology is not necessarily a different polymorph but might be important for future pharmaceutical formulations. The new crystals' thermal behaviour was observed by utilising a thermal microscope, DSC and TGA. FT-IR would verify should the product have different molecular groups/bindings. PXRD and ESEM were only performed should the newly formed product differ from DDS. DDS is light sensitive; the purchased DDS was stored in an opaque air-tight container. The glass container containing the recrystallised products was protected from light by covering it with foil whenever it was removed from the dark cupboard for analysis. The characterisation and analysis results are summarised in table 5.2 and will be explained in detail in this chapter.

Table 5.2: Observation and analysis of the products recrystallised from the various solvents according to morphological shape, and whether they differed from DDS (✓) or not (×) using analysis techniques such as DSC, TGA, TM and FT-IR.

Code	Crystal shape	DSC	TGA	TM behaviour	FT-IR	PXRD
ACE	Bladed	×	×	×	×	~
ACL	Tabular	×	×	×	×	~
1BT	Bladed	×	×	×	×	~
2BT	Acicular	×	×	×	×	~
CLF	Tabular (trapezium)	×	×	×	×	~
DCM	Acicular	✓	✓	✓	✓	✓
DMF	Tabular	×	×	×	×	~
DMSO	Tabular	×	×	×	×	~
DXN	Flaky	✓	✓	✓	✓	✓
EOH	Bladed	×	×	×	×	~
MOH	Prismatic	×	×	×	×	~
1PR	Bladed	×	×	×	×	~
2PR	Bladed	×	×	×	×	~
THF	Prismatic	✓	✓	✓	✓	✓
H2O	Bladed & tabular	✓	~	✓	~	~

✓ Indicate that the specific product showed significant difference to that of DDS when compared to the analysis done using the indicated technique.

× Signify that no differences were observed between the recrystallised product and DDS when using the indicated analysis technique.

~ Signifies that the analysis technique was not carried out on this specific product.

5.4.1 **Three solvates and a hydrate**

Samples were dispersed in mineral oil to visually verify gas evolution (images can be found in annexure A and on the included CD). The only samples where gas evolution was visible were the products from DCM, DXN, H_2O and THF. Upon heating these crystals became more opaque even before the gas was released from the structure. The exact nature of the evolved gas cannot be verified using TM, nor can the stoichiometric relationship between the solvent and DDS be calculated using this technique alone. Most information regarding the DDS solvates will be described in the next chapter and annexure B.

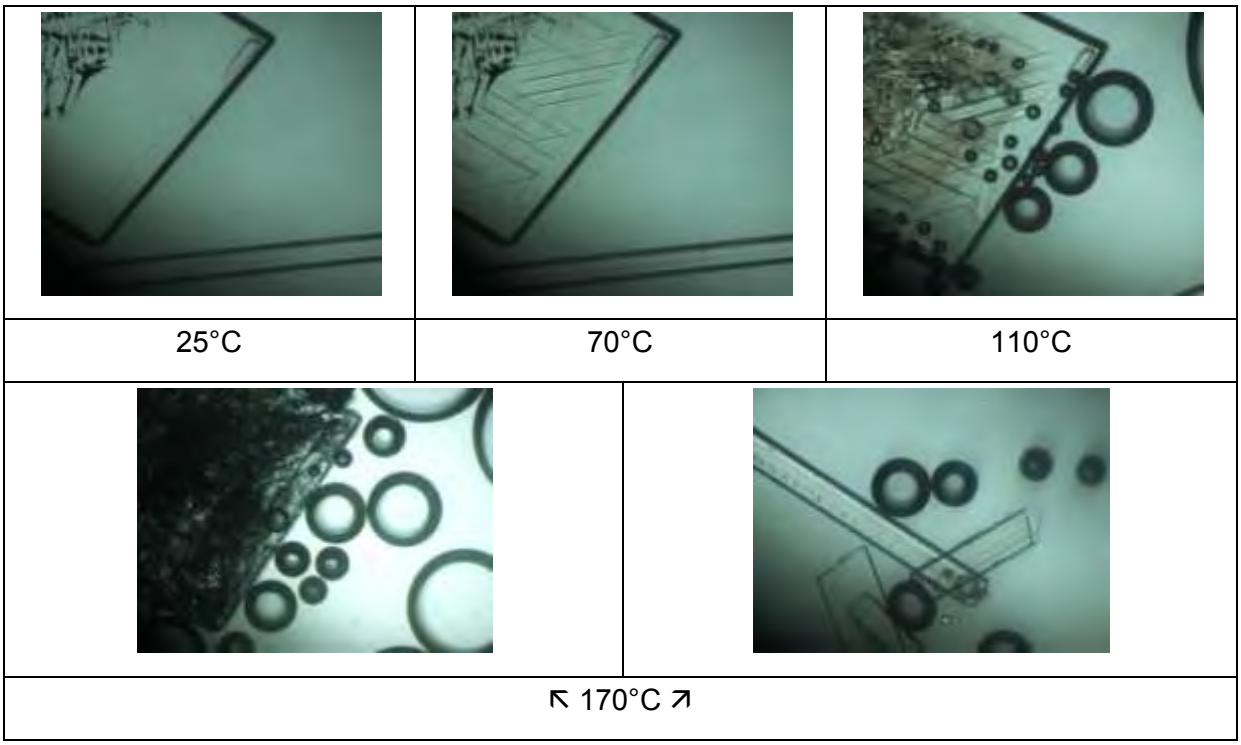

Figure 5.4: Micrographs of the two different crystals shapes recrystallised from water as seen at 25°C, one being tabular and the other bladed. Small grooves appeared at 70°C on the tabular shaped crystal, gas-evolution started at 110°C. At 170°C the tabular crystal appears opaque while the bladed crystals have not shown any activity or change. Not shown here is melting. The desolvated tabular crystals melted first (at 172°C) followed by the bladed crystals at 179°C.

It was interesting to find that two different habits recrystallised from water (figure 5.4), one being tabular and the other bladed. Very little product was formed because of DDS's poor water solubility (0.4 g DDS was dissolved in 1 L of boiling water). Observation using the TM produced fascinating results. The tabular crystals showed grooves, started turning opaque and evolved gas during this heating period while the bladed crystals stayed the same until melting. It can be concluded that these two crystal habits are also two different polymorphs. The Cambridge Structural Database (CSD) reported that a hydrate, DDS•0.33(H_2O) has been submitted into this database by three different research groups in the past. Since the hydrate is a known entity (Cambridge Structural Database and Cambridge Structural Database System, Version 5.32, 2011), has extremely low yield and is sure to have even poorer water solubility than the anhydrate (Pudipeddy & Serajuddin, 2005), this form was not further pursued.

5.5 THERMAL BEHAVIOUR OF DDS RECRYSTALLISED FROM VARIOUS SOLVENTS

The DSC and TGA traces of all recrystallised products can be seen as simplified stacks in figures 5.5 and 5.7 – 5.113. Each product's DSC traces will be discussed.

5.5.1 **Dapsone (DDS)**

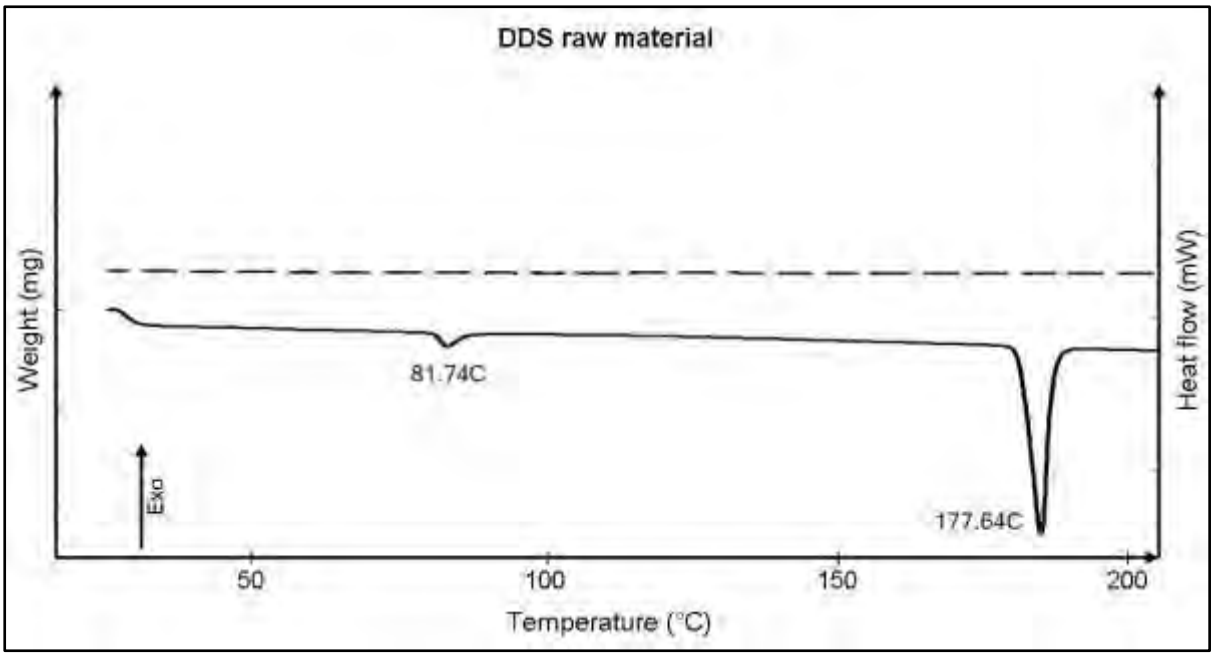

Figure 5.5: Simplified DSC and TGA (broken line) overlay of DDS to illustrate the solid-solid phase transition- and melting endotherms.

No weight loss can be seen over the temperature range of 25 – 200°C; this is in accordance with the BP which states that DDS may not lose more than 1.5 % weight when being dried at 105°C (British Pharmacopoeia, 2011).

The first endothermic event that is seen in figure 5.4 is that of the solid-solid phase transition found at 82 ± 1°C. The melting endotherm is a sharp peak found at 178 ± 1°C.

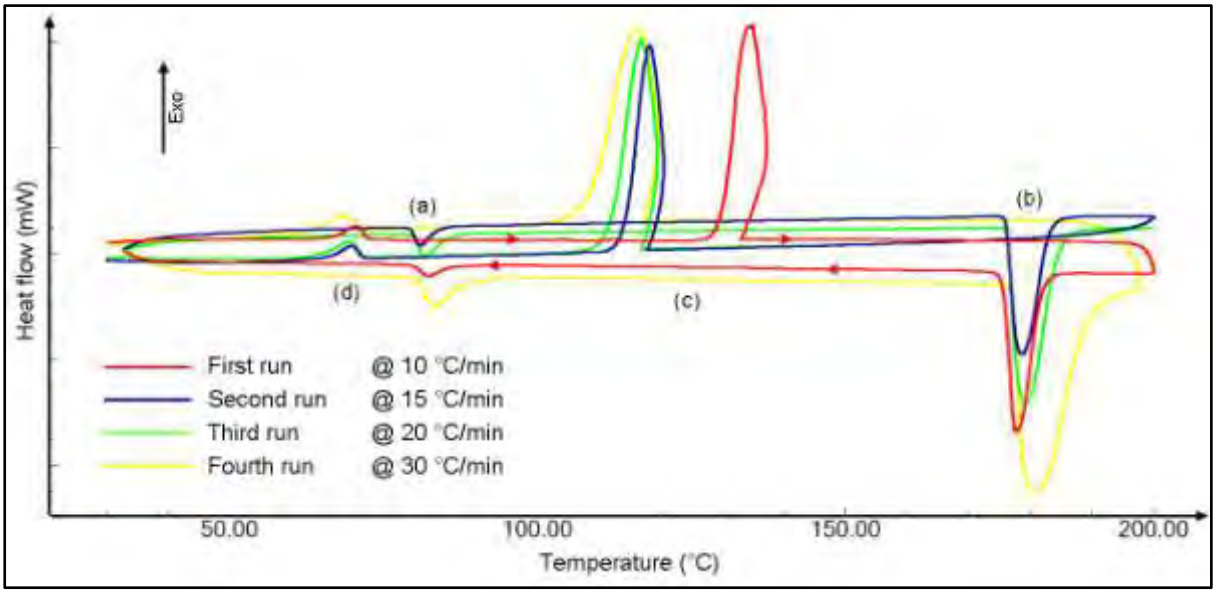

Figure 5.6: DSC thermogram overlay of the same DDS sample first heated and cooled at 10°C.min^{-1}, followed by runs with respective heating/cooling rates of 15°C.min^{-1}, 20°C.min^{-1} and 30°C.min^{-1}. The phase transition upon heating the DDS form III sample can be seen as an endotherm at ~82°C (a), melting of the DDS form II sample takes place at ~177°C (b), cooling of the sample leads to recrystallisation from the melt which is seen as an exothermic event (c), a solid-solid phase transition takes place upon further cooling and is also seen as an exothermic event at ~70°C (d).

There exists an endothermic relationship between DDS form III (which is most stable at room temperature and also the commercially available form) and form II (which melts at 177°C) as stated by Kuhnert-Brandstätter and Moser (1979); this relationship can be clearly seen in figure 5.6. Initial heating of DDS form III leads to a solid-solid phase transition at ~82°C (a), DDS is now in form II since it melts at 177°C (b).

An exothermic event can be seen upon cooling of the melt (c). This event does not always take place at the same temperature but can usually be found around 115-135°C. After recrystallising of the melt DDS is mostly found as form II again, further cooling leads to an exothermic conversion back to form III at 70°C (d). The heating/cooling cycle can be repeated several times and DDS will present basically the same behaviour. A lag in response was seen as the heating rate was increased.

Decomposition took place after melting of the samples; this was seen from the diffraction patterns of the variable temperature x-ray diffractometer (VTXRD) and modulated temperature differential scanning calorimeter (MTDSC), but not on conventional DSC. It is possible that the nitrogen atmosphere in the DSC protected DDS against oxidation.

5.5.2 **Acetone (ACE)**

DDS is very soluble in ACE. The recrystallised product consists of blade-shaped crystals. No weight loss was found over the heating range. According to the DSC thermogram this product behaved exactly like DDS, generating two endotherms at 82°C and 177°C.

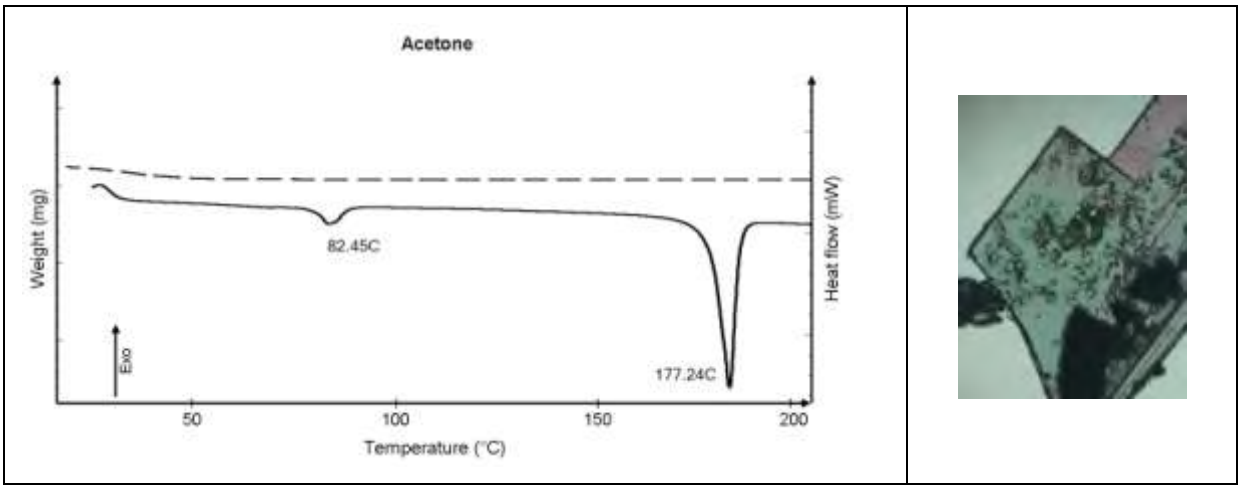

Figure 5.7: Simplified DSC and TGA (broken line) overlay and a micrograph (taken at 25°C) of the product recrystallised from acetone.

5.5.3 **Acetonitrile (ACL)**

DDS is also very soluble in ACL, producing tabular-shaped crystals which did not show any weight loss during heating (figure 5.8). A slightly broader melting endotherm was observed on the DSC trace with its peak temperature at 179.52°C; this could mean that it converted to DDS form I during the melting of DDS form II.

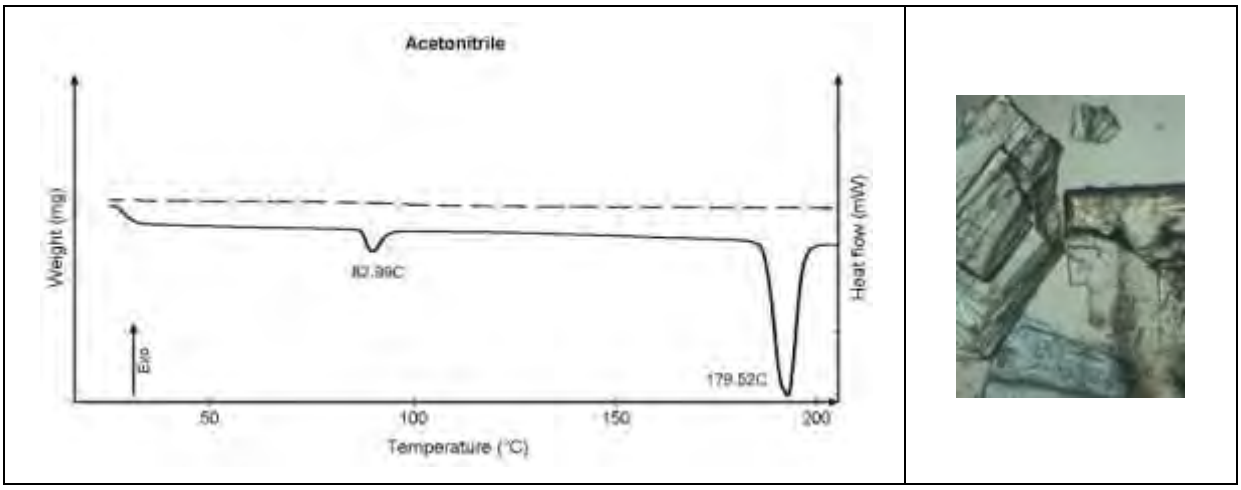

Figure 5.8: Simplified DSC and TGA (broken line) overlay and a micrograph (taken at 25°C) of the product recrystallised from acetonitrile.

5.5.4 **1-Butanol (1BT)**

The product that recrystallised from 1BT was very thin blade-shaped crystals. It formed a closely stacked mesh which made it difficult to remove all excess solvent between the crystals and therefore weight loss can be seen from the very beginning indicating a "wet" sample. This finding can be verified by the TM micrographs which did not show any evolved gas from the crystals.

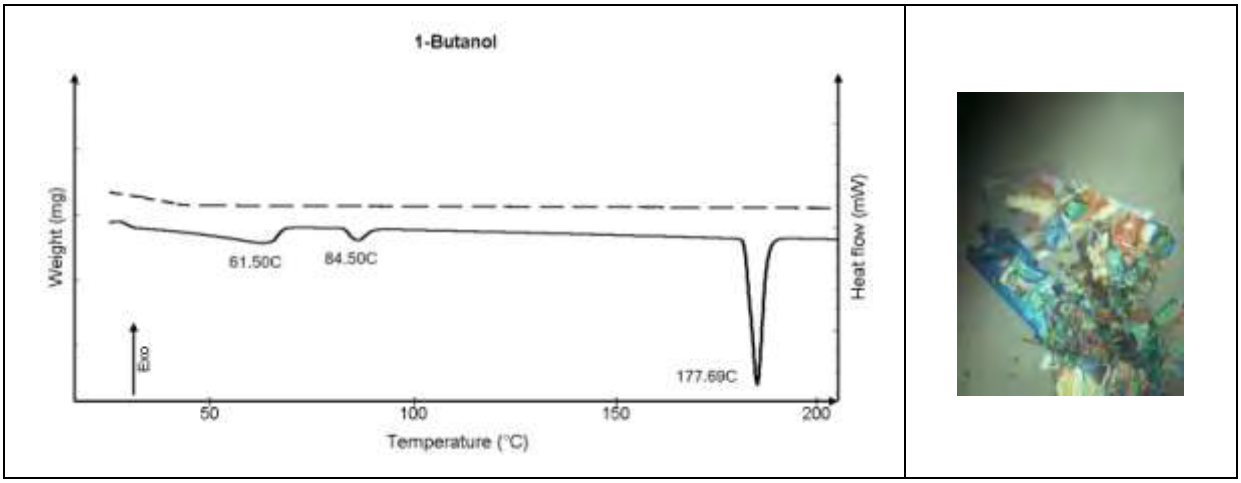

Figure 5.9: Simplified DSC and TGA (broken line) overlay and a micrograph (taken at 25°C) of the product recrystallised from 1-butanol.

5.5.5 2-Butanol (2BT), chloroform (CLF) and *N,N*-dimethylformamide (DMF)

Recrystallised products from 2BT and CLF did not produce anything of interest. The product that recrystallised from DMF showed a broad melting peak with a peak temperature of 179°C; this could mean that DDS form I crystallised from the melt of DDS form II.

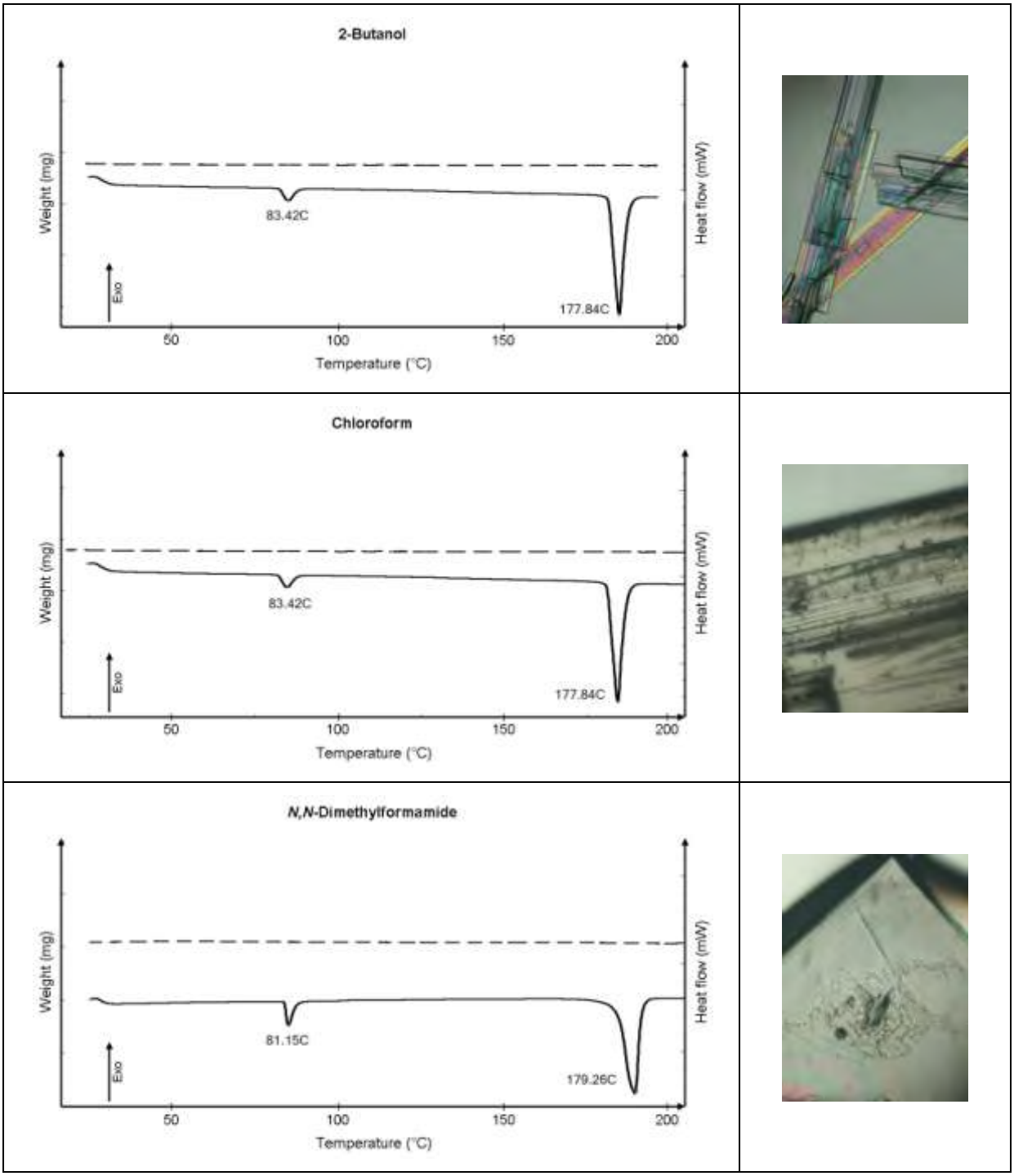

Figure 5.10: Simplified DSC and TGA (broken line) overlays and micrographs (taken at 25°C) of the products recrystallised from 2-butanol, chloroform and *N,N*-dimethyl formamide.

5.5.6 **Dimethyl sulfoxide (DMSO)**

The boiling point of DMSO (189°C) is higher than the melting point of DDS which goes against the conventional rules of recrystallisation (Mullin, 1961), but it was still interesting to see what happens. The recrystallisation of DDS from DMSO took a long period of time, and the end product was beautiful tabular-shaped blocks stacked onto one another. Because of DMSO's high viscosity it was difficult to "dry" the sample completely before analysis without compromising its integrity. This could be the reason for the very different DSC thermogram. The amount of DDS that was required to form a super-saturated solution in DMSO was extremely high, i.e. 2.5 g DDS in 1 ml DMSO. Two small endotherms can be seen, possibly indicating that DDS could dissolve in the small amount of DMSO left on the crystal and slowly melt before DMSO could reach its boiling point and evaporate. A mixture's boiling/melting point would almost always be lower than when the substance with the highest boiling/melting point is tested alone (Martin, 1993). The crystals were verified to be that of DDS form III by FT-IR analysis (results not shown here) and not another polymorphic form.

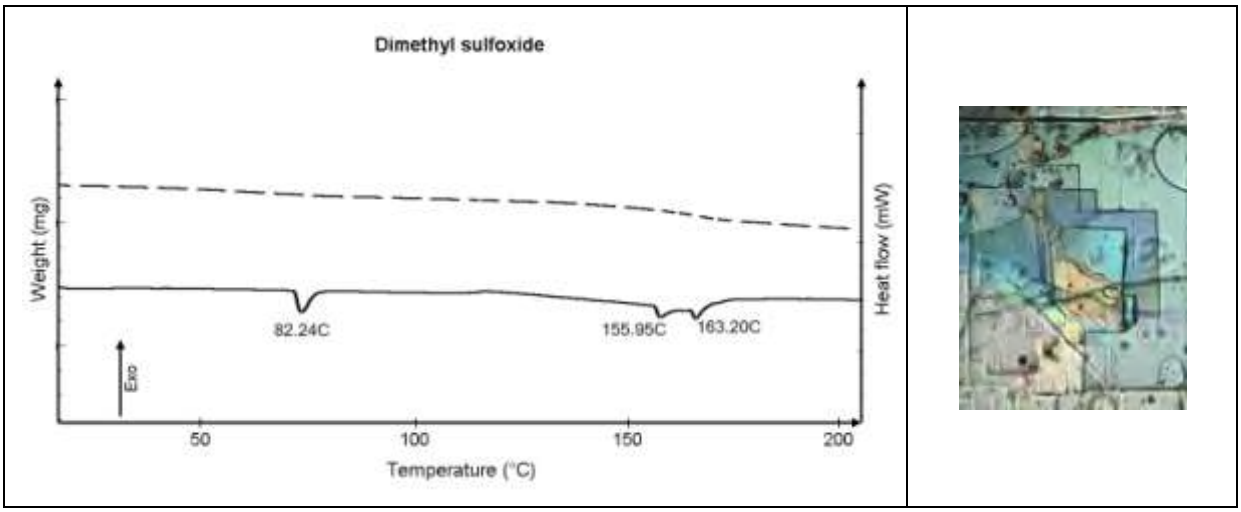

Figure 5.11: Simplified DSC and TGA (broken line) overlay and a micrograph (taken at 25°C) of the product recrystallised from dimethyl sulfoxide.

5.5.7 **Ethanol (EOH) and methanol (MOH)**

The recrystallisation products of EOH and MOH both lost about 1 - 1.3% of its weight as determined with TGA. This event was not observed when analysing samples from the same batch on the DSC. The theoretical percentage weight loss for a one-to-one solvate containing DDS with EOH or MOH is 15.65% and 11.43% respectively; the experimental

weight loss was too small in relation to the theoretical percentage to be deemed a solvate. The melting endotherms of these two products were also slightly higher and broader than other recrystallised products, indicating that conversion to DDS form I might have taken place.

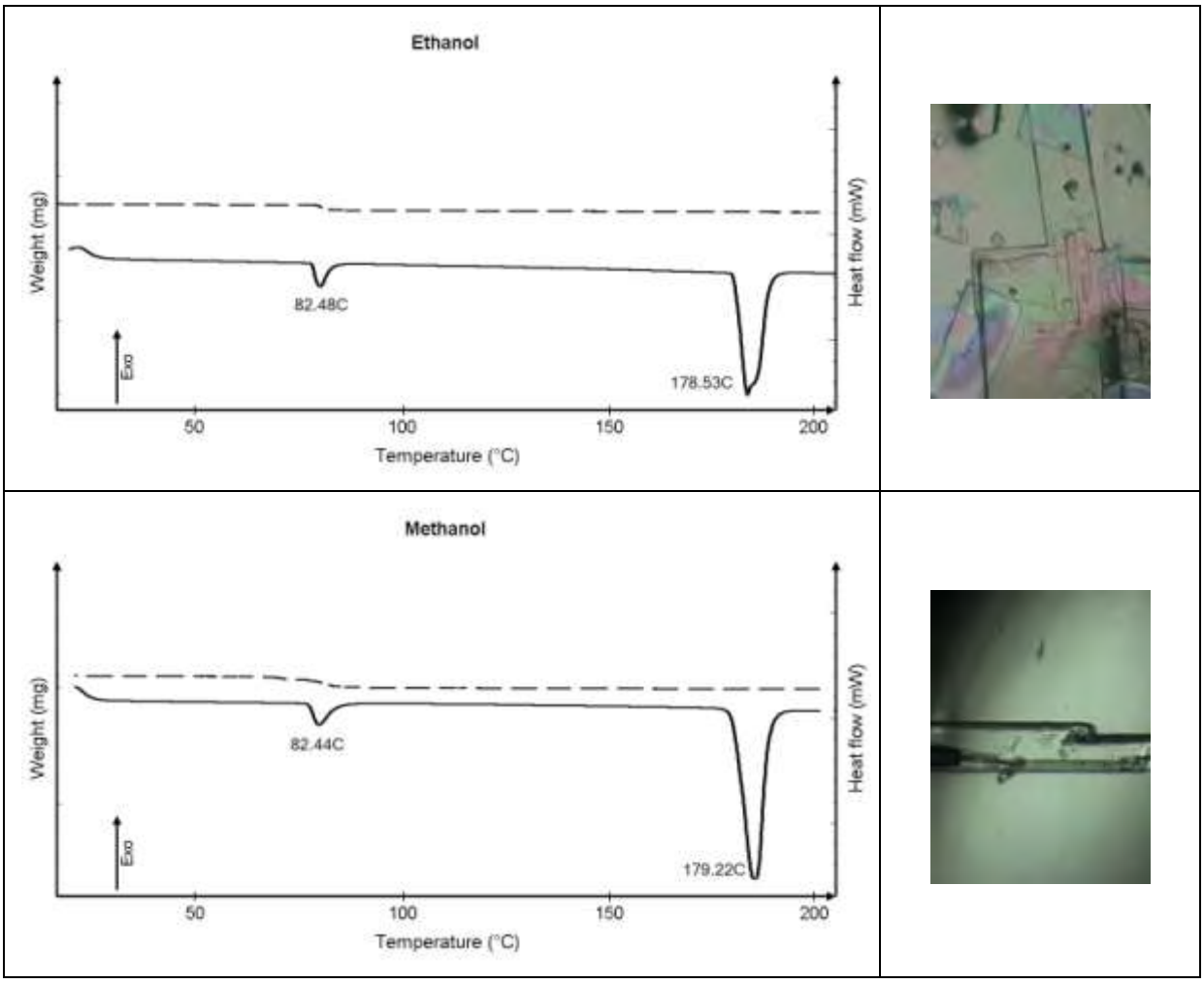

Figure 5.12: Simplified DSC and TGA (broken line) overlays and micrographs (taken at 25°C) of the product recrystallised from ethanol and methanol.

5.5.8 **1-Propanol (1PR), 2-propanol (2PR) and toluene (TOL)**

Recrystallisation of DDS from 1PR, 2PR or TOL did not produce anything other than recrystallised DDS form III crystals. No weight loss was seen over the heating range and no temperature-peak shift was observed.

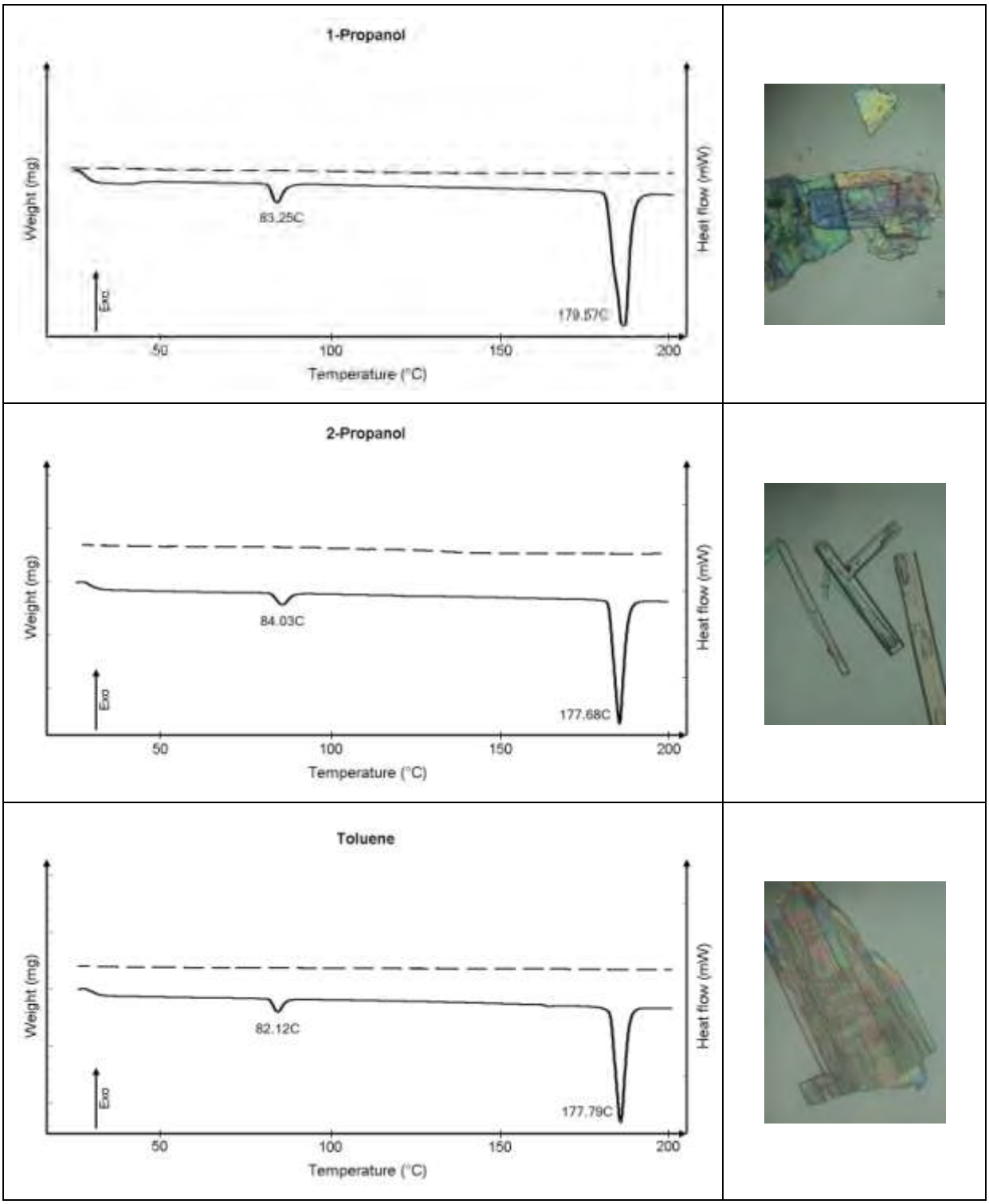

Figure 5.13: Simplified DSC and TGA (broken line) overlay and micrographs (taken at 25°C) of the product recrystallised from 1-propanol, 2-propanol and toluene.

5.6 MELTING POINTS OF RECRYSTALLISED DDS AND ITS POLYMORPHIC FORMS

The recrystallised products can be divided into two groups: those that melted at 177.6 ± 0.2°C and those that showed a broad melting endotherm with its peak melting temperature at ~179.5 ± 0.5°C. The products that melted at ~177.6°C include recrystallisations from ACE, 1BT, 2BT, CLF, 2PR, TOL, desolvated DXN and desolvated THF crystals. The higher melting point was seen with fewer recrystallised products, namely those from ACL, DMF, EOH, MOH, 1PR and desolvated DCM.

The general assumption is that the polymorph with the higher melting point would be more stable. If this was true why is the prevalence of the higher melting point less than that of the lower melting point? The answer may be given by Ostwald's Rule: "When leaving a given state and in transforming to another state, the state which is sought out is not the thermodynamically stable one, but the state nearest in stability to the original state" (Threlfall, 2003).

To further investigate the question previously stated in section 4.3.1.1 about whether the transition point of DDS form I takes place before or after the melting of DDS II; it is important to evaluate the TM micrographs and DSC results.

Conventional DSC traces are not capable of showing all the underlying thermal events taking place. DSC traces of the higher melting point crystals showed a broad melting peak when compared to the lower melting point endotherm; thus it was not possible to verify whether the transition took place before or after melting using this technique. DDS and its solvates were analysed using MTDSC and VTXRD (chapter 6 and annexure B) to further investigate this phenomenon.

Evaluation of the TM micrographs did not show any crystallisation taking place within the melt of the "higher melting peak" crystals. This is consistent with previous observations that the transition took place before melting of DDS form II.

5.7 CONCLUDING REMARKS

Investigation of DDS and its recrystallised products from various neat solvents was absolutely necessary to evaluate the facts and results provided in previous publications since not much was known about the interrelationships of DDS's polymorphs.

Analysis of these recrystallised products led to several discoveries regarding DDS's different polymorphic forms, their appearance, behaviour and also their relation to one another. The

solid-solid phase transition found at ~82°C was examined using various techniques. From SEM and TM micrographs this phase transition can be seen as a wave moving from one side of a crystal to the other.

Recrystallisation of DDS predominantly favoured form III at room temperature. It was possible to establish that the transition for DDS form I takes place before the melting of DDS form II, since no crystallisation was seen in the melt of the higher melting peak's crystals on the TM.

The most interesting discovery that came from the recrystallisations would be the existence of three novel solvate forms for DDS. Their crystal structures were elucidated using SCXRD and this information was deposited into the CSD for future reference regarding DDS. All results regarding the DDS solvates can be found in chapter 6, annexure A and B.

5.8 REFERENCES

AMIDON, G.L., LENNERNAS, H., SHAH, V.P. & CRISON, J.R. 1995. A theoretical basis for a biopharmaceutical drug classification: the correlation of in vitro drug product dissolution and in vivo bioavailibility. *Pharmaceutical Research*, 12(3):413-420.

BLAGDEN, N., DE MATAS, M., GAVAN, P.T. & YORK, P. 2007. Crystal engineering of active pharmaceutical ingredients to improve solubility and dissolution rates. *Advanced Drug Delivery Reviews*, 59(7):613-630.

BRITISH PHARMACOPOEIA. 2011. London: The Stationary Office. 639-640p.

CAMBRIDGE STRUCTURAL DATABASE AND CAMBRIDGE STRUCTURAL DATABASE SYSTEM, VERSION 5.32. 2011. Cambridge Crystallographic Data Centre. Cambridge.

DOUROUMIS, D & FAHR, A. 2006. Nano- and micro-particulate formulations of poorly water-soluble drugs by using a novel optimized technique. *European Journal of Pharmaceutica and Biopharmaceutics*, 63(2):173-175.

KUHNERT-BRANDSTÄTTER, M. & MOSER, I. 1979. Zur Polymorphie von dapson und ethambutoldihydrochlorid. *Microchimica Acta*, 71(1):125-136.

LINDENBERG, M., KOPP, S & DRESSMAN, J.B. 2004. Classification of orally administered drugs on the World Health Organization Model list of essential medicines according to the biopharmaceutics classification system. *European Journal of Pharmaceutics and Biopharmaceutics*, 58(2):265-278.

LÖBENBERG, R. & AMIDON, G.L. 2000. Modern bioavailability, bioequivalence and biopharmaceutics classification sytem. New scientific approaches to international regulatory standards. *European Journal of Pharmaceutics and Biopharmaceutics*, 50(1):3-12.

LOFTSSON, T. 2002. Cyclodextrins and the biopharmaceutics classification system of drugs. *Journal of Inclusion Phenomena and Macrocyclic Chemistry*, 44(1):63-67.

MARTIN, A. 1993. Physical pharmacy: physical chemical principles in the pharmaceutical sciences. Philadelphia: Lippincott Williams & Wilkins. 622p.

MILLER, J.M., BEIG, A., CARR, R.A., WEBSTER, G.K. & DAHAN, A. 2012. The solubility-permeability interplay when using co-solvents for solubilization: revising the way we use solubility-enabling formulations. *Molecular Pharmaceutics*, 9(3):581-590.

MIRMEHRABI, M. & ROHANI, S. 2005. An approach to solvent screening for crystallization of polymorphic pharmaceuticals and fine chemicals. *Journal of Pharmaceutical Sciences*, 94(7):1560-1576.

MULLIN, J.W. 1961. Crystallization. London: Butterworths. 268p.

PORTER, C.J.H., TREVSKIS, N.L. & CHARMAN, W.N. 2007. Lipids and lipid-based formulations: optimizing the oral delivery of lipophilic drugs. *Nature Reviews*, 6:231-248.

PUDIPEDDY, M. & SERAJUDDIN, A.T.M. 2005. Trends in solubility of polymorphs. *Journal of Pharmaceutical Sciences*, 94(5):929.

SEEDHER, N. & KANOJIA, M. 2008. Micellar solubilization of some poorly soluble antidiabetic drugs: a technical note. *AAPS PharmSciTech*, 9(2):431-436.

SERAJUDDIN, A.T.M. 2007. Salt formation to improve drug solubility. *Advanced Drug Delivery Reviews*, 59(7):603-616.

THRELFALL, T. 2003. Structural and thermodynamic explantions of Ostwald's rule. *Organic Process Research & Development*, 7(6):1017-1027.

Chapter 6

DDS solvates

6.1 INTRODUCTION

Solvates were formed by exposing DDS to DCM, DXN and THF under the previously described recrystallisation conditions.

An investigation of the solid-solid phase transition and desolvation characteristics of DDS solvates follow. Attempting to answer the question of whether desolvation or the phase transition first occurred in the dapsone solvates seems oddly reminiscent of the age old conundrum: what came first, the chicken or the egg? In this work, we wish to shed some light on these previously unexplored areas of the DDS solvate's solid-state properties.

6.2 DSC AND TG ANALYSIS RESULTS FOR THE SOLVATES

6.2.1 Dichloromethane (DCM)

The product of recrystallisation in DCM led to the formation of a solvate. Equation 32 was used to calculate the hypothetical percentage mass loss necessary for a one-to-one API to solvent relationship; in the case of a DDS:DCM it would be 28.5 %. Experimental weight loss of 14.9 ± 0 % was predicted by the TGA; this meant that the DCM-solvate was established in a 2DDS to 1DCM ratio. DDS•0.5(DCM) might be deemed a "stable" compound (calculated with equation 31) since the onset of desolvation temperature (80 ± 2°C)is higher than the boiling point of DCM (41°C).

Heating of DDS•0.5(DCM) crystals leads to multiple peaks seen at the end of the DSC thermogram. Since it was known from Chapter 4 that the hemi-hydrate melts at 170°C; it was believed that water was somehow captured into the crystal structure. This hypothesis was tested by determining the amount of water in the compound; KF confirmed the absence of water (0.25 %) therefore it could not be a hemi-hydrate combination. The exact nature of these two new endotherms remains a mystery but some light will be shined on it later in this chapter.

6.2.2 1,4-Dioxane (DXN)

Crystals formed in DXN presented as yellow thin flakes which was sometimes stacked like a Christmas tree or a star. Weigh loss initiated at 101 ± 4.4°C according to the DSC (under our specific conditions). This is very close to DXN's boiling point, but because of the huge percentage weight loss calculated by the TGA and also the evidence provided by TM micrographs it was confirmed to be a solvate.

According to equation 32 the percentage weight loss that will be characteristic of a one-to-one DDS:DXN solvate is 26.2 %. The experimental weigh loss was 27.7 % which is slightly higher than the 1:1 ratio but still in the expectable norms.

6.2.3 Tetrahydrofurane (THF)

Weight loss initiated at 68 ± 2°C according to the TGA (74.6 ± 0.3°C according to the DSC conditions). Onset temperatures are defined as the temperatures where the tangents at the midpoint intersected the baseline; this would mean a slight over-estimation but would rule out any bias. The percentage weight loss calculated for a one-to-one solvate was 22.5%, the experimental value calculated was 23.6 ± 0.4 %; therefore it has to be a one-to-one solvate.

According to equation 31 this solvated-compound is deemed relatively stable since its onset of desolvation is slightly higher than the boiling point for THF alone.

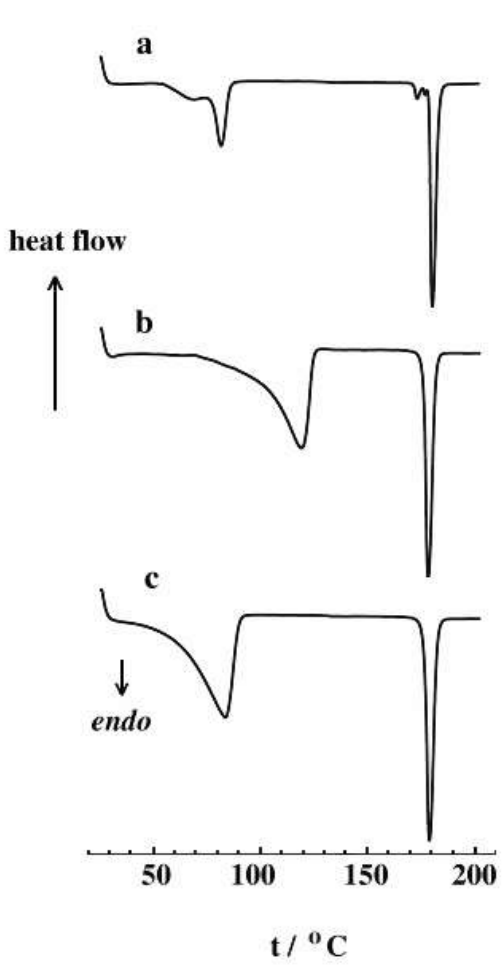

Figure 6.1: Simplified DSC trace stack for (a) DDS•0.5(DCM); (b) DDS•DXN; and (c) DDS•THF over temperature (°C).

Table 6.1: Thermogravimetric for DDS solvates (Standard deviations in parentheses refer to the last digit)

Solvate	Desolvation onset (°C)	Calculated TG mass loss (%) (1:1)	Experimental TG mass loss (%)	DDS:Solvent Ratio
DDS•0.5(DCM)	80 (2)	28.5	14.9	2:1
DDS•DXN	101 (4)	26.2	27.7	1:1
DDS•THF	68 (2)	22.51	23.6	1:1

6.3 SCANNING ELECTRON MICROSCOPY (SEM)

The original crystal habit of DDS was not distinguishable since it was bought in powder form, which was milled. DDS•0.5(DCM) looks like a bunch of straws stacked together. This crystal was previously characterised as acicular by observation on the TM. It is possible to see how the flaky DDS•DXN crystals were stacked onto one another to form bigger and thicker flakes. DDS•THF can be described as a boat-shaped crystal.

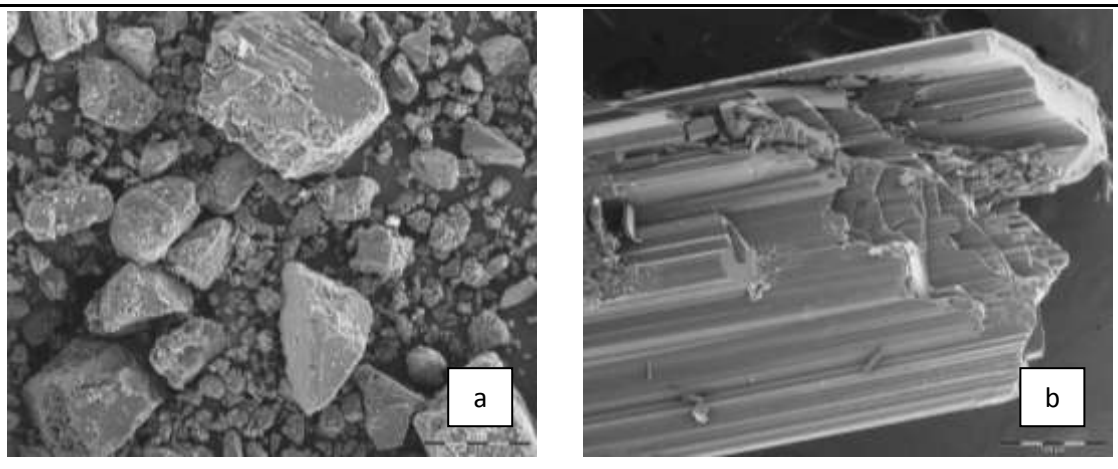

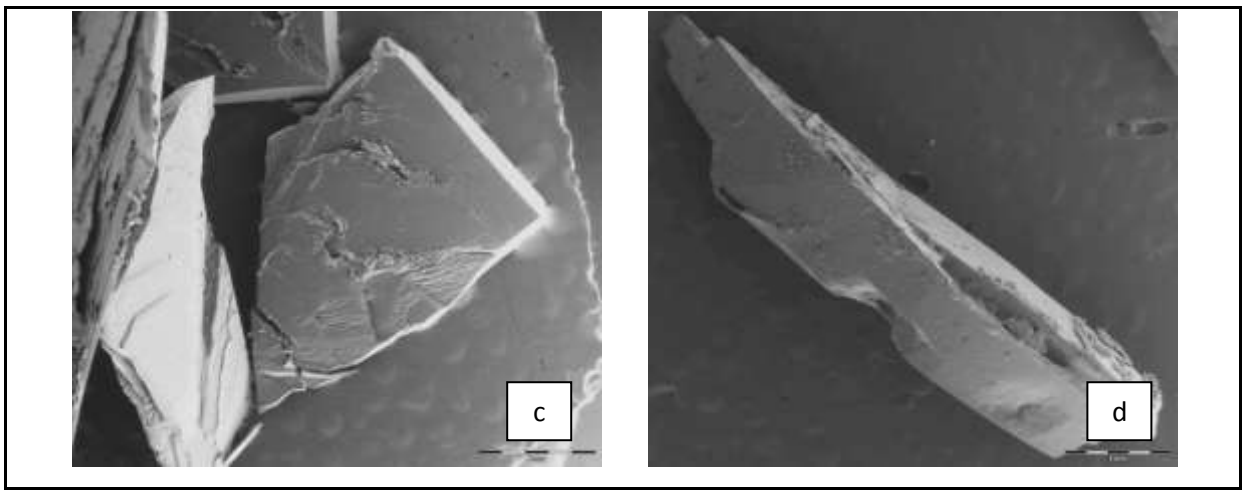

Figure 6.2: SEM micrographs of milled DDS (a), DDS•0.5(DCM) (b), DDS•DXN (c) and DDS•THF (d).

6.4 FOURIER TRANSFORM INFRARED SPECTROSCOPY (FT-IR)

The FT-IR spectra of the recrystallisation products were identical to that of DDS form III, except for the DCM-, DXN- and THF-solvates'. By zooming in on 3500 – 2800 cm^{-1} region of the FT-IR it was possible to identify and describe the differences between the compounds. Kuhnert-Brandstätter and Moser's IR results provided us with a unique opportunity to compare the solvate structures with that of the different DDS forms. Unfortunately, it was not possible for us to analyse the heated samples as was done for DDS forms II and I (Kuhnert-Brandstätter & Moser, 1979).

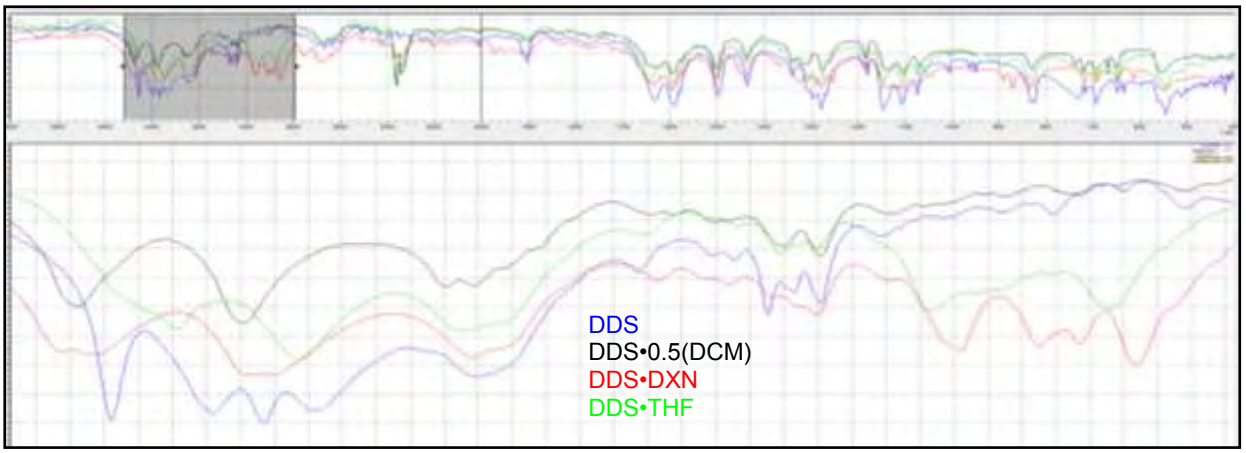

Figure 6.3: FT-IR patterns (enlarged) for DDS (blue); DDS•0.5DCM (black); DDS•DXN (red) and DDS•THF (green) zooming in on 3500 – 2800 cm^{-1} region.

Table 6.2: Comparison of the IR-spectra for the wavenumber region 3500-2800 cm^{-1} at room temperature for DDS III, DDS•0.5(DCM), DDS•DXN and DDS•THF. The IR-spectral data for DDS II and DDS I was obtained from Kuhnert-Brandstätter and Moser (1979) which was measured above 80°C.

DDS III	DDS II	DDS I	DDS•0.5(DCM)	DDS•DXN	DDS•THF
3456	3460	3483	3476	3468	3418
3396	3413		3379	3375	3347
3366	3372			3360	
3334	3340				
3236		3232	3242	3242	3225 / 3248
3146					3144
3102			-	-	-
3089			-	-	3088
3070			-	-	-
3054			3061	-	3063
3038			3038	3042	3040
-	-	-	-	2957	2974
-	-	-	-	2911	2945
-	-	-	-	2886	2903
-	-	-	-	2853	2868

There are absorption peaks listed around 2800-3000 cm^{-1} for DDS•DXN and DDS•THF (less intense), this absorption area is dedicated to the alkanes (C-H).

The peaks at wavenumbers between 3200-3500 cm^{-1} are of particular interest since it indicates symmetric and asymmetric NH-bond vibrations. Kuhnert-Brandstätter and Moser

(1979) heated the DDS past its phase transition (80 ± 2°C) where they then studied forms II and I in terms of their spectral data, the peak maxima shifts can be seen in table A.1.

The peaks at wavenumbers between 3100-3000 cm^{-1} are an indication of alkene (=C-H) bonds. This can be found in all of our samples, although the solvates' spectral data differ significantly from that of DDS.

6.5 POWDER X-RAY DIFFRACTION (PXRD)

Definite differences can be seen between DDS form III and the respective solvates at 25°C.

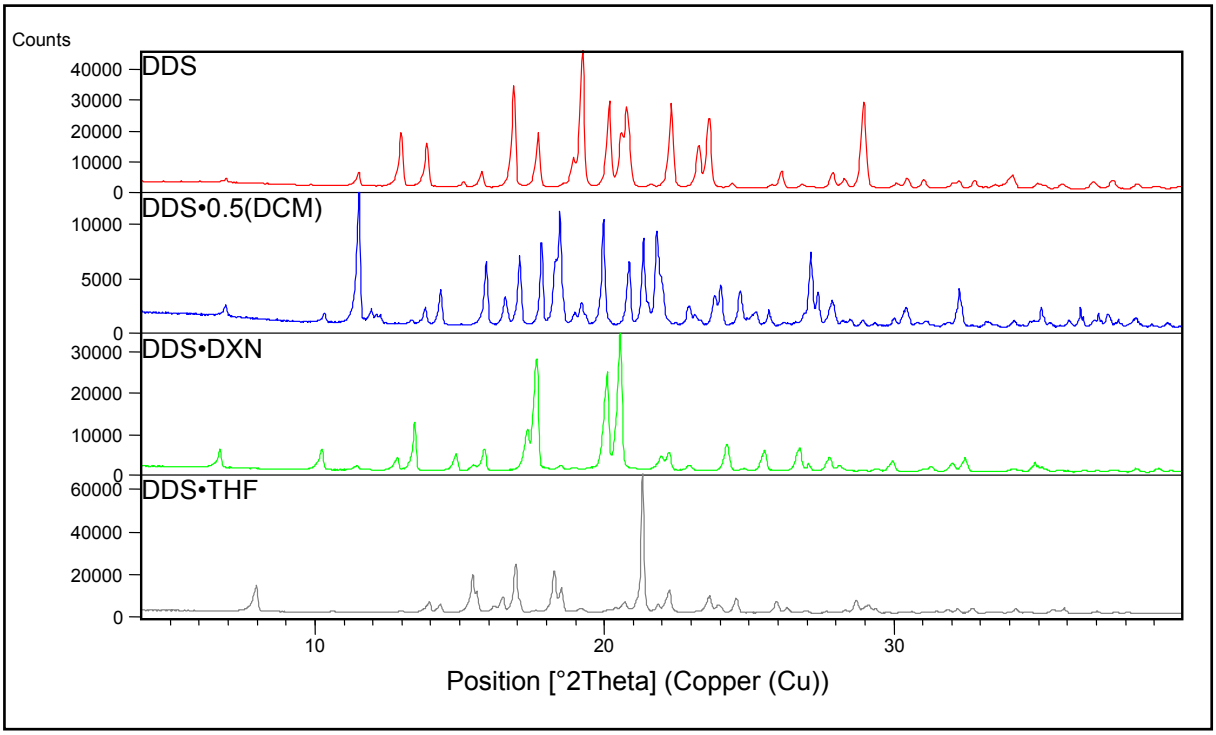

Figure 6.4: PXRD patterns of DDS and the three solvates at 25°C.

Each solvate was desolvated in an oven at 100°C for 120 minutes, afterwards each sample was analysed using the PXRD. The extent of desolvation was confirmed with the TGA. After desolvation of the solvates they all converted back to DDS (form III) which is most stable at room temperature. In other words, after losing the solvent molecules from their crystal structure (which was initially completely different from DDS), they did not convert into a new polymorphic or amorphous form but rather converted back to DDS (form III).

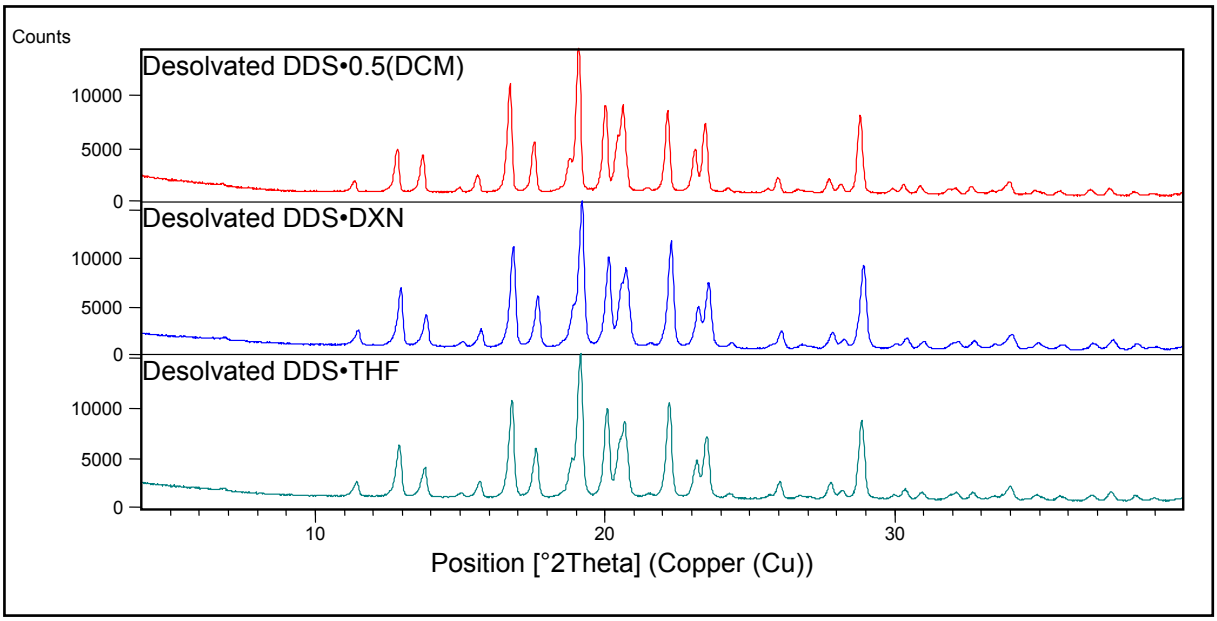

Figure 6.5 : PXRD spectral data of the desolvated solvates at 25°C.

6.6 SOLUBILITY

The solubility determination in this study was conducted according to a modified saturation shake-flask method. This method is based on the technique that was developed by Higuchi and Connors (1965). The apparatus used in this study consists of a solubility bath with a horizontal rotating axis (54 rpm) submerged in the water. The temperature of the water bath was maintained at 37 ± 2°C. A surplus of sample powder was added to each test tube, and the solvent then added. Each test tube was sealed with Parafilm® (Pechiney, USA) inside the screw cap to prevent leaking. The test tubes were placed in the solubility bath for a period of 24 hours. The sample was collected and the content of each test tube was filtered using a PVDF 0.45 µm disposable filter.

The analysis of the solubility samples was done manually with quartz cuvettes using a Shimadzu UV-1800 (Shimadzu, Japan). A calibration curve was set up using DDS raw material at several known concentrations within the specific solvent (each concentration was prepared in triplicate and then each was further analysed in triplicate), by following the Beer-Lambert law.

One aim of this study was to investigate the possibility of preparing new polymorphs of dapsone in an attempt to improve some of its physicochemical properties like solubility. Equilibrium solubility (after 24 hours) was employed as a quick and easy way to compare the

solubility of DDS to that of its solvates. DCM, DXN and THF all have a high carcinogenic risk. For this reason the solubility of the de-solvated solvates was also tested. If the solubility of the desolvates shows a significant improvement in the solubility, it may be commercialised into a pharmaceutically acceptable product.

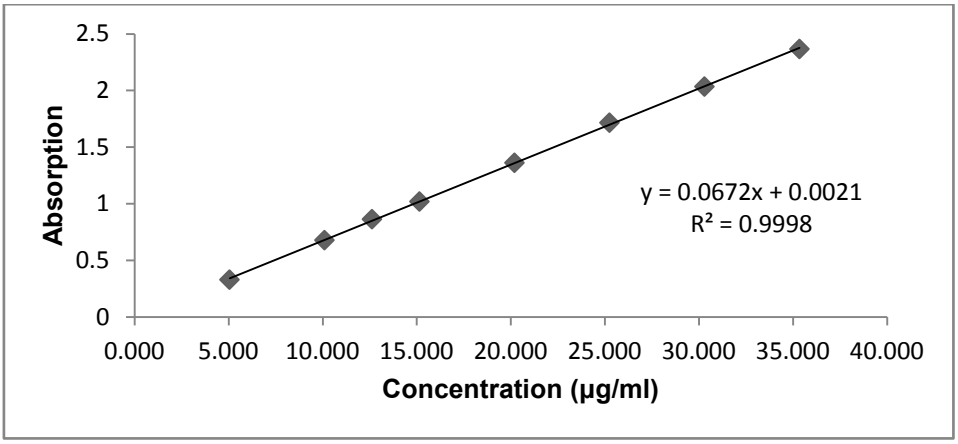

Figure 6.6: Standard concentration curve constructed after completely dissolving known amounts of DDS in pure water at 37°C (n = 3).

The solubility values of DDS•DXN and DDS•THF and their respective desolvates were higher than that of DDS (table 6.3). The decreased aqueous solubility values of DDS•0.5(DCM) can possibly be ascribed to the immiscible nature of DCM and the inherently low aqueous solubility of DDS. The desolvated products of the solvates should be in range with DDS since they converted back to DDS form III at room temperature. There were, however, no significant differences between the dioxane and THF solvates and their respective desolvates.

Further studies on the solubility should be done to investigate possible phase transformations and to obtain repeatable results with lower standard deviation (SD) values. Also, to ensure 24 hours was enough time to reach solubility equilibrium.

Table 6.3: Solubility of DDS, the solvates and also their desolvated products in pure water at 37°C after 24 hours (n = 5)

Product	**Solubility ($\mu g.ml^{-1}$)**	
DDS	36.34	± 2.08
DDS•0.5(DCM)	31.65	± 0.63
Dry DDS•DCM	36.99	± 0.27
DDS•DXN	42.74	± 3.03
Dry DDS•DXN	39.77	± 1.94
DDS•THF	42.32	± 0.41
Dry DDS•THF	41.17	± 2.28

6.7 SINGLE CRYSTAL X-RAY DIFFRACTION (SC-XRD)

The crystal structures of DDS and DDS•0.33(H_2O) were submitted to the CSD. By comparing the PXRDs of the solvates to the data already found in the CSD it was possible to verify that the structures of these solvates were not elucidated before.

The details of the previously published forms of DDS can be seen in table 4.3. Table 6.4 provides the details of the solvates, further details can be found in Annexure A. The crystal system of DDS•DXN is orthorhombic like that of DDS while the crystal systems of DDS•0.5(DCM) and DDS•THF are monoclinic which is the same as that of DDS•0.33(H_2O).

The order of density are DDS•0.5(DCM) >> DDS•0.33(H_2O) > DDS > DDS•DXN > DDS•THF when comparing these results with that of the published data for DDS and DDS•0.33(H_2O). This density results were interesting since the relative melting points for the desolvated products are DDS•0.5(DCM) >> DDS ≈ DDS•DXN ≈ DDS•THF >> DDS•0.33(H_2O).

Table 6.4: Crystallographic data and experimental details for DDS solvates.

	DDS·0.5(DCM)	**DDS·DXN**	**DDS·THF**
Ratio	2:1 DDS:dichloromethane	1:1 DDS:1,4-dioxane	1:1 DDS:tetrahydrofuran
Empirical formula	$2(C_{12}H_{12}N_2O_2S)\bullet CH_2Cl_2$	$C_{12}H_{12}N_2O_2S\bullet C_4H_8O_2$	$C_{12}H_{12}N_2O_2S\bullet C_4H_8O$
Formula weight	581.52	336.40	320.40
Temperature, °C	-100(2)	-100 (2)	-100 (2)
Crystal system	Monoclinic	orthorhombic	monoclinic
Space group	$P2_1/n$	*P*bca	$P2_1/n$
a, Å	8.3000(2)	11.1008(5)	5.8587(3)
b, Å	16.5991(4)	11.3387(5)	12.6787(7)
c, Å	19.9138(4)	26.628(1)	21.8078(12)
α, deg	90.0	90.0	90.0
β, deg	98.660(1)	90.0	91.335(1)
γ, deg	90.0	90.0	90.0
Volume, ($Å^3$)	2712.3(1)	3351.6(3)	1619.5(2)
Z	4	8	4
d_{calcd} (Mg/m^3)	1.424	1.333	1.314
abs coeff, mm^{-1}	0.432	0.214	0.214
Crystal size, mm^3	0.10 x 0.18 x 0.23	0.10 x 0.15 x 0.19	0.15 x 0.22 x 0.28

Theta range for data collection	3.49 – 27.48	1.53 – 28.32	1.86 – 28.38
Index ranges	h: -10, 10	h: -14, 14	h: -7, 7
	k: -21, 21	k: -15, 15	k: -16, 15
	l: -25, 25	l: -35, 34	l: -29, 29
Reflections collected	246760	46588	23300
Independent reflections	6196 [R(int) = 0.0677]	4158 [R(int) = 0.0546]	4040 [R(int) = 0.0341]
Completeness, %	99.7%	99.6%	99.7%
Absorption correction	empirical (SADABS)	none	none
Max and min transmission	0.9071 and 0.9580	0.9604 and 0.9789	0.9426 and 0.9687
Refinement method	full-matrix least-squares on F^2	full-matrix least-squares on F^2	full-matrix least-squares on F^2
Data/restraints/ parameters	6196/4/350	4158/12/203	4040/7/218
Goodness-of-fit on F^2	1.044	1.046	1.018
Final *R* indices [$I > 2\sigma(I)$]	*R1* = 0.0413, *wR2* = 0.0977	*R1* = 0.0642, *wR2* = 0.1775	*R1* = 0.0399, *wR2* = 0.1009
Largest diff peak and hole, eÅ^{-3}	0.30 and -0.44	0.76 and -0.70	0.38 and -0.30

6.8 THERMAL KINETICS AND TM MICROGRAPHS

Solid-state kinetic studies were performed on each solvate to elucidate the possible mechanism of desolvation.

Brown *et al.* (1980) urged that special care should be taken when preparing a sample for kinetic analysis since the formation of desolvation nuclei are very sensitive to superficial imperfections in the crystal, and the reaction often initiates within these damaged regions. In recent kinetic studies, researchers refrained from crushing (Khawam & Flanagan, 2008) and even from sieving crystals (Koradia *et al.*, 2010), since this would lead to formation of crystal defects which may conceal the actual desolvation/dehydration mechanism and rate of the reaction. For this reason intact crystals were used in this study.

The solid-solid phase transition did not influence the results obtained from isothermal TGA results since no weight loss was observed over the heating range (figure 5.4).

Model-free data analysis (table 6.5) was done using the standard isoconversional method over the conversion fraction (α) range of 0.15 – 0.90. As expected from reactions in the solid state (Vyazovkin & Wight, 1997; Vyazovkin, 2000; Khawam & Flanagan, 2006; Koradia *et al.*, 2010) the E_a did not remain constant throughout the α-range.

Model-fitting results (table 6.6) for the desolvation of these samples resulted in good correlation for several of the models derived from nucleation growth and/or geometric contraction mechanisms. This phenomenon is not uncommon; it was also illustrated by the desolvation of sulfameter solvates (Khawam & Flanagan, 2008) and the dehydration of nitrofurantoin monohydrate (Koradia *et al.*, 2010). The activation energy obtained by use of the model-fitting results all lay in the area of standard deviation for the results obtained with the model-free method. Zhou & Grant (2004) investigated the model dependence of the activation energy using simulated data. They found that the obtained activation energy was independent of the model chosen for isothermal kinetic data.

Because of the small difference between the correlation values of the solid-state kinetics done on the desolvation of our solvate crystals closer inspection was necessary. From the micrographs of DDS•0.5(DCM) it can be seen that desolvation starts at the ends of the crystals, initially moving in one direction as expected for a ***R***2 model (figure 6.7). Statistically the nucleation and growth model (***A***2) was chosen to predict the kinetic parameters; although the contribution of both models cannot be neglected. Model-fitting results for the desolvation of the DDS•DXN samples follow the ***A***2 nucleation and growth model under the specific conditions. The micrographs confirm this model-fitting result (figure 6.8). DDS•THF samples followed the geometric contracting area (***R***2) model under the specific conditions. This model assumes that the solid particle has a certain geometric shape (e.g. cylindrical or

rectangular for ***R***2 models) and the reaction would swiftly take place on the outside surface of the crystals. Micrographs of the DDS•THF crystal illustrate that the outer surface of the crystal turns opaque before any bubbles can be seen (figure 6.9). Unfortunately, it is not possible to conclude and verify a definitive kinetic model from microscopic observation. [Please see Annexure A and/or the included CD for the micrographs of the desolvating samples].

Table 6.5: Activation energies (E_a) calculated for the desolvation of each solvate using model-free analysis.

	DDS•0.5(DCM)		**DDS•DXN**		**DDS•THF**	
α	Average E_a (kJ.mol^{-1})		Average E_a (kJ.mol^{-1})		Average E_a (kJ.mol^{-1})	
0.15	164.7	± 23.4	179.8	± 5.8	150.2	± 0.1
0.20	159.0	± 23.4	175.4	± 5.3	152.1	± 0.1
0.25	155.9	± 21.8	172.5	± 5.2	153.2	± 0.1
0.30	154.5	± 22.0	170.5	± 4.8	154.3	± 0.1
0.35	152.8	± 20.8	168.4	± 4.5	155.7	± 0.1
0.40	152.1	± 20.9	167.0	± 4.6	156.9	± 0.1
0.45	151.0	± 19.4	166.2	± 4.6	158.0	± 0.1
0.50	150.5	± 18.6	165.6	± 4.6	159.3	± 0.1
0.55	150.4	± 17.5	165.7	± 4.7	160.2	± 0.1
0.60	150.0	± 16.7	166.0	± 5.1	160.5	± 0.0
0.65	149.1	± 14.8	166.5	± 5.6	162.1	± 0.0
0.70	149.3	± 14.2	168.3	± 6.7	163.8	± 0.0
0.75	148.3	± 12.5	169.8	± 7.9	165.8	± 0.0
0.80	147.1	± 10.9	171.0	± 9.7	166.7	± 0.0
0.85	147.3	± 11.2	172.3	± 11.1	166.6	± 0.0
0.90	146.3	± 9.5	172.9	± 12.8	165.0	± 0.0

Table 6.5: Calculated E_a (in kJ.mol^{-1}) and correlation values compared to each solid-state kinetic model for the desolvation of each solvate.

	DDS•0.5(DCM)			**DDS•DXN**			**DDS•THF**		
	Average E_a		R^2	Average E_a		R^2	Average E_a		R^2
A2	140.9	± 7.2	0.998	170.0	± 14.4	0.999	154.2	± 18.3	0.993
A3	140.6	± 6.6	0.989	170.0	± 14.1	0.977	156.0	± 18.0	0.977
A4	140.2	± 6.8	0.978	170.7	± 14.5	0.901	155.8	± 18.5	0.962
B1	140.7	± 6.7	0.980	170.0	± 14.8	0.971	155.3	± 18.2	0.957
R2	141.0	± 7.4	0.996	172.7	± 14.3	0.997	154.7	± 18.2	0.998
R3	140.7	± 7.6	0.985	173.0	± 12.9	0.994	151.9	± 18.7	0.992
F1	141.4	± 7.8	0.947	169.2	± 12.2	0.969	153.8	± 18.8	0.955
F2	143.3	± 8.1	0.642	168.5	± 10.1	0.692	153.9	± 20.2	0.651
F3	145.1	± 7.9	0.399	168.3	± 9.2	0.449	154.0	± 21.6	0.404
D1	140.8	± 7.3	0.979	168.2	± 14.2	0.983	154.8	± 18.3	0.989
D2	141.3	± 7.8	0.949	174.4	± 5.9	0.966	155.8	± 19.0	0.962
D3	141.1	± 8.0	0.863	177.9	± 0.1	0.896	154.6	± 18.8	0.877
D4	140.5	± 9.0	0.925	159.0	± 24.8	0.948	154.9	± 18.7	0.939

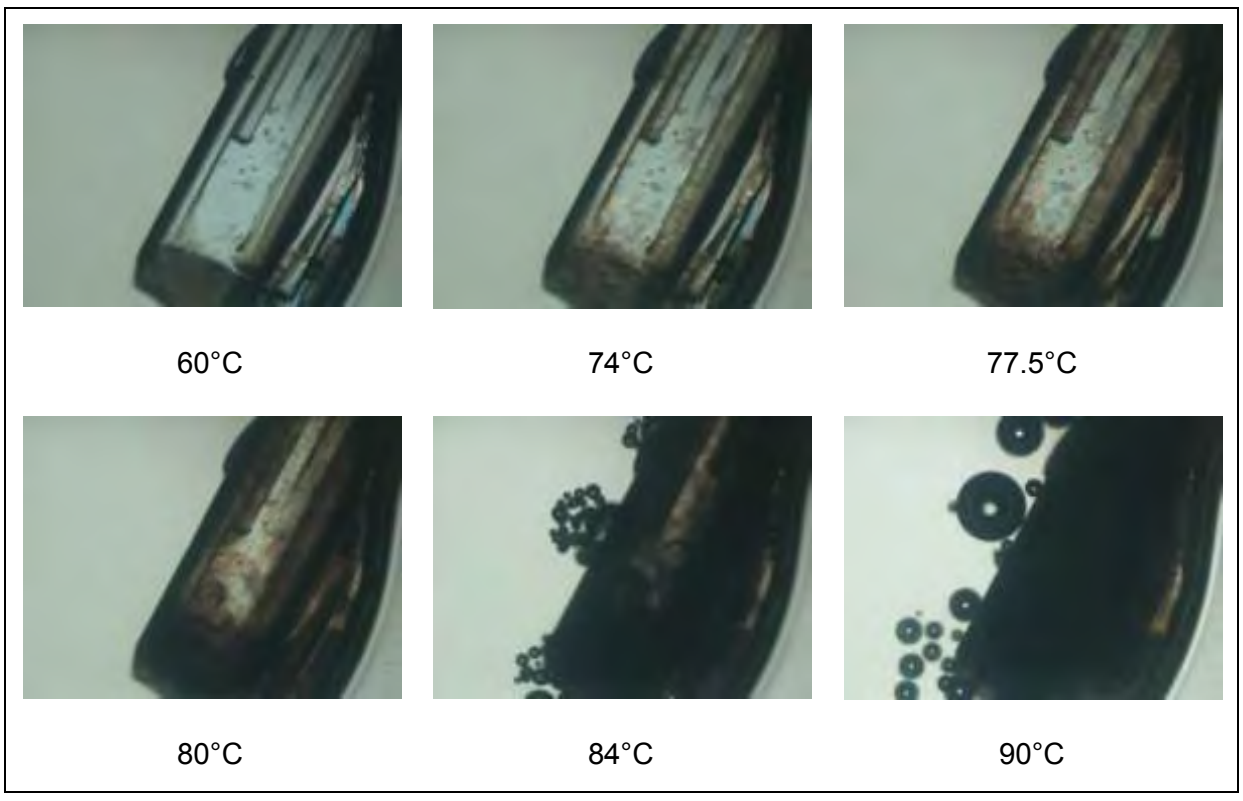

Figure 6.7: Micrographs of a desolvating DDS•0.5(DCM) crystal under non-isothermal heating.

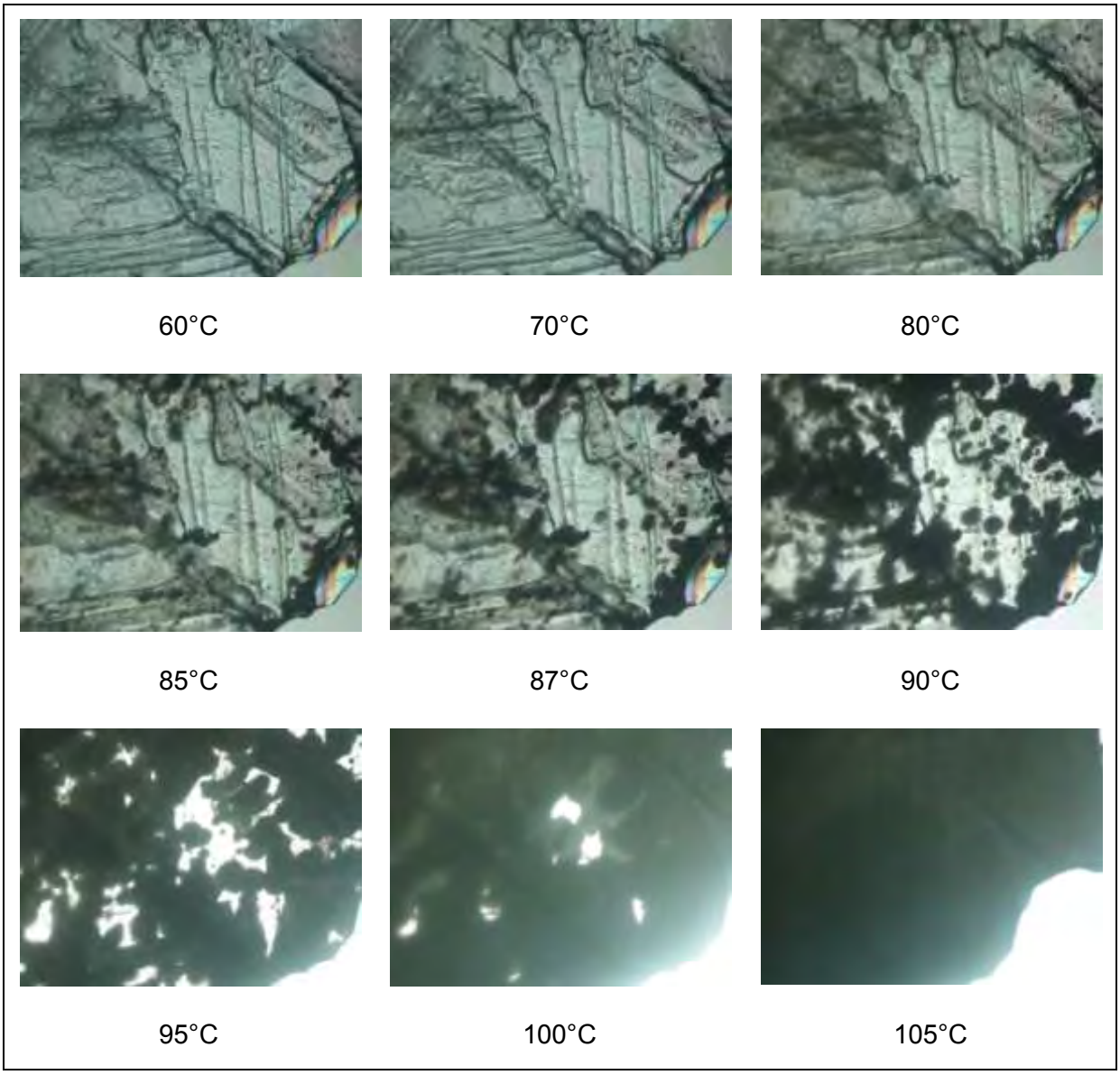

Figure 6.8: Micrographs of a desolvating DDS·DXN crystal, under non-isothermal heating conditions in the absence of mineral oil.

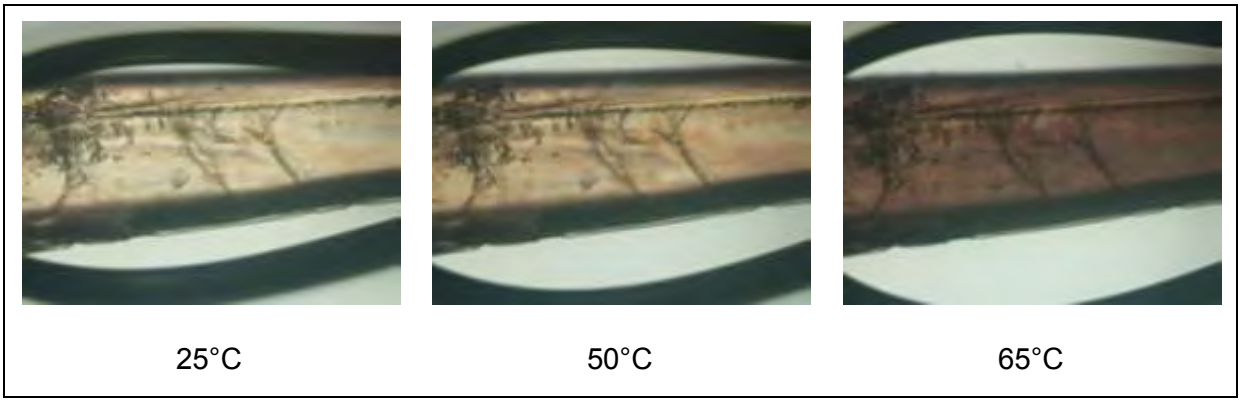

Figure 6.9: Micrographs of a DDS·THF crystal desolvating under non-isothermal heating conditions.

6.9 VARIABLE TEMPERATURE X-RAY DIFFRACTION (VTXRD) AND MODULATED TEMPERATURE DIFFERENTIAL SCANNING CALORIMETRY (MTDSC)

Extensive research concerning DDS and its solvates was done using VTXRD to investigate changes in the internal structure of the products when exposed to increased temperatures. VTXRD data supplied us with important information regarding the solid-solid phase transition found at ~ 82°C and also clarified the process of desolvation for each solvate. More results can be found in the attached articles as Annexure B.

Conventional DSC is simplistic in its operation and sample preparation, but does not always show the complete picture of the thermal events taking place. MTDSC has the advantage of separating the total heat flow into reversing and non-reversing heat signals. Melting endotherms can generally be seen in the reversing and non-reversing heat signals. The solid-solid phase transition at ~82°C was also observed in both the reversing and non-reversing heat signals. This transition was seen for DDS, DDS•0.5(DCM) and DDS•THF although it was obscured by the desolvation for DDS•DXN. All three the solvates initially showed a decrease in the reversing heat signal (the heat capacity), but after complete desolvation it increased to the level where it stayed for the rest of the MTDSC trace. This indicates that the crystals initially experienced a decrease in mobility within its system which changed after desolvation.

Two distinct endothermic peaks and one exothermic peak can be seen in the non-reversing signal for all samples in the temperature range of 175 – 185°C.

In the case of DDS•0.5(DCM) one large and two small endotherms were seen in the reversing heat signal; the two small peaks in the non-reversing signal are at 172°C and 177°C. The endotherm at 177°C was not seen in the reversing heat signal. This peak might have been caused by the melting of a small amount of DDS form II. The endotherms at ~172°C and ~180°C are repeated in both the reversing and non-reversing heat signals. The endotherm found at 172°C is that of the solid-solid phase transition for DDS form II to DDS form III; this event can also be seen from the VTXRD data in figure 6.8. Form I was described by Kuhnert-Brandstätter and Moser to melt at 179°C and that it recrystallised from the melt of form II (which melts at 177°C). According to them there exists an enantiotropic relationship between form I and form II and also between form I and form III. An enantiotropic relationship is only possible if the transition point takes place prior to melting (Giron, 1995) as was the case for the melting of the desolvated DDS•0.5(DCM). The endothermic peak at ~180°C seen in the reversing and non-reversing heat signals was caused by the melting of DDS form I.

An exothermic peak can be seen for all of the samples after the melting endotherm. This was caused by decomposition of the melting sample, but was not observed in conventional DSC traces. The DSC and MTDSC were both purged with nitrogen gas and pierced pans were used in the DSC while non-pierced, crimped pans were used in the MTDSC. Decomposition was observed on the MTDSC traces due to its greater sensitivity and its ability to separate different simultaneous thermal events from one another. Samples were purged with compressed air in the VTXRD which would have a higher oxygen concentration and possibly lead to more oxidative decomposition.

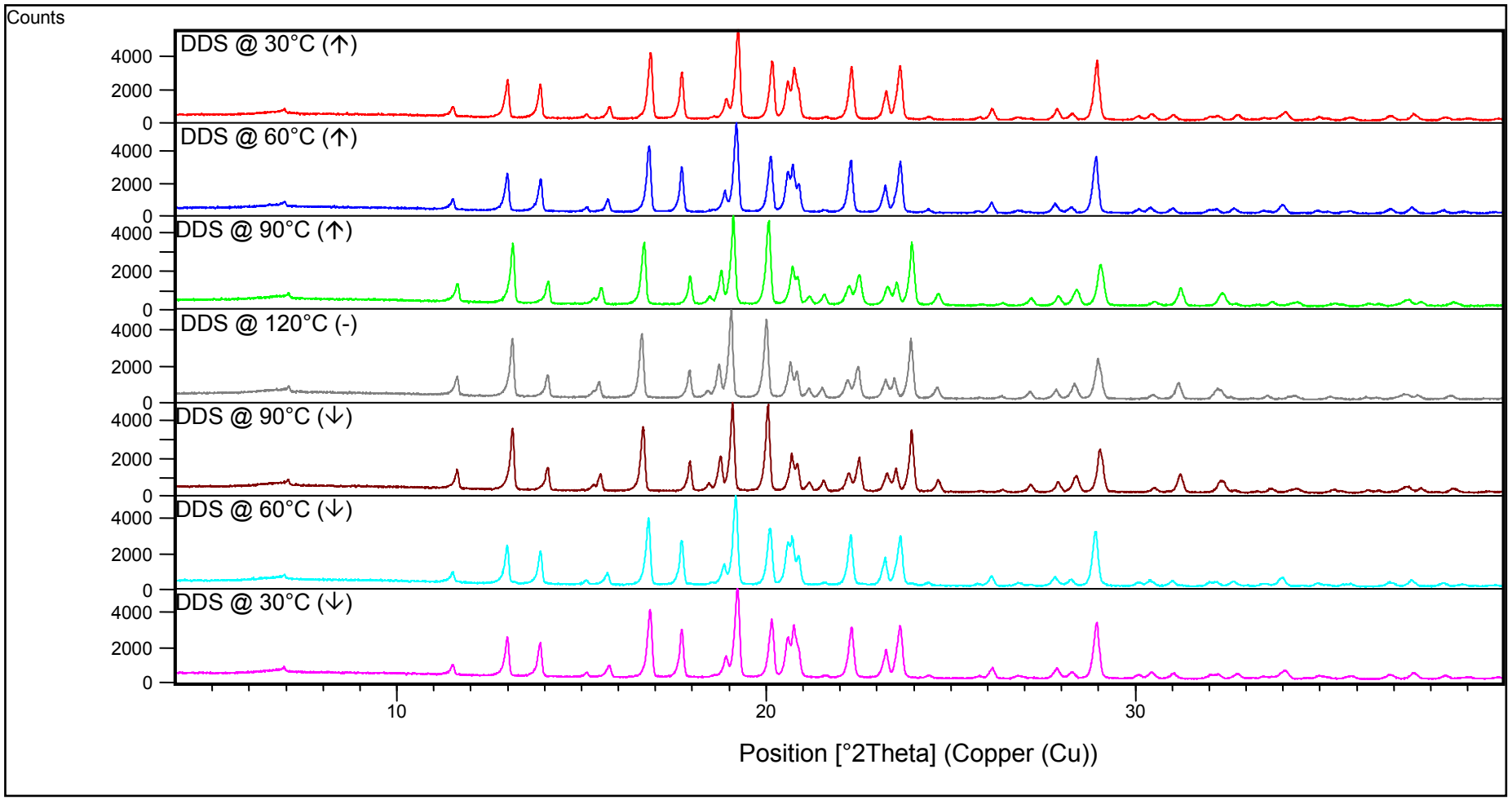

Figure 6.10: VTXRD patterns composed from the heating (↑) of DDS to 120°C and the cooling (↓) thereof back to room temperature.

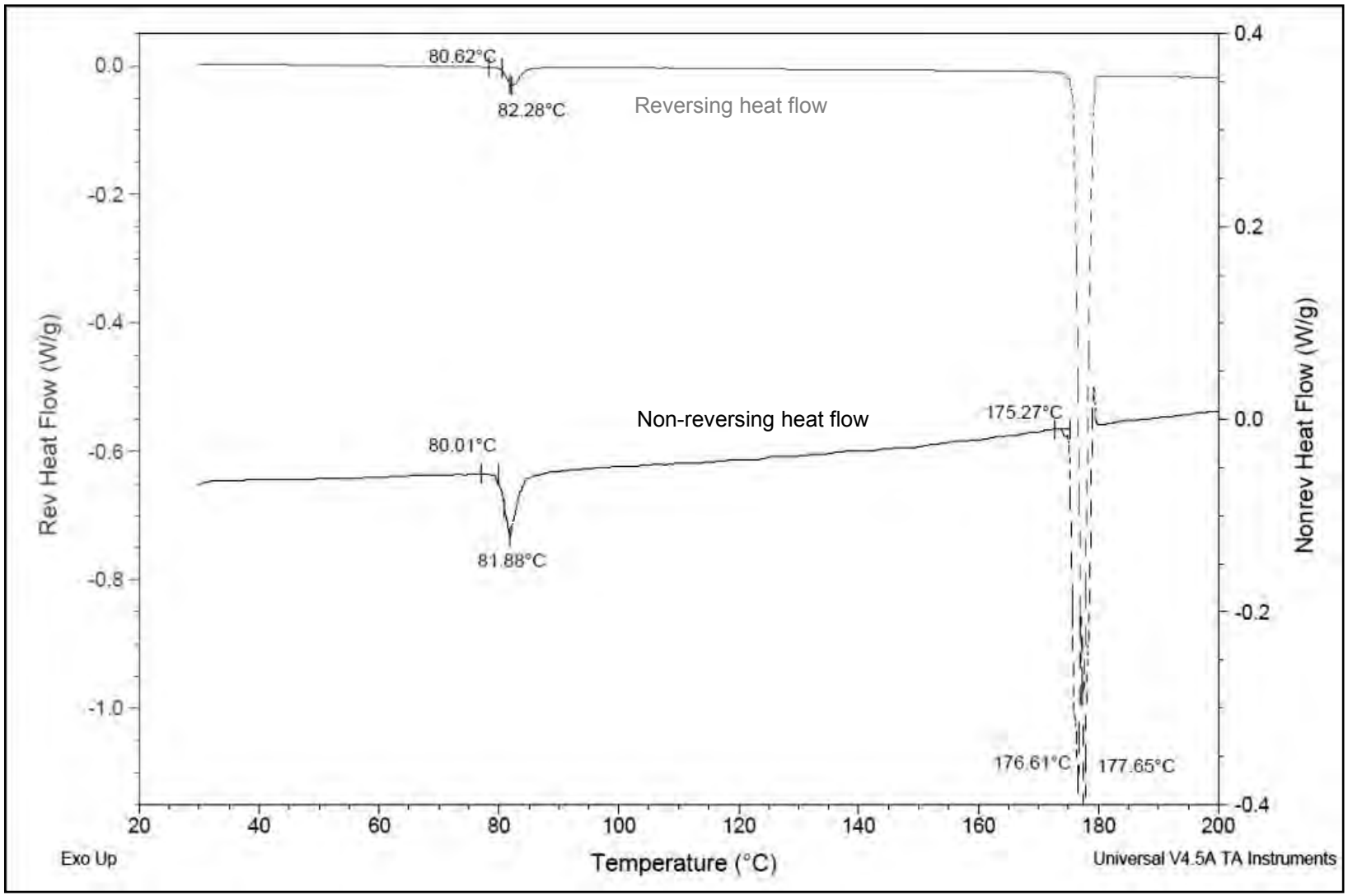

Figure 6.11: MTDSC for DDS heated to 200°C. Heat flow curves include the reversing (gray) and non-reversing heat signals (black).

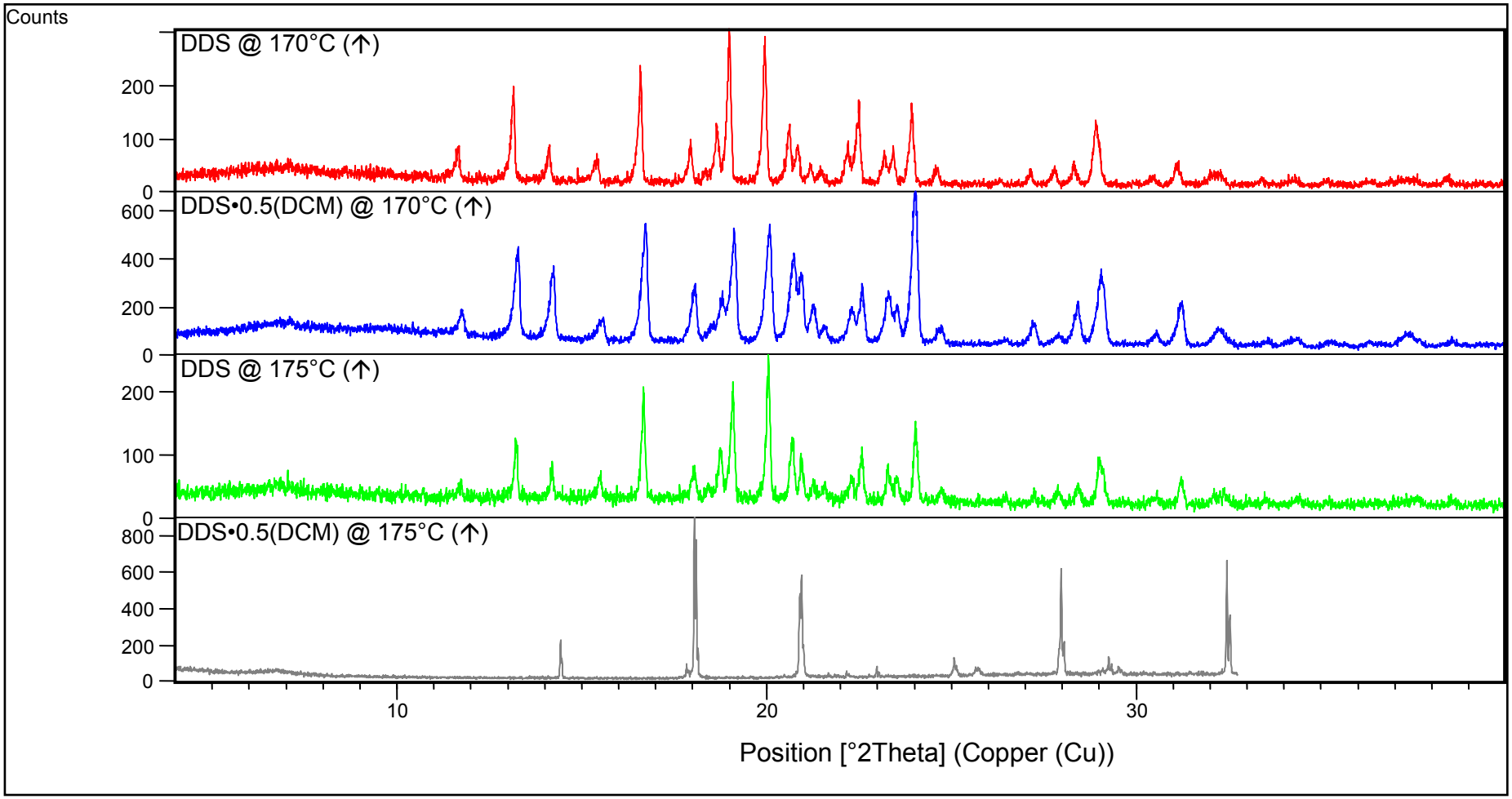

Figure 6.12: VTXRD patterns for the events taking place upon heating (↑) of DDS and DDS•0.5(DCM) samples before melting (temperature range 170 – 175 ± 5°C).

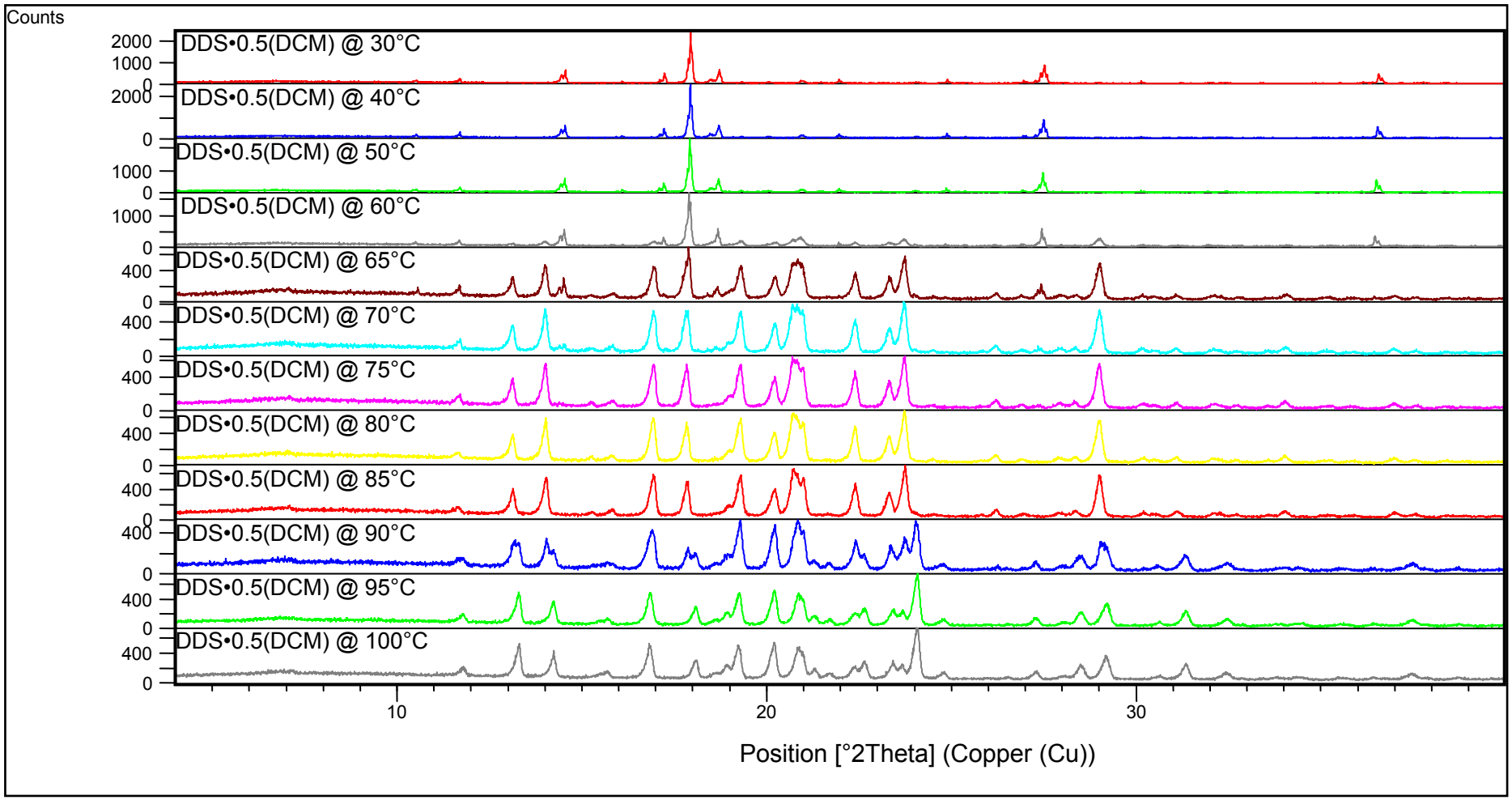

Figure 6.13: VTXRD data for the events taking place in DDS•0.5(DCM) during heating (temperature range 25 – 100°C).

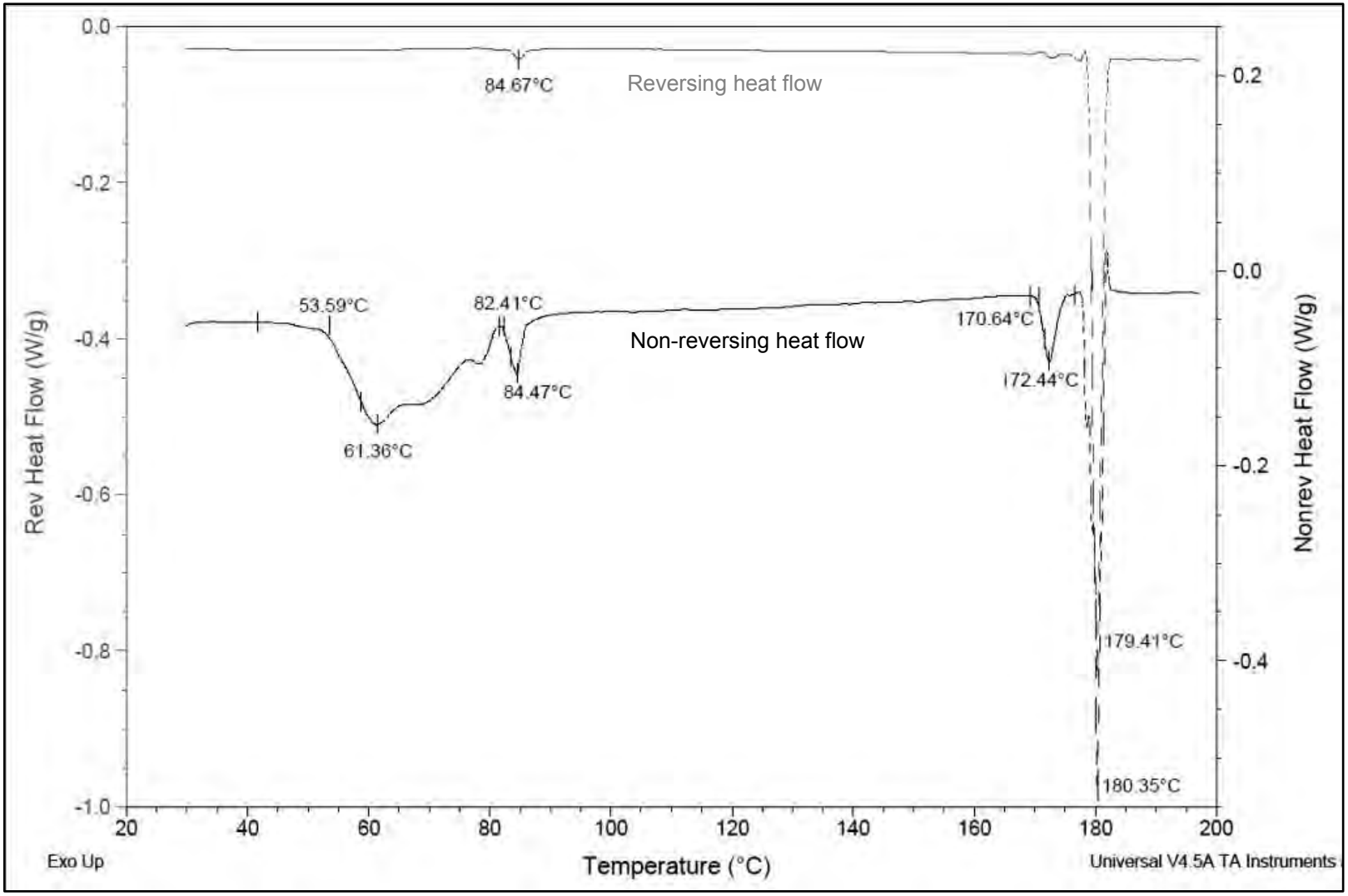

Figure 6.14: MTDSC for DDS•0.5(DCM) heated to 200°C. Heat flow curves include the reversing (gray) and non-reversing heat signals (black).

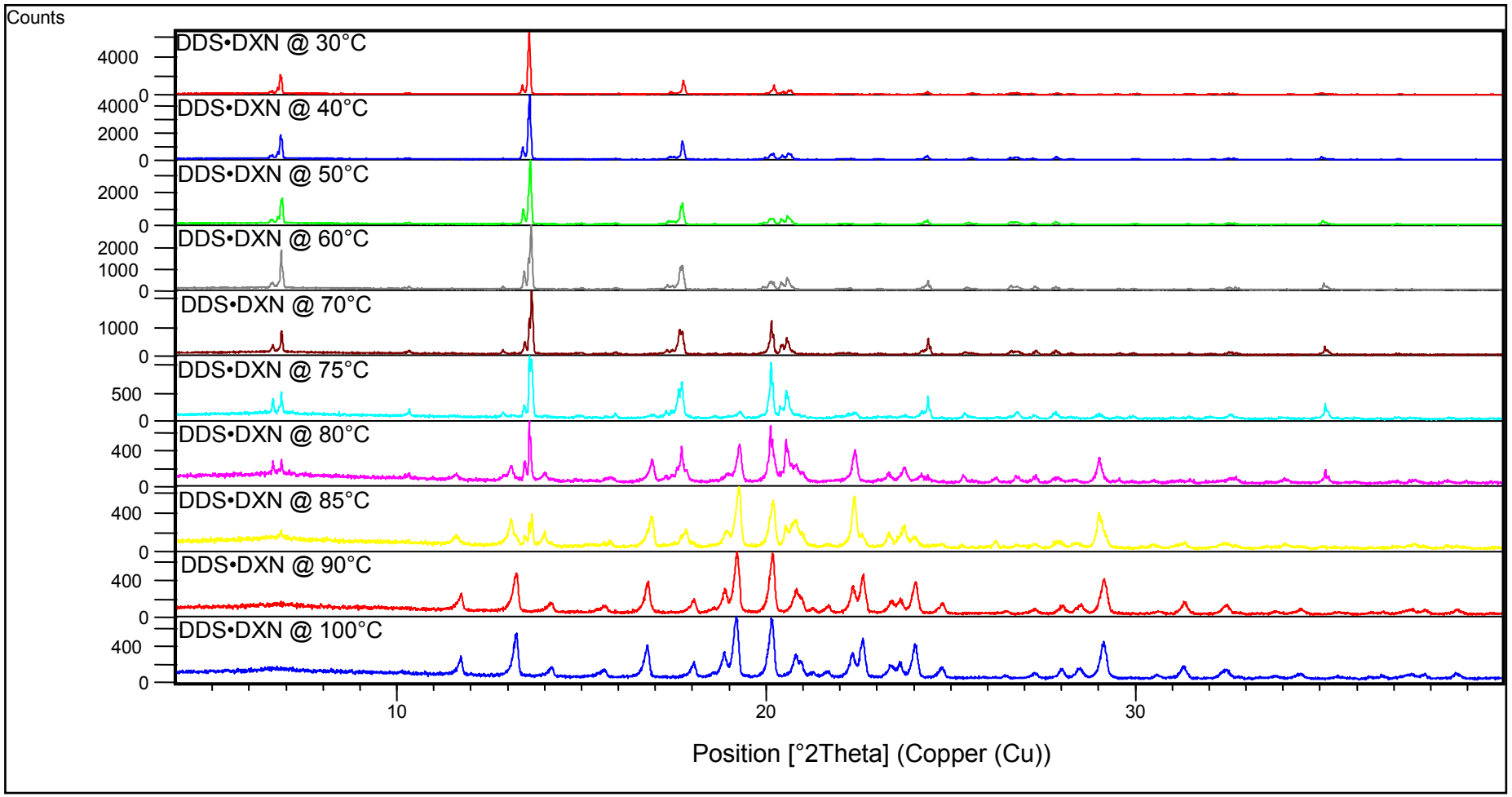

Figure 6.15: VTXRD spectral data for the desolvation of DDS•DXN.

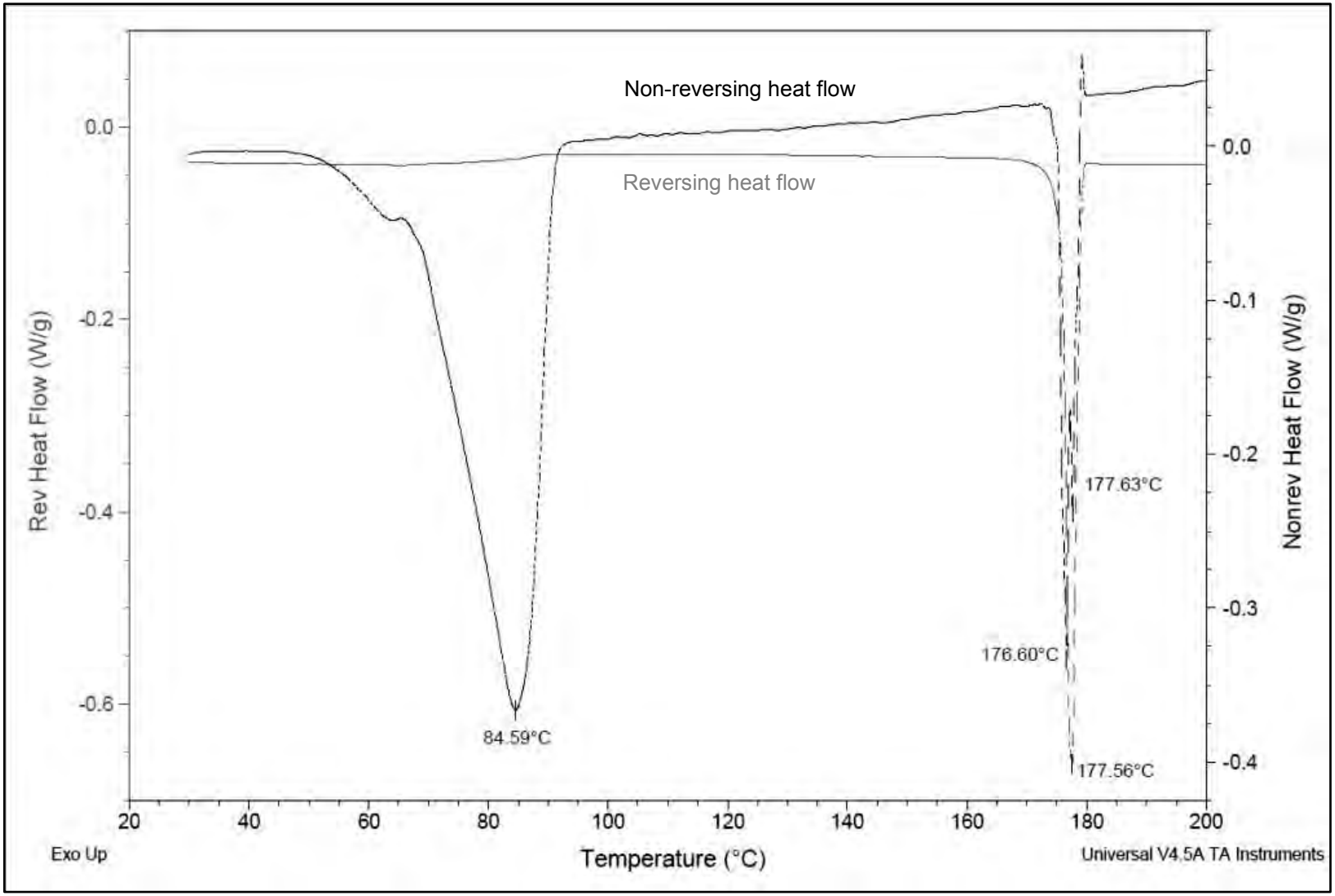

Figure 6.16: MTDSC for DDS•DXN heated to 200°C. Heat flow curves include the reversing (gray) and non-reversing heat signals (black).

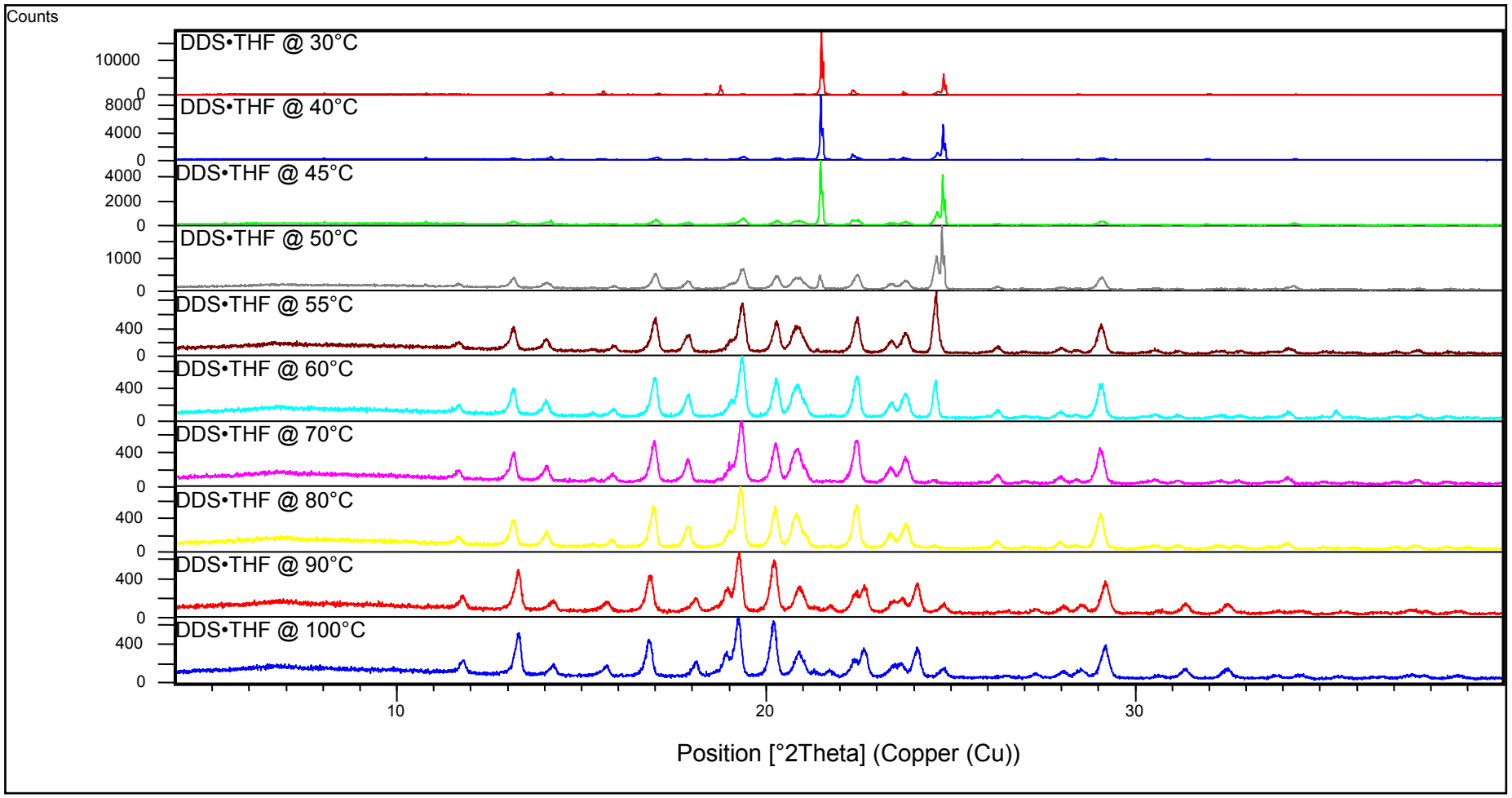

Figure 6.17: VTXRD stack for the desolvation and phase transition of DDS•THF.

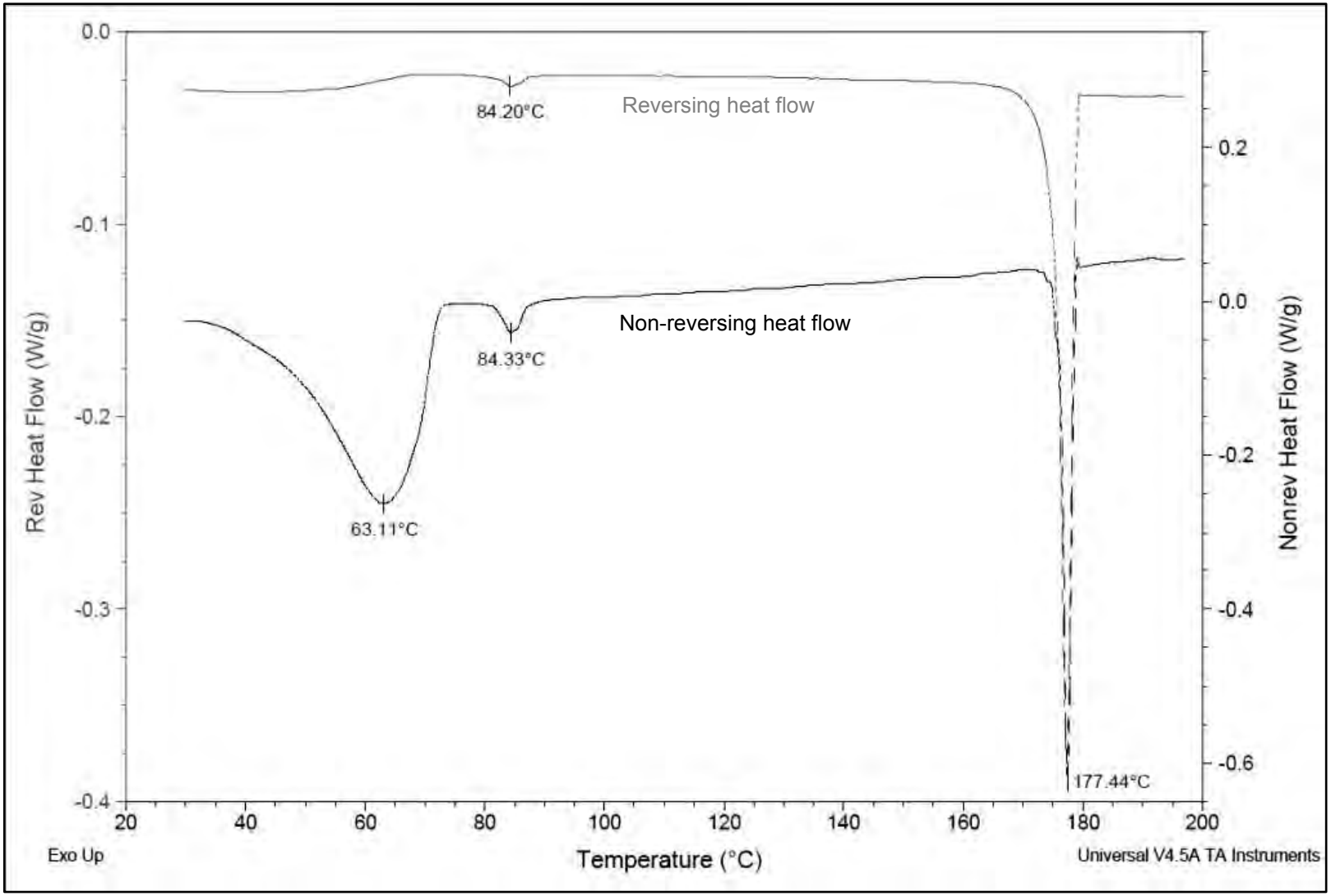

Figure 6.18: MTDSC for DDS•THF heated to 200°C. Heat flow curves include the reversing (gray) and non-reversing heat signals (black).

6.10 CONCLUDING REMARKS

Desolvation of DDS•THF preceded the phase transition point. Desolvation of DDS•0.5(DCM) also took place before phase transition point; but another form may be seen up to 90°C on the VTXRD patterns. MTDSC traces of DDS•DXN did not show the phase transition as was seen from the other products in both the reversing- and non-reversing heat signals. Elucidation of desolvation and the phase-transition was also not possible using VTXRD. This results conclude that it is not possible to have the one event without the other in the case of the DDS•DXN solvate during non-isothermal heating.

The three solvates crystallised into different crystal systems; DDS•DXN is orthorhombic which is the same as DDS. The crystal system for DDS•0.5(DCM) and DDS•THF is monoclinic; this coincides with the already published hemi-hydrate. The desolvated products correspond perfectly to the orthorhombic DDS form found at room temperature.

It was mostly possible to reconcile the calculated desolvation kinetics with the crystal's morphology and crystal structure. Isothermal solid-state kinetics was done on each solvate at three different temperatures. The order for thermal stability between the solvates are as follows; DDS•0.5(DCM) >> DDS•THF > DDS•DXN.

Despite the variety of solvates with their different modes of solvent inclusion and mechanism of desolvation; desolvation leads to the complete conversion back to DDS and not a polymorph or amorphous phase thereof.

6.11 REFERENCES

BROWN, M.E., DOLLIMORE, D & GALWEY, A.K. 1980. 22 vols. Reactions in the solid state. (*In*: BAMFORD, C.H. & TIPPER, C.F.H, *eds*. *Comprehensive chemical kinetics*, Amsterdam: Elsevier. 340 p).

GIRON, D. 1995. Thermal analysis and calorimetric methods in the characterisation of polymorphs and solvates. *Thermochimica Acta*, 248:1-59.

KHAWAM, A & FLANAGAN, D.R. 2006. Basics and applications of solid-state kinetics: a pharmaceutical perspective. *Journal of Pharmaceutical Sciences*, 95(3):472-498.

KHAWAM, A. & FLANAGAN, D.R. 2008. Desolvation kinetics of sulfameter solvates. *Journal of Pharmaceutical Sciences*, 97(6):2160-2175.

KORADIA, V, LOPEZ DE DIEGO, H, ELEMA, M.R. & RANTANEN, J. 2010. Integrated approach to study the dehydration kinetics of nitrofurantoin monhydrate. *Journal of Pharmaceutical Sciences*, 99(9):3966-3976.

KUHNERT-BRANDSTÄTTER, M. & MOSER, I. 1979. Zur Polymorphie von dapson und ethambutoldihydrochlorid. *Microchimica Acta*, 71(1):125-136.

VYAZOVKIN, S. 2000. Kinetic concepts of thermally stimulated reaction in solids: a view from a historical perspective. *International Reviews in Physical Chemistry*, 19(1):45-60.

VYAZOVKIN, S. & WIGHT, C.A. 1997. Kinetics in solids. *Annual Review of Physical Chemistry*, 48(1):125-149.

ZHOU, D. & GRANT, D.J.W. 2004. Model dependence of the activation energy derived from nonisothermal kinetic data. *Journal of Physical Chemistry A*, 108(19):4239-4246.

Chapter 7

Conclusion

The chemotherapeutic activity of dapsone (DDS) was first published in 1937 but still not much is known about the interrelationships of its polymorphic forms or the possibility of solvate formations. This type of knowledge is fundamentally important with regards to the manufacturing and storage of the drug. A complete polymorphic study was done on DDS using a variety of common and modern techniques.

Recrystallisation of DDS from various neat solvents was done; the products that formed from recrystallisation included some habit modifications, a hydrate and three solvates.

DDS III (anhydrous dapsone at 25°C) is able to convert to DDS form II *via* a reversible solid-solid phase transition at 82°C. This event was observed as a wave moving from one side of a crystal to the other for all recrystallised products when exposed to polarised light using a thermal microscope (TM).

The melting point for the greater majority of the recrystallised products were at ~177°C (as expected for DDS form II) while some of the products melted at a higher melting point (~180°C). The higher melting point was first mentioned in 1953 and was subsequently named DDS form I by Kuhnert-Brandstätter and Moser in 1979. Ostwald's rule may explain why the prevalence of the lower melting polymorph is higher than that of the higher melting point polymorph. From our experiments using various visual and thermal analysis techniques we were able to conclude that DDS form I converts *via* a solid-solid phase transition before the melting of DDS form II. It would be interesting to identifying the internal crystal structure of DDS form II and I and evaluating their respective structures to that of DDS form III as a future perspective.

DDS•(0.33)H_2O has been discovered before by several research groups. A hydrate would be even less water soluble than the anhydrated DDS and was therefore not pursued further.

DDS solvates have not been reported before in the literature. Solvates recrystallised from dichloromethane (DCM), 1,4-dioxane (DXN) and tetrahydrofuran (THF) in stoichiometric relationships of DDS•0.5(DCM), DDS•DXN and DDS•THF. The crystal structures of the solvates were elucidated using single-crystal X-ray diffraction and the results were deposited into the Cambridge Structural Database (CSD). The crystal system of DDS•DXN is orthorhombic like that of DDS form III while the crystal systems of DDS•0.5(DCM) and DDS•THF are monoclinic which is the same as that of DDS•0.33(H_2O). The fact that we have found only three solvates and a hydrate so far for this pharmaceutically important drug does not mean that other polymorphic forms/solvates does not exist, it just indicates that we have not created the necessary conditions to re-crystallise and/or preserve them.

The desolvation of these solvates was extensively studied. The activation energy (E_a) and kinetic model that each solvate followed during desolvation was calculated using isothermal thermogravimetric analysis (TGA) and verified by micrographs obtained by using a hot stage microscope. The nucleation and growth model (***A***2) was statistically chosen to explain the desolvation process for DDS•0.5(DCM) although the contribution of the geometric contracting area (***R***2) model cannot be neglected. Model-fitting results for the desolvation of DDS•DXN and DDS•THF concluded that they respectively followed the ***A***2 and ***R***2 model; the micrographs confirmed these model-fitting results. The order for thermal stability between the solvates are as follows: DDS•0.5(DCM) >> DDS•THF > DDS•DXN. The calculated E_a values followed the opposite trend being 141 ± 7 kJ.mol^{-1} for DDS•0.5(DCM), 155 ± 19 kJ.mol^{-1} for DDS•THF and 170 ± 14 kJ.mol^{-1} for DDS•DXN. Unfortunately accurate assumptions about E_a may not be reliable since these three solvates are not isostructural. After desolvation of the solvates it completely converted back to the crystal structure of DDS form III at room temperature.

The water solubility of these solvates and their desolvated products were calculated. The recrystallisation solvents are toxic; therefore the desolvated products were also tested to see whether a safe and improved pharmaceutical product might be obtained. There was, however, no significant differences between the dioxane and THF solvates and their respective desolvates; DDS•0.5(DCM) was even less soluble than DDS. Further studies on the solubility should be exploited to investigate possible phase transformations and to obtain repeatable results with lower SD values and also, to ensure 24 hours was enough time to reach solubility equilibrium.

The polymorphism and physicochemical data obtained from this study can enable future researchers or manufacturers to develop improved pharmceutical dossage forms to address the pharmaceutical and/or pharmacological issues of dapsone.

Annexure A

Published Article

Published in *Crystal Growth & Design*, 2012 12(3): 1683-1692.

Title: Solvatomorphism of the Antibacterial Dapsone: X-ray Structures and Thermal Desolvation Kinetics

The journal primarily covers the following:

- Crystal engineering (e.g., organic, inorganic, and hybrid solids)
- Crystal growth of inorganic, organic, and biological substances (e.g., biomineralization)
- Polymorphism, polytypism
- Development of new nanostructured phases
- Intermolecular interactions in the solid state (e.g., hydrogen bonding, lattice energies)
- Modeling of crystal growth processes
- Prediction of crystal structure and crystal habit
- Determination and calculation of electronic distribution in the solid state
- Nucleation theory
- Molecular kinetics and transport phenomena in crystal growth
- Phase transitions
- Solvation and crystallization phenomena, modeling of crystallization processes
- Purification techniques, industrial crystallization.

Paper included as it was published in *Crystal Growth & Design*.

CRYSTAL GROWTH & DESIGN

Article

pubs.acs.org/crystal

Solvatomorphism of the Antibacterial Dapsone: X-ray Structures and Thermal Desolvation Kinetics

Helanie Lemmer,[†] Nicole Stieger,[†] Wilna Liebenberg,[†] and Mino R. Caira*[,‡]

[†]Unit for Drug Research and Development, Faculty of Health Sciences, North-West University, Potchefstroom, 2531, South Africa
[‡]Department of Chemistry, University of Cape Town, Rondebosch 7701, South Africa

Supporting Information

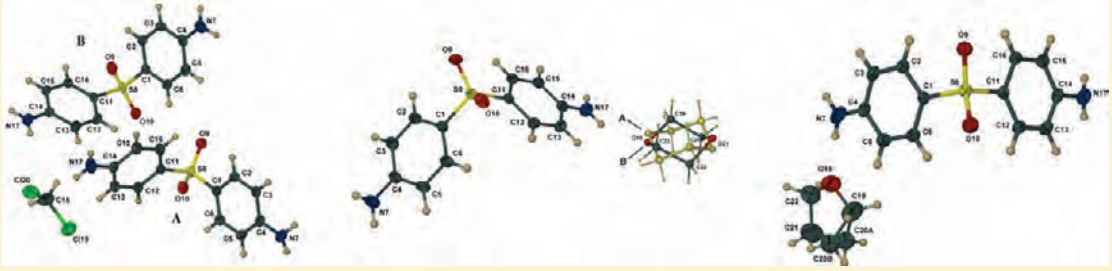

ABSTRACT: Three non-isostructural solvates of the antibacterial dapsone (DDS) containing dichloromethane [**DDS·0.5(DCM)**], 1,4-dioxane [**DDS·DXN**], and tetrahydrofuran [**DDS·THF**] were prepared and characterized by X-ray diffraction (XRD) and thermal analysis, the latter including hot stage microscopy (HSM), thermogravimetric analysis (TGA) and differential scanning calorimetry (DSC). In addition, their thermal desolvation was investigated by isothermal kinetic studies which indicated the A2 model as the best fit for desolvation of the DCM and DXN solvates, while the R2 model was indicated for the THF solvate. Activation energies for desolvation of these new species were in the range 141−173 kJ mol^{-1}. Attempts were made to reconcile the kinetic models with the observed HSM desolvation behavior and the modes of solvent inclusion within the solvate crystals determined by XRD (viz. isolated sites for the DCM solvate and channel-type for the others).

INTRODUCTION

Dapsone [4,4′-sulfonylbisbenzeneamine; 4,4′-sulfonyldianiline; 4,4′-diaminodiphenyl sulfone; hereinafter DDS] (Figure 1) is a drug with a fascinating history of having "reinvented" itself several times to treat a diversity of diseases including tuberculosis, leprosy, malaria, and AIDS-related pneumonia.[1] Interestingly, following its synthesis in 1908, with no particular consideration being given to possible medicinal applications, it lay dormant until the 1930s, when its potent antibacterial properties were first recognized and its potential as an antitubercular drug, in particular, was beginning to be explored. During subsequent decades, new indications for the drug, including those listed above, were successively identified and DDS gained widespread use. Currently, the drug remains a powerful therapeutic tool in the treatment of leprosy, dermatitis herpetiformis, and malaria, and in the prophylaxis of pneumocystosis, a serious infection common among AIDS patients.[2] Figure 1 shows the chemical structure of dapsone.

Our interest in the solid-state chemistry of DDS stems from its use in the treatment of opportunistic infections associated with AIDS, and the present account focuses on the possibility of obtaining different solid forms of the drug. If such species (polymorphs, solvates) should inadvertently arise during recrystallization from contaminated solvents and be incorporated into solid dosage forms, they could compromise both the safety and the performance of the drug. We recently reported

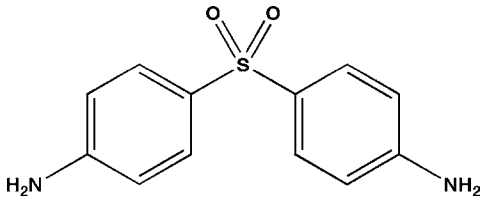

Figure 1. Chemical structure of dapsone (DDS).

such an eventuality in connection with the antitubercular rifampicin, which is able to form stable solvates by entrapping toxic ethylene glycol and diethylene glycol during crystallization.[3] Although solvatomorphism of DDS derivatives has been reported,[4] only a hydrate of the parent drug with formula **DDS·0.33H$_2$O** is known (CSD ref code ANSFON02).[5] The crystal structure of this species and that of unsolvated DDS (CSD ref code DAPSUO10)[5] have been reported, but no solvate structures containing organic solvents have been documented to date. As in the case of the antiretroviral neviparine, for which we recently reported extensive solvatomorphism,[6,7] the presence of strong hydrogen bonding functions in the molecule of DDS suggests that it should interact with polar

Received: January 6, 2012
Revised: February 6, 2012
Published: February 9, 2012

Table 1. Crystallographic Data and Experimental Details for DDS Solvates

	DDS·0.5(DCM)	DDS·DXN	DDS·THF
ratio	2:1 DDS/dichloromethane	1:1 DDS/1,4-dioxane	1:1 DDS/tetrahydrofuran
empirical formula	$2(C_{12}H_{12}N_2O_2S)\cdot CH_2Cl_2$	$C_{12}H_{12}N_2O_2S\cdot C_4H_8O_2$	$C_{12}H_{12}N_2O_2S\cdot C_4H_8O$
formula weight	581.52	336.40	320.40
temperature, K	173(2)	173(2)	173(2)
crystal system	monoclinic	orthorhombic	monoclinic
space group	$P2_1/n$	*Pbca*	$P2_1/n$
a, Å	8.3000(2)	11.1008(5)	5.8587(3)
b, Å	16.5991(4)	11.3387(5)	12.6787(7)
c, Å	19.9138(4)	26.628(1)	21.8078(12)
α, deg	90.0	90.0	90.0
β, deg	98.660(1)	90.0	91.335(1)
γ, deg	90.0	90.0	90.0
volume, (Å^3)	2712.3(1)	3351.6(3)	1619.5(2)
Z	4	8	4
d_{calcd} (Mg/m^3)	1.424	1.333	1.314
abs coeff, mm^{-1}	0.432	0.214	0.214
crystal size, mm^3	0.10 × 0.18 × 0.23	0.10 × 0.15 × 0.19	0.15 × 0.22 × 0.28
theta range for data collection	3.49−27.48	1.53−28.32	1.86−28.38
index ranges	*h*: −10, 10	*h*: −14, 14	*h*: −7, 7
	k: −21, 21	*k*: −15, 15	*k*: −16, 15
	l: −25, 25	*l*: −35, 34	*l*: −29, 29
reflections collected	246760	46588	23300
independent reflections	6196 [R(int) = 0.0677]	4158 [R(int) = 0.0546]	4040 [R(int) = 0.0341]
completeness, %	99.7	99.6	99.7
absorption correction	empirical (SADABS)	none	none
max and min transmission	0.9071 and 0.9580	0.9604 and 0.9789	0.9426 and 0.9687
refinement method	full-matrix least-squares on F^2	full-matrix least-squares on F^2	full-matrix least-squares on F^2
data/restraints/parameters	6196/4/350	4158/12/203	4040/7/218
goodness-of-fit on F^2	1.044	1.046	1.018
final *R* indices [$I > 2\sigma(I)$]	R_1 = 0.0413, wR_2 = 0.0977	R_1 = 0.0642, wR_2 = 0.1775	R_1 = 0.0399, wR_2 = 0.1009
largest diff peak and hole, e·Å^{-3}	0.30 and −0.44	0.76 and −0.70	0.38 and −0.30

solvent molecules and thus possibly incorporate them during recrystallization. To anticipate the appearance of such solvated forms of DDS, we therefore attempted to generate a series of them by recrystallization of the drug from various solvents. Herein, we report the preparation of three crystalline solvates of DDS isolated by recrystallization from dichloromethane (DCM), 1,4-dioxane (DXN), and tetrahydrofuran (THF), with the respective abbreviated formulas **DDS·0.5(DCM)**, **DDS·DXN**, and **DDS·THF**, their X-ray structures, as well as thermodynamic and kinetic data for their thermal desolvation.

EXPERIMENTAL SECTION

Crystal Preparation. Samples were prepared by adding a requisite amount of the anhydrous dapsone (Ria International LLC, East Hanover, USA, batch 20100128) to the pure solvents and heating the mixtures to their respective boiling points. The hot, saturated solutions were loosely covered with parafilm and allowed to crystallize by spontaneous cooling to room temperature (~293 K) in a dark cupboard. **DDS·DXN** formed yellow platy crystals upon cooling, while slow evaporation led to the formation of colorless, acicular, and prismatic crystals of **DDS·0.5(DCM)** and **DDS·THF**, respectively.

Thermal Analysis. Single crystals were heated under silicone oil on a Leitz Wetzlar hot stage, and micrographs were recorded using a Nikon Eclipse E400 equipped with a Nikon DS-Fil camera. NIS-Elements F 2.30 image-capturing software was employed. For differential scanning calorimetry (DSC) measurements, temperature and enthalpy values were recorded using a Shimadzu DSC-60A instrument (Japan) with TA60 version 2.11 software. Samples in the range 4−8 mg were weighed, placed in an aluminum crucible with a pierced lid, and heated at 10 K/min in an inert nitrogen atmosphere. The instrument was calibrated with high purity indium and tin standards.

Thermogravimetric analysis (TGA) was performed using a Shimadzu DTG-60 (Japan) instrument and TA60 version 2.11 software. For non-isothermal kinetic studies using TGA, mass losses were recorded using 3−10 mg samples heated from 298 to 473 K at 10 K/min in open aluminum crucibles purged with nitrogen (35 mL/min). For isothermal kinetic studies, crystals of mass ~3 mg were broken into identical pieces (dimensions 3 × 1 × 1 mm^3 for **DDS·0.5(DCM)** and **DDS·THF**, and 1 × 1 × 1 mm^3 flakes in the case of **DDS·DXN**) under solvent two days before analysis. To prevent spontaneous desolvation, they were not crushed or sieved. Isothermal analysis was performed in duplicate at temperatures in the range 323−333 K for **DDS·0.5(DCM)**, 333−343 K for **DDS·DXN**, and 313−323 K for **DDS·THF**.

The mass loss data were transformed into fractional extent of reaction (α). Both the standard isoconversional and model-fitting methods were used.[8,9] The isoconversional ("model-free") method generates activation energies (E_a) for each progressive α value without modelistic assumptions. The conventional modelistic method generates the kinetic triplet (frequency factor *A*, rate constant *k*, and activation energy E_a) by two subsequent model fittings. The first model fitting identifies the appropriate kinetic model by comparison of experimental and theoretical curves and yields the value of *k*. Isothermal data have been analyzed on the assumption that a single set of Arrhenius parameters *A* and E_a are applicable over the full range of α at each temperature.

Single-Crystal X-ray Diffraction. Intensity data for **DDS·0.5(DCM)** were collected on a Nonius Kappa CCD four-circle diffractometer using graphite-monochromated MoKα radiation (λ = 0.71073 Å). The data-collection strategy was evaluated using

Table 2. Thermogravimetric and Calorimetric Data for DDS Solvates

solvate	experimental TG mass loss (%)	DDS/solvent ratio	calculated TG mass loss (%)	desolvation onset temperature (K)	ΔH for desolvation (J/g)
DDS·0.5(DCM)	14.9	2:1	14.6	353(2)	64(1)
DDS·DXN	27.7	1:1	26.2	374(4)	148(2)
DDS·THF	23.6	1:1	22.5	348	148(1)

COLLECT[10] software, and intensity data were scaled and reduced using DENZO-SMN software.[11] Absorption corrections based on the multiscan method using program SADABS were applied.[12] For **DDS·DXN** and **DDS·THF**, intensities were measured on a Bruker Kappa DUO APEX II diffractometer and processed using APEX2 and SAINT software.[13] All crystals were mounted on cryogenic loops using Paratone N oil (Exxon, USA) and cooled to 173(2) K in a constant stream of nitrogen vapor produced at a flow rate of 20 mL/min by a Cryostream cooler (Oxford Cryosystems, UK). Structures were solved using SHELXS-97[14] and refined by full-matrix least-squares on F^2 using SHELXL-97[15] via the program interface X-Seed.[16] Non-hydrogen atoms of the DDS molecules were refined anisotropically. Disorder of all atoms of the 1,4-dioxane molecule in solvate **2** precluded anisotropic refinement, and all 12 non-H atoms were treated isotropically. In solvate **3**, one C atom of the included tetrahydrofuran molecule was disordered over two positions and both components were treated isotropically. Suitable distance restraints (C−C, C−O) were applied to the disordered solvent molecules to maintain reasonable geometries. All H atoms were initially located in difference electron density maps, and those with standard geometries were subsequently placed in idealized positions and refined isotropically in a riding model with U_{iso} values 1.2−1.5 times those of their parent atoms. Distance restraints for N−H bonds (0.88 Å, σ = 0.005 Å) were imposed on amino groups of DDS molecules that displayed pyramidal geometry. Table 1 lists data-collection and refinement details.

Powder X-ray Diffraction (PXRD). PXRD traces were recorded at 298 K on a PANalytical X'Pert-PRO diffractometer with CuKα-radiation and a minimum step size of 0.001° 2θ. Generator settings were 45 mA, 40 kV.

RESULTS AND DISCUSSION

Preliminary Characterization. Thermogravimetric analysis was initially employed to establish the DDS/solvent ratios and to gauge the thermal stabilities of the solvates. Figure 2 shows the TG and DSC traces from which desolvation onset temperatures and enthalpies were derived. The data are summarized in Table 2.

In all cases, there is an apparent one-step solvent mass loss, the percentages listed in Table 2 indicating the reported solvate stoichiometries. DSC traces are shown in Figure 2. Each solvate displays an endotherm corresponding to desolvation and a fusion endotherm with common features for the resultant DDS phase. This is consistent with the fact that on desolvating all three solvates in an oven at 363 K for 150 min, the resulting PXRD traces all corresponded to that of the bulk DDS material. Furthermore, we ascertained that the common desolvated product corresponds to the known orthorhombic form of dapsone (ref code DAPSUO05, space group $P2_12_12_1$).[5] All relevant PXRD patterns are provided as Supporting Information.

For desolvation events, the difference between the desolvation onset temperature and the boiling point of the pure solvent ($\Delta T = T_{on} - T_b$) has been suggested as one simple measure of solvate thermal stability.[17] The T_b values for solvents DCM, DXN, and THF are 313, 374, and 339 K respectively, and the ΔT values for the corresponding DDS solvates are +40, ∼0, and +9 K, yielding the thermal stability order **DDS·0.5(DCM)** ≫ **DDS·THF** > **DDS·DXN**.

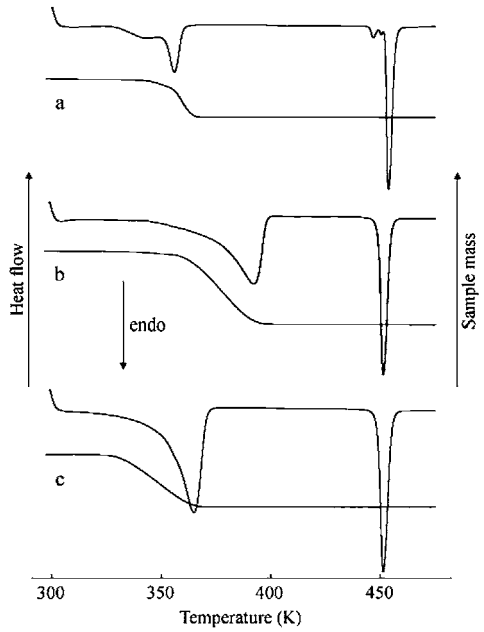

Figure 2. DSC and TGA traces for (a) **DDS·0.5(DCM)**; (b) **DDS·DXN**; (c) **DDS·THF**.

Molecular and Crystal Structures of the Solvates. Figure 3 shows the crystallographic asymmetric units with the atomic labeling. The conformations of the four independent DDS molecules in these crystals, reflected in four representative dihedral angles around the C−S bonds, are summarized in Table 3.

At first glance, the molecules of DDS shown above appear to have C_{2v} symmetry but all show significant deviations from this idealized symmetry that are conveniently gauged from values of the torsion angles τ_1−τ_4 listed in Table 3. These parameters measure the extents of rotation of the individual phenyl ring planes with respect to the respective SO_2 groups and they would all have the same magnitudes in the idealized geometry. Even larger ranges of the torsion angles τ_1−τ_4 than those indicated in Table 3 are observed when the values for the four independent molecules of dapsone in the structures of **DDS·0.33H$_2$O** (CSD ref code ANSFON02)[5] and unsolvated DDS (DAPSU005)[5] are considered. Thus, the DDS molecule adapts its conformation to the local environment in its various crystalline forms; the relevant intermolecular interactions in the solvates reported here are described below.

Another structural feature of interest in the DDS molecule is the variation in the stereochemistry of the amino groups, which also depends on intermolecular interactions, in particular hydrogen bonding. As noted above, during X-ray structure solution, all H atoms were located and modeled according to the observed geometries, namely, trigonal planar or pyramidal. Specifically, in each of the two independent drug molecules A and B in the DCM solvate, as well as in the DDS molecule in

dx.doi.org/10.1021/cg300019f | Cryst. Growth Des. 2012, 12, 1683−1692

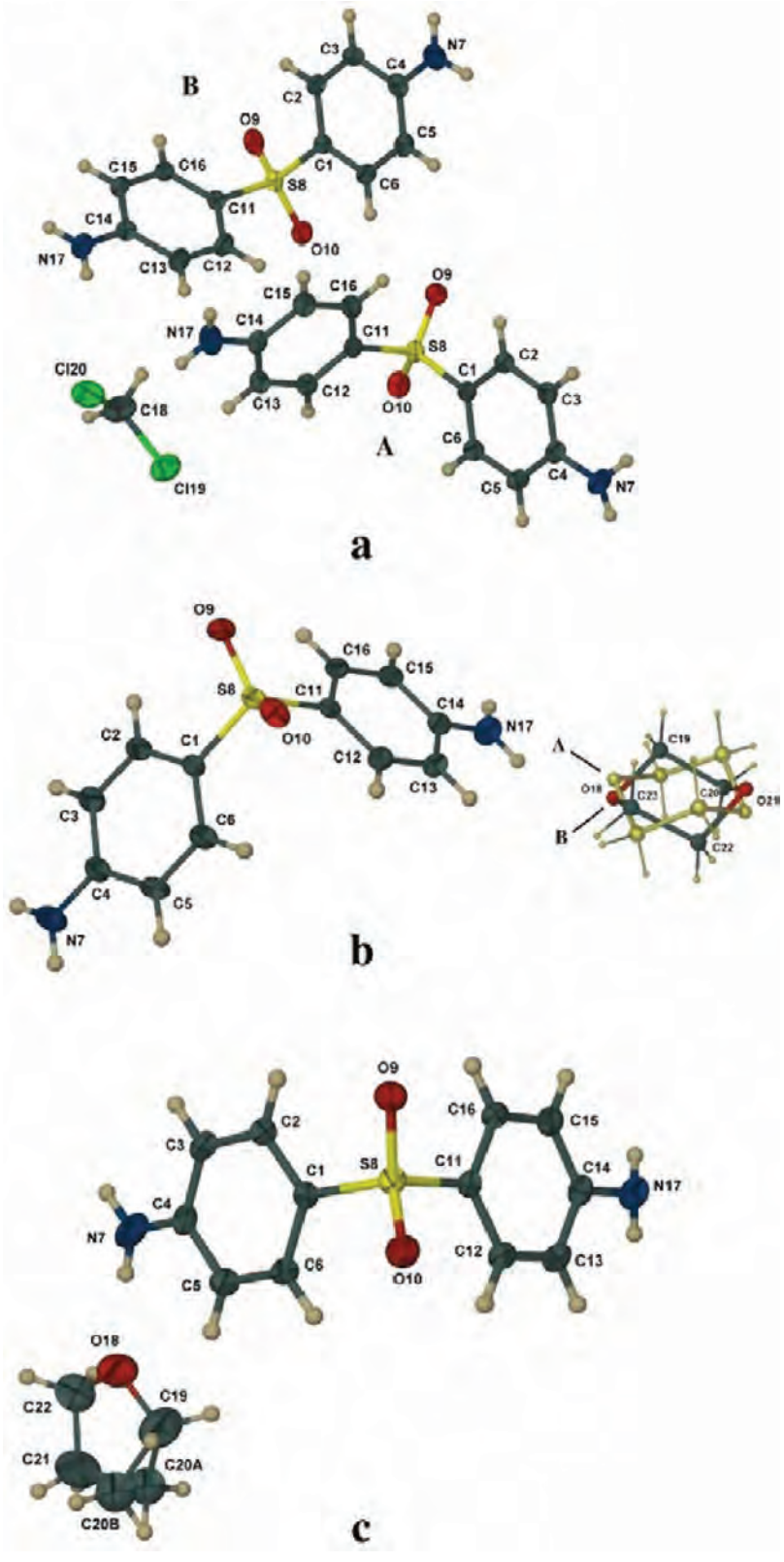

Figure 3. Crystallographic asymmetric units in solvates (a) **DDS·0.5DCM**; (b) **DDS·DXN**; (c) **DDS·THF**. Thermal ellipsoids are drawn at the 50% probability level.

the THF solvate, one $-NH_2$ group is trigonal planar while the other is pyramidal. Instead in the DXN solvate, both $-NH_2$ groups of the DDS molecule have trigonal planar geometry. These features are consistent with the observed H-bonding in the respective crystals. For example, pyramidization occurs in the DCM solvate as the amino H atoms strive to optimize H-bonding with neighboring sulfonyl oxygen acceptor atoms, while in the THF solvate, pyramidization arises from H-bond donation normal to the plane of the $-NH_2$ group in question. H-bond details appear in Table 4.

dx.doi.org/10.1021/cg300019f | *Cryst. Growth Des.* 2012, 12, 1683−1692

Table 3. Representative Dihedral Angles (deg) Reflecting DDS Conformations in the Solvates

dihedral angle (deg)[a]	DDS·0.5(DCM)	DDS·DXN	DDS·THF
τ_1 C2−C1−S8−O9	A: 30.2; B: 29.6	13.7	20.5
τ_2 C6−C1−S8−O10	A: −20.0; B: −24.1	−37.3	−32.4
τ_3 C16−C11−S8−O9	A: −36.7; B: −12.6	−17.4	−24.6
τ_4 C12−C11−S8−O10	A: 17.1; B: 42.2	34.8	28.5

[a]esd range 0.1 −0.3 deg.

In the solvate **DDS·0.5(DCM)**, solvent molecules associate in isolated pairs at centers of inversion. Figure 4 shows how such a pair (at 0, 1/2, 1/2) is enclathrated by a cage comprising several DDS molecules engaged in extensive hydrogen bonding via seven unique intermolecular N−H···O bonds between amino residues and sulfonyl oxygen atoms (Table 4).

Figure 5 is a packing diagram showing the extended crystal structure of the DCM solvate viewed down [100]. Isolated pairs of encapsulated solvent molecules as well as the complex network of hydrogen bonds are clearly evident. Only one unique C−H···O H-bond contributes to crystal cohesion. The shortest π-stacking interaction between phenyl rings has a centroid−centroid distance of 4.365 Å.

In the 1,4-dioxane solvate, **DDS·DXN**, the solvent molecule is disordered over two positions as shown earlier in Figure 3b, the major component (A) having a site-occupancy factor of 0.58(1). All four oxygen atoms of the disordered pair [O18A, O21A, O18B, O21B, shown in Figure 3b] are acceptors in hydrogen bonding to amino groups of DDS molecules (Table 4). For clarity, in the figures that follow, only the major component of the solvent molecule is included.

In the crystal of **DDS·DXN**, the solvent molecules are aligned in channels parallel to the crystal *b*-axis. They are not in direct contact, however, their van der Waals surfaces being separated by distances of ∼1−2 Å. Figure 6 (top) shows three representative stacked DXN molecules encapsulated within a tube-like, hydrogen-bonded network of DDS molecules. Each solvent molecule is tethered to the network by two N−H···O hydrogen bonds, as indicated for the central DXN molecule in the array. Below this is another view of the solvent-filled channel with all atoms drawn in space-filling mode.

It appears from the above analysis of the topology of solvent inclusion that migration of DXN molecules along the channel might be feasible upon heating the solvate, demanding only relatively small rotations of the phenyl rings of host DDS molecules. This point is revisited below when the desolvation processes are discussed.

Figure 7 is a packing diagram illustrating channel occupation by guest 1,4-dioxane molecules in the highly symmetrical structure of the solvate **DDS·DXN**.

The tetrahydrofuran molecule in the solvate **DDS·THF** (Figure 3c) has atom C20 disordered over two positions, C20A and C20B. Each position corresponds to a distinct five-membered ring conformation, namely, an envelope on C21 when C20A is present (site-occupancy 0.65(1)) and a twist form (twist on C19−C20B) when C20B is present (site-occupancy 0.35(1)). In the figures that follow, only the major component is included for clarity.

Figure 8 shows that each solvent molecule is partially accommodated within the V-shaped groove of a DDS molecule and is linked to the DDS molecule associated with an inversion-related THF molecule via a hydrogen bond N7−H7A···O18.

This unit is repeated by translation along the *x*-direction ($a \sim 6$ Å) in two inversion-related strands. The THF molecules within a strand are in contact along the *x*-direction and the two strands are likewise in contact. In Figure 9, the crystal structure of **DDS·THF** is viewed parallel to the linear channels that accommodate the THF molecules. The double strands of included solvent molecules are seen to be encaged in a large cyclic hydrogen bonded assembly comprising four DDS molecules. These cyclic assemblies are directly linked along the unit cell diagonals but are separated by smaller ("empty") hydrogen bonded cyclic motifs located at the midpoints of the unit cell axes. The latter motifs are stabilized by a π-stacking interaction between a phenyl ring and its inversion-related counterpart (centroid−centroid distance = 4.321 Å). The H-bonding network that maintains the DDS framework is indicated in detail and the geometrical parameters for the

Table 4. Hydrogen Bond Data for the Solvates[a]

solvate	D−H···A	*d*(D−H) (Å)	*d*(H···A) (Å)	*d*(D···A), Å	∠(DHA), deg
DDS·0.5(DCM)	N7A−H7A···O9B^{i}	0.88	2.44	3.257(2)	155(2)
	N7A−H7B···O10A^{ii}	0.88	2.21	3.063(2)	165(2)
	N7B−H7C···O9B^{ii}	0.88	2.26	3.104(2)	160(2)
	N17A−H17A···O9B^{iii}	0.88	2.59	3.351(3)	145
	N17A−H7B···O9A^{iv}	0.88	2.15	3.015(3)	169
	N17B−H17C···O10A^{iii}	0.88	2.11	2.970(2)	164
	N17B−H17D···O10B^{iii}	0.88	2.21	3.027(2)	154
DDS·DXN	N7−H7A···O10^{v}	0.88	2.15	3.018(4)	167
	N17−H17A···O10^{vi}	0.88	2.37	3.089(4)	139
	N7−H7B···O21A^{vii}	0.88	2.48	3.190(6)	139
	N7−H7B···O21B^{vii}	0.88	2.56	3.201(6)	131
	N17−H17B···O18A	0.88	2.15	2.981(6)	156
	N17−H17B···O18B	0.88	2.11	2.875(6)	145
DDS·THF	N7−H7A···O18	0.88	2.12	2.998(3)	175(2)
	N7−H7B···N17^{viii}	0.88	2.31	3.172(3)	166(2)
	N17−H17A···O10^{ix}	0.88	2.18	3.055(2)	174(2)
	N17−H17B···O9^{x}	0.88	2.27	2.955(2)	135(2)

[a]Symmetry codes: (i): 3/2 + *x*, 1/2 − *y*, 1/2 + *z*; (ii): 1 + *x*, *y*, *z*; (iii) 1/2 − *x*, 1/2 + *y*, 1/2 − *z*; (iv) 3/2 − *x*, 1/2 + *y*, 1/2 − *z*; (v): −1/2 + *x*, *y*, 1/2 − *z*; (vi): −1/2 + *x*, 1/2 − *y*, 1 − *z*; (vii): 3/2 − *x*, 1 − *y*, −1/2 + *z*; (viii): −1/2 + *x*, 1/2 − *y*, −1/2 + *z*; (ix): 3/2 − *x*, 1/2 + *y*, 3/2 − *z*; (x): 1/2 − *x*, 1/2 + *y*, 3/2 − *z*.

dx.doi.org/10.1021/cg300019f | *Cryst. Growth Des.* 2012, 12, 1683−1692

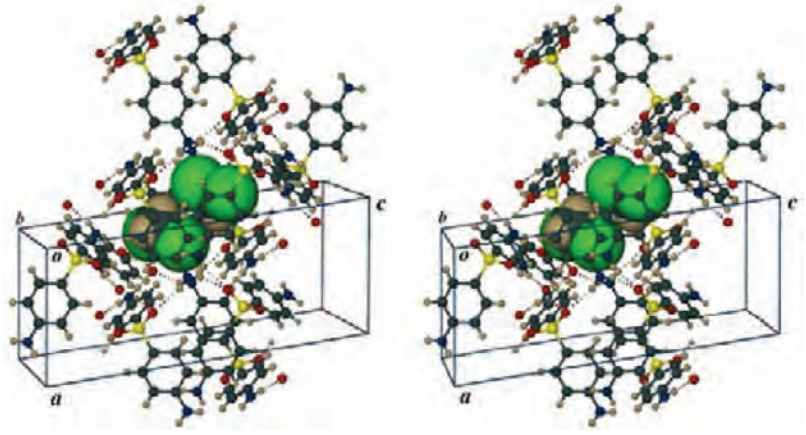

Figure 4. Stereoview showing details of the encapsulation of a pair of DCM molecules in solvate **DDS·0.5(DCM)**. DCM molecules are drawn in space-filling mode and DDS molecules are in ball-and-stick mode.

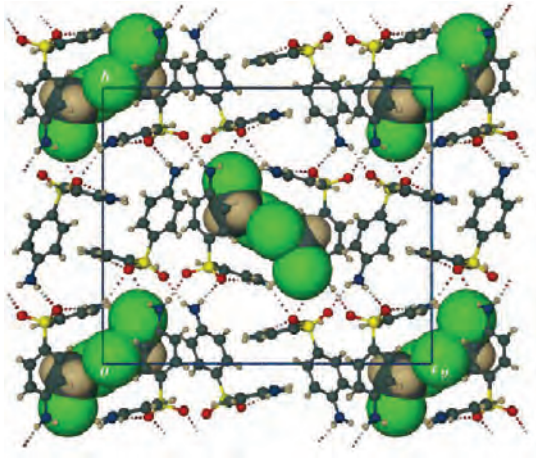

Figure 5. Packing diagram for **DDS·0.5(DCM)** viewed along [100].

relevant N–H···O and N–H···N hydrogen bonds are listed in Table 4.

In summary, as far as the solvent inclusion modes in the three solvates are concerned, the solvate with DCM is unique in containing isolated pairs of solvent molecules in the crystal, whereas both the DXN and THF solvates contain solvent molecules within linear channels, with the differences noted above. In **DDS·DXN**, the 1,4-dioxane molecules form infinite single-stranded rows with gaps between contiguous molecules, whereas in **DDS·THF**, double-stranded rows of tetrahydrofuran molecules are present and close contacts are maintained between solvent molecules.

The experimental PXRD patterns for the three solvates (recorded at ∼294 K) were compared with the computed patterns from the single crystal X-ray structures at 173 K (see Supporting Information). In general, there is a sufficient level of agreement to indicate that no phase changes occurred on cooling the crystals for single crystal XRD studies. There is some variation in the intensity values for corresponding peaks due to preferred orientation effects and the significant difference in the temperatures of the samples.

It is of interest to attempt to reconcile the thermal stability order **DDS·0.5(DCM)** ≫ **DDS·THF** > **DDS·DXN**, deduced earlier using the simplistic parameter $\Delta T = T_{on} - T_b$, with the structural results. The highest stability, associated with the

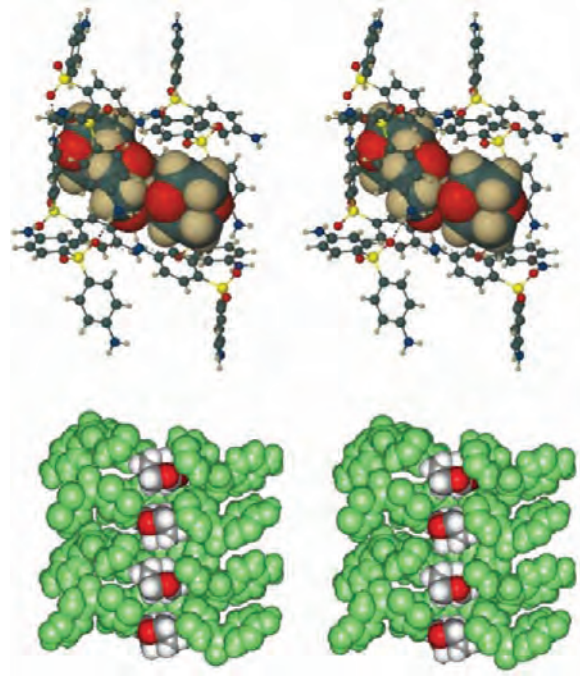

Figure 6. Stereoviews of the encapsulation of DXN molecules within a channel in the crystal of **DDS·DXN** viewed roughly parallel to the channel direction (top) and in cross-sectional view normal to the channel direction (bottom). The DDS molecules that contribute to forming the channel are drawn in green.

DDS·0.5(DCM) solvate, is consistent with the established mode of inclusion of its solvent molecules, requiring complete disruption of the host framework for DCM molecules to be released from the solvated crystals. In contrast, for the less stable solvates **DDS·DXN** and **DDS·THF**, solvent molecules are located in channels that should facilitate their diffusion out of the respective crystals. (Predicting the relative stabilities of the latter solvates on the basis of their crystal structures is not straightforward since they do not have an isostructural host framework. In addition, there are distinct differences in host–guest hydrogen bonding as well as differences in channel topology and occupation in these solvates).

Kinetics of Desolvation. An isothermal kinetic study has been carried out on the three solvates in order to elucidate the

dx.doi.org/10.1021/cg300019f | *Cryst. Growth Des.* 2012, 12, 1683–1692

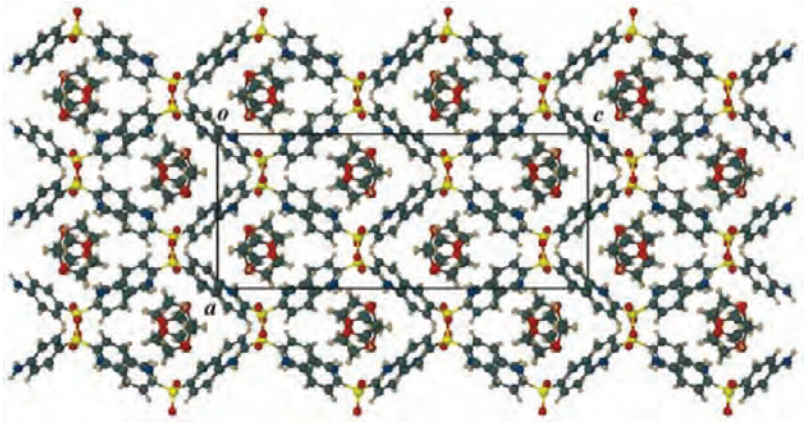

Figure 7. Crystal structure of **DDS·DXN** viewed along [010].

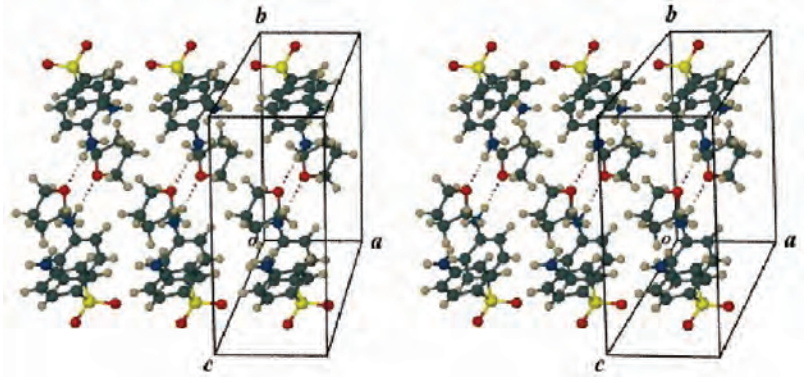

Figure 8. Stereoview illustrating the host–guest interactions in solvate **DDS·THF**.

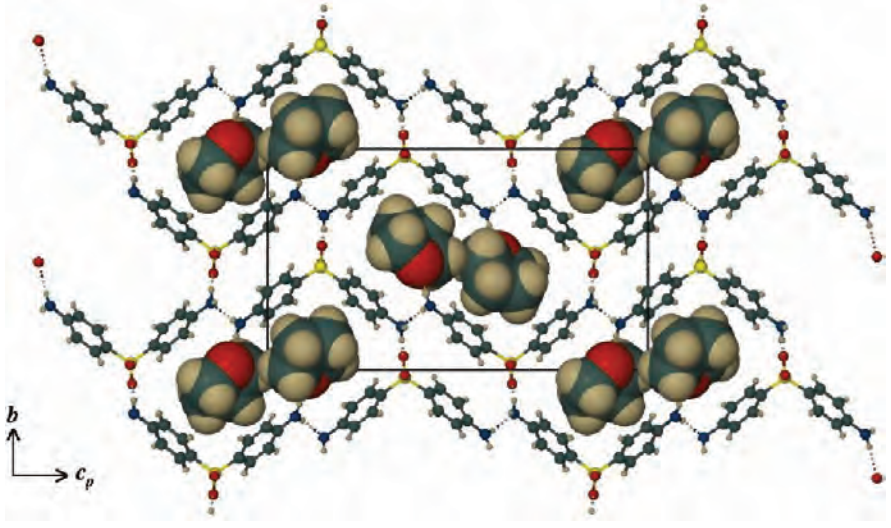

Figure 9. Projection of the crystal structure of solvate **DDS·THF** along [100].

possible mechanisms and activation energies involved in guest release. Good fits (r^2 > 0.99) of the experimental data were obtained for three models; the values of the derived activation energies and r^2 for these models are listed in Table 5. The models include the Avrami-Erofe'ev (A) and geometrically based (R2, R3) models. For each solvate, all of the models predict similar activation energy values based on the Arrhenius relationship of the isothermal model-fitting for the desolvation process; the independence of isothermal kinetic activation energy on the fitted reaction model has been noted previously.[18]

Model-free data analysis was performed using the standard isoconversional method over the α-range 0.15–0.90. Desolvation of **DDS·DXN** yielded the highest average activation energy of the three solvates investigated and would therefore be the most kinetically stable using this criterion. As expected for

dx.doi.org/10.1021/cg300019f | *Cryst. Growth Des.* 2012, 12, 1683–1692

Table 5. Kinetic Models for Desolvation, Activation Energies and Measures of Correlation

	kinetic model	E_a (kJ mol^{-1})	r^2
DDS·0.5(DCM)	A2	140.9 (7)	0.998[a]
	R2	141.0 (7)	0.996
DDS·DXN	A2	170.0 (14)	0.999[a]
	R2	172.7 (14)	0.997
	R3	173.0 (13)	0.994
DDS·THF	A2	154.2 (18)	0.993
	R2	154.7 (18)	0.998[a]
	R3	151.9 (19)	0.992

[a]Statistical model of choice.

reactions in the solid phase, the E_a values did not remain constant throughout their respective α-ranges (Figure 10).[19−21]

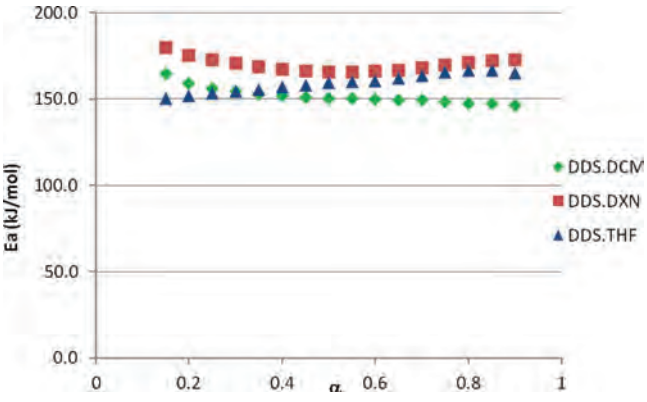

Figure 10. The activation energy, E_a, plotted as a function of the conversion fraction, α, for the desolvation process as obtained from model-free analysis.

Insofar as it is possible, the desolvation kinetics may be reconciled with various aspects of crystal morphology and crystal structure. From Table 5 we observe that the r^2 values for the A2 and R2 models for desolvation of **DDS·DCM** crystals are almost indistinguishable. Statistically, the desolvation followed the random nucleation and growth model (A2); the initial one-dimensional growth pattern can be observed from the micrographs in Figure 11, although the influence of the geometrical contracting area (R2) model cannot be neglected toward the end of the desolvation process.

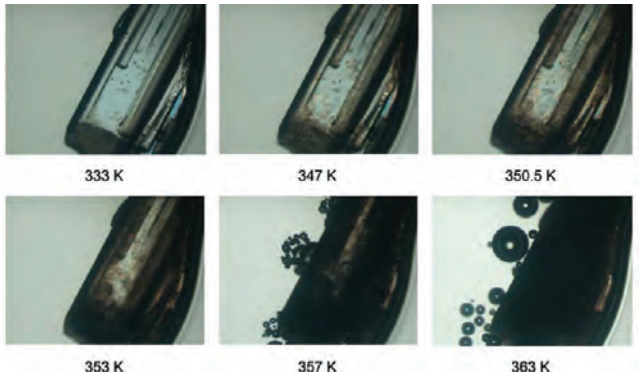

Figure 11. Micrographs of a desolvating **DDS·DCM** crystal under non-isothermal heating.

In the case of solvate **DDS·DXN**, it was noted above that the 1,4-dioxane molecules are aligned in channels parallel to the crystal *b*-axis, and migration of solvent molecules along this direction might be feasible, facilitated by small rotations of the phenyl rings of host DDS molecules. Model-fitting results for the desolvation of our **DDS·DXN** samples follow the nucleation and growth (A2) model under the experimental conditions specified in this report. Figure 12 depicts a desolvating **DDS·DXN** crystal (in the absence of mineral oil) subjected to a non-isothermal heating run. Random nucleation occurred but the growth of the nuclei took place in two dimensions, rather than one, as expected for the A2 model. This change in process dimensions was explained by Khawam and Flanagan[22] who studied the isothermal and non-isothermal desolvation of crystals containing various solvent molecules in constricted channels with cavities of narrowest width ∼2 Å. The latter topology of solvent inclusion had been demonstrated in an earlier study of the isostructural series of sulfameter (5-methoxysulfadiazine) solvates containing DXN, THF, and chloroform based on X-ray analysis and non-isothermal kinetic studies of their desolvation.[23] The detailed study of Khawam and Flanagan[22] focused on a larger series of solvates of sulfameter, showing that on isothermal heating runs, the desolvation of some of them (including those containing DXN and THF) occurred in one dimension (A2), while non-isothermal runs led to desolvation in one or more dimensions (A2 or A3). There is thus good correspondence between the results obtained for the solvate **DDS·DXN** in the present study and the solvates of sulfameter with DXN and THF[22] with respect to the analogous channel-type mode of solvent inclusion and a common A2 model for their desolvation.

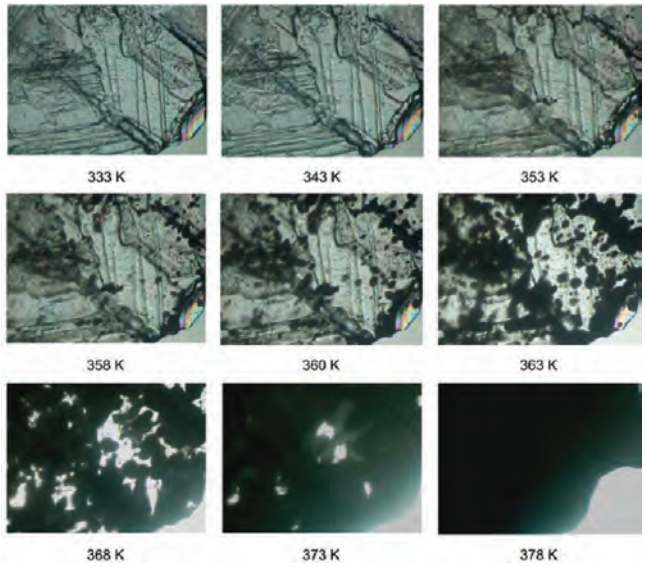

Figure 12. Micrographs of a desolvating **DDS·DXN** crystal, under non-isothermal heating conditions in the absence of mineral oil.

The mechanism for the desolvation of the third solvate, **DDS·THF**, was identified as the contracting area geometrical model (R2), which involves rapid nucleation of the particle surface and a phase-boundary controlled reaction for cylindrical particles. A desolvating single crystal of **DDS·THF** is shown in Figure 13.

The necessary disruption of the hydrogen bond between the THF molecule and the DDS host matrix corresponds to the

dx.doi.org/10.1021/cg300019f | *Cryst. Growth Des.* 2012, 12, 1683−1692

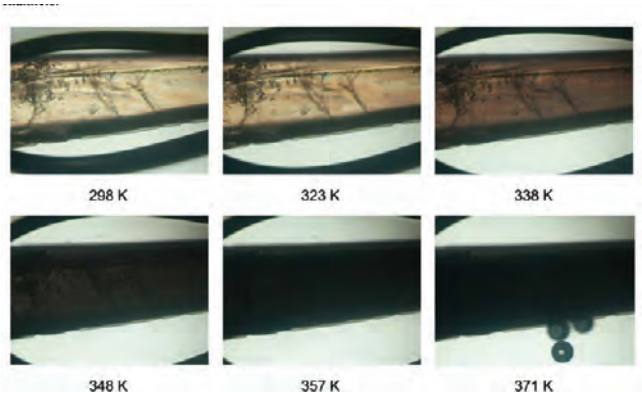

Figure 13. Micrographs of a **DDS·THF** crystal desolvating under non-isothermal heating conditions.

inward advance of the phase boundary from the surface to the center of the crystals; release of these molecules by diffusion through the channels evidently plays a minor role in the desolvation process. The geometrical contracting area model (R2) is not uncommon for guest molecules located in channels.[24−26]

The magnitudes of the activation energies for the respective desolvation processes are in the order **DDS·DXN** > **DDS·THF** > **DDS·0.5(DCM)**. We note that although the DCM solvent molecules are accommodated in isolated cages in **DDS·0.5-(DCM)**, the solvent molecules are not linked to the surrounding host molecules via hydrogen-bonds as in the case of the DXN and THF solvates. Whether this influences the ranking of the E_a values is, however, not easily determined: we have previously highlighted the limits of interpretation that can be placed on activation energies for solid-state reactions that do not involve isostructural host frameworks,[27] as is the case in the present study.

CONCLUSIONS

This study has demonstrated that the antibacterial DDS has a tendency to form solvated crystals, a result substantiated with strong evidence, including single crystal X-ray structural elucidation. Despite the longevity of this drug, the only crystal structures reported hitherto are those of the unsolvated form and the hydrated species with a 3:1 stoichiometric ratio of DDS to water. The facile crystallization of the new species from common solvents indicates that they could arise inadvertently during purification of DDS, with negative implications for product safety and performance. The presence of these solvates can be readily established by comparison of their experimental PXRD patterns with the reference PXRD patterns provided as Supporting Information. Single crystal XRD revealed a variety of hydrogen bonding motifs in the solvate crystals and elucidated the modes of solvent inclusion. Desolvation of all three solvates produced the orthorhombic form of DDS, the only polymorph of dapsone whose structure has been reported in the CSD.[5]

The thermodynamic stabilities, based on the simplistic parameter $T_{on} - T_b$ are in the order **DDS·0.5(DCM)** ≫ **DDS·THF** > **DDS·DXN**, while the isothermal kinetics of desolvation yielded activation energies in the reverse order. It is noted, however, that such intercomparison of the values of thermal data, as well as activation energies, for a series of solvates which are not based on a common, isostructural host framework, is questionable. The derived values of E_a may be considered as useful empirical data that characterize the individual crystalline solvates under the conditions of their desolvation described in this study. Instead, somewhat more emphasis is placed here on the observed similarities and differences in the nature of the best-fitting kinetic models for desolvation obtained by isothermal kinetics, since some level of reconciliation with the observed crystal structures and/or crystal morphologies can in this case be made.

ASSOCIATED CONTENT

Supporting Information

X-ray crystallographic data for the three crystal structures (PDF); they have also been deposited at the Cambridge Crystallographic Data Centre, CCDC Nos. 836169−836171. Experimental and computed PXRD patterns for the solvates and their desolvation products are also provided. This material is available free of charge via the Internet at http://pubs.acs.org/.

AUTHOR INFORMATION

Corresponding Author

*Fax: 27 21 650 5195. Phone: 27 21 650 3071. E-mail: Mino.Caira@uct.ac.za.

Notes

The authors declare no competing financial interest.

ACKNOWLEDGMENTS

We are grateful to the University of Cape Town, North-West University, and the National Research Foundation of South Africa for financial support.

REFERENCES

(1) Justin, B. *J. Hist. Med. Allied Sci.* **2011**, *66*, 425−67.
(2) Wolf, R.; Orni-Wasserlauf, R. *Int. J. Dermatol.* **2000**, *39*, 779−783.
(3) De Villiers, M. M.; Caira, M. R.; Li, J.; Strydom, S. J.; Bourne, S. A.; Liebenberg, W. *Mol. Pharmaceutics* **2011**, *8*, 877−888.
(4) Yang, C.-P.; Woo, E. M.; Jou, G.-L. *J. Therm. Anal. Calorim.* **2003**, *74*, 843−852.
(5) *Cambridge Structural Database and Cambridge Structural Database system*, Version 5.32; Cambridge Crystallographic Data Centre, University Chemical Laboratory: Cambridge England, May 2011.
(6) Caira, M. R.; Stieger, N.; Liebenberg, W.; De Villiers, M. M.; Samsodien, H. *Cryst. Growth Des.* **2008**, *8*, 17−23.
(7) Stieger, N.; Liebenberg, W.; Wessels, J. C.; Samsodien, H.; Caira, M. R. *Struct. Chem.* **2010**, *21*, 771−777.
(8) Brown, M. E.; Dolimore, D.; Galwey, A. K. In *Comprehensive Chemical Kinetics*; Bamford, C. H.; Tipper, C. F. H., Eds.; Elsevier: Amsterdam, Netherlands, 1980; Vol. *22*, 340.
(9) Vyazovkin, S. *Mikrochim. Acta* **2000**, *355*, 155−163.
(10) Hooft, R. *Collect*; Nonius B. V.: Delft, The Netherlands, 2002.
(11) Otwinowski, Z.; Minor, W. In *International Tables for Crystallography*; Rossman, M. G., Arnold, E., Eds.; Kluwer: Dordrecht, 2000; Vol. *F*.
(12) Sheldrick, G. M. *SADABS v2.01*, 2000.
(13) *SAINT-Plus (including XPREP)*, Version 7.12; Bruker AXS Inc.: Madison, WI, 2004.
(14) Sheldrick, G. M. In *Crystallographic Computing*; Sheldrick, G. M.; Kruger, C.; Goddard, R., Eds.; Oxford University Press: Oxford, U.K., 1985; Vol. 3, p 175.
(15) Sheldrick, G. M. *SHELXL-97, Program for Crystal Structure Refinement*; University of Göttingen: Göttingen, Germany.
(16) Barbour, L. J. *J. Supramol. Chem.* **2003**, *1*, 189−191.
(17) Caira, M. R.; Nassimbeni, L. R. Phase transformations in inclusion compounds, kinetics and thermodynamics of enclathration. In *Comprehensive Supramolecular Chemistry*; Atwood, J. L., Davies, J. E.,

D. Macnicol, D. D.; Vögtle, F., Eds.; Pergamon: New York, 1996; Vol. 6, Chapter 25 .
(18) Zhou, D.; Grant, D. J. W. *J. Phys. Chem. A* **2004**, *108*, 4239−4246.
(19) Vyazovkin, S.; Wight, C. A. *Annu. Rev. Phys. Chem.* **1997**, *48*, 125−149.
(20) Vyazovkin, S. *New J. Chem.* **2000**, *24*, 913−917.
(21) Khawam, A.; Flanagan, D. R. *J. Pharm. Sci.* **2006**, *95*, 472−498.
(22) Khawam, A.; Flanagan, D. R. *J. Pharm. Sci.* **2008**, *97*, 2160−2008.
(23) Caira, M. R.; Mohamed, R. *Supramol.Chem.* **1993**, *2*, 201−207.
(24) Caira, M. R.; Coetzee, A.; Nassimbeni, L. R.; Weber, E.; Wierig, A. *Supramol. Chem.* **1999**, *10*, 35−241.
(25) Coetzee, A.; Nassimbeni, L. R.; Su, H. *J. Chem. Research S* **1999**, *7*, 436−437.
(26) Nassimbeni, L, R.; Su, H. *Acta Crystallogr.* **2001**, *B57*, 394−398.
(27) Caira, M. R. Isostructurality of Inclusion Compounds. In *Encyclopedia of Supramolecular Chemistry*; Atwood, J. L.; Steed, J. W., Eds.; Marcel Dekker Inc.: New York, 2004; pp 767−775.

Annexure B

Manuscripts to be submitted to

Thermochimica Acta

Thermochimica Acta is an international journal concerned with all aspects of thermoanalytical and calorimetric methods and their application to experimental chemistry, physics, biology and engineering.

The journal particularly welcomes papers from newly emerging areas as well as from the traditional strength areas:

- New and improved instrumentation and methods
- Thermal properties and behaviour of materials
- Kinetics of thermally stimulated processes

Each paper submitted for publication should clearly present:

- Scientific motivation (i.e., why this study is of interest);
- Relevance to the stated scope of *Thermochimica Acta* (i.e., why thermal methods play a crucial role in the study, or why this study is important for the use and development of thermal methods);
- General significance of the obtained results (i.e., how this study contributes to the advancement of knowledge in the general area of the study). Note that novelty of a study does not necessarily imply general significance of the results.

In reporting DSC data; this journal prefers the exothermic reactions to be plotted downward.

The literature references in Annexure B & C were done according to this journal's guide lines.

Annexure B

Thermal evaluation and enantiotropic polymorphism of dapsone

H. Lemmer[a,*], N. Stieger[a], H.J.R. Lemmer[a], L.R. Tiedt[b], Mino R. Caira[c], W. Liebenberg[a]

[a] Unit for Drug Research and Development, Faculty of Health Sciences, North-West University, Potchefstroom, South Africa

[b] Laboratory for Electron Microscopy, Faculty of Natural Sciences, North-West University, Potchefstroom, South Africa

[c] Department of Chemistry, University of Cape Town, Rondebosch, South Africa

* Corresponding author: H. Lemmer

Tel.: +27 84 445 2221

E-mail address: helanie.lemmer@gmail.com

Postal address: Helanie Lemmer

Internal box 36

Private bag X6001

Potchefstroom

South Africa

2520

There are still some aspects of this article that will have to be investigated before it can ultimately be submitted for publication.

Thermal evaluation and enantiotropic polymorphism of dapsone

Abstract

Multiple enantiotropically-related polymorphic transitions exist for dapsone. Anhydrous dapsone (DDS form III) undergoes a solid-solid phase transition at ~82°C to DDS form II; which then melts at ~177°C. The desolvated form of a solvate that recrystallised from dichloromethane (DCM) presented us with an opportunity to study the transition to DDS form I. DDS form I was previously reported to melt at ~180°C and to crystallise from the melt of DDS form II.

Keywords: Dapsone; Phase transition; Melting point; Enantiotropic.

1. Introduction

Dapsone (DDS), an antibacterial drug is used clinically for the treatment of leprosy as well as opportunistic infections in HIV-positive patients. Despite the age of this drug not much is known about the solid-solid phase transformations or the interrelationships between the polymorphs except for the work published by Kuhnert-Brandstätter and Moser [1]. At ambient conditions the dapsone anhydrate exists as the crystalline form III. Upon heating, this form converts *via* a solid-solid enantiotropic phase transition at 82 ± 2°C to form II which then melts at ~177°C. For this reason the melting point of DDS form III cannot be obtained [2,1].

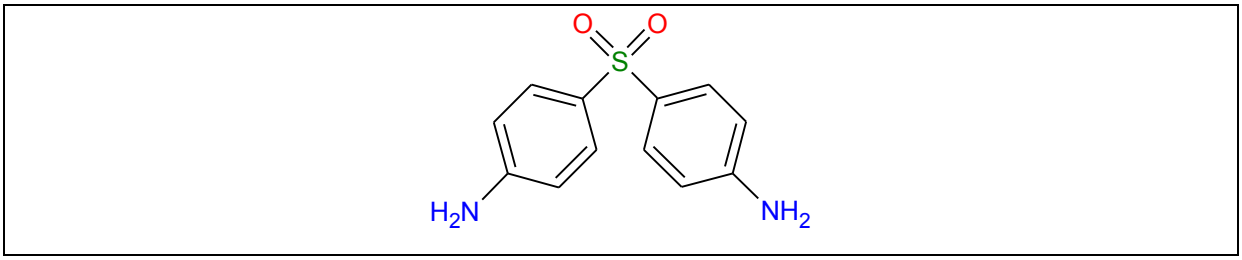

Figure 1. Chemical structure of dapsone (DDS).

Butt [3] first suggested in 1953 that DDS exists in more than one form: one that melts at 177°C and another form that melts at 180.5°C. He was able to produce the higher melting

form by grinding samples or by leaving a DDS sample that would normally melt at 177°C in an oven at 50°C for several days. He also mentioned that it was not possible to recapture this higher melting form by dissolving and recrystallising it; since it did not reproduce the higher melting form, but rather the form that melts at 177°C. Reinvestigation of DDS's complex energy-temperature relationship with regards to its possible forms has been proposed before [4].

According to Kuhnert-Brandstätter and Moser [1], form I melts at 179°C but is recrystallised from the melt of form II and an enantiotropic relationship exists between form I and form II and additionally between form I and III. The hydrated form of DDS was named DDS form IV and its dehydrated form melts at 170°C.

The thermal behaviour described above is inconsistent with the provided pressure versus temperature phase diagram (figure 2) and also some discrepancies exist. The first discrepancy can be observed from the pressure versus vapour plot: DDS form III is the most stable form at room temperature and should therefore have the lowest vapour pressure at that temperature, but according to the plot (figure 2(a)) it is DDS form IV and not III. This discrepancy can easily be fixed by switching the titles of DDS form III and IV as was done in figure 2(b). DDS form IV has no interrelationship with any other DDS polymorphs; the exact nature of form IV will still have to be investigated. The second discrepancy is that of the statement that DDS form I crystallises from the melt of DDS form II and that there exists an enantiotropic relationship between DDS forms I and II. This statement does not match that of the provided plot (figure 2(a)) and also, two polymorphs can only be enantiotropic in nature if the transition takes place prior to melting. Reinvestigation of the interrelationships between the DDS polymorphs using modern techniques will be necessary to evaluate and reconstruct a possible truth about the interrelationship of DDS polymorphs especially with regard to DDS form I.

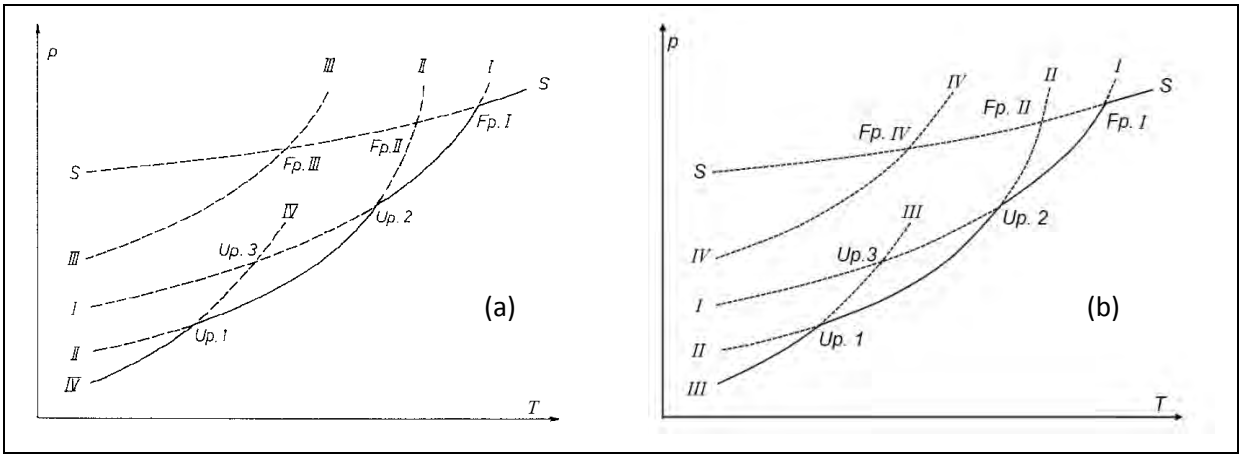

Figure 2. Enantiotropic relationship between the polymorphs of DDS (**a**) Pressure versus temperature phase diagram of the four modifications of DDS according to the article published by Kuhnert-Brandstätter and Moser in 1979; where S indicates the melt, Fp is the melting point and Up indicates the phase transitions. (**b**) Proposed corrected pressure versus temperature phase diagram of the four modifications of DDS.

Process-induced transformation from one polymorph into another can take place during storage or processing when the temperature and/or pressure are elevated [5]. These different crystalline forms have different physicochemical characteristics which include melting and sublimation temperatures, heat capacity, conductivity, volume, density, viscosity, crystal hardness, crystal shape, colour, refractive index, solubility, dissolution rate, stability, hygroscopicity and solid state reactions [6].

DDS formed a solvate when recrystallised from dichloromethane (DCM); the single crystal structure of this solvate has been elucidated and submitted into the Cambridge Structural Database, it can be found *via* the internet at http://pubs.acs.org/. DDS•0.5(DCM) crystallised in the stoichiometric relationship of one DCM molecule to two DDS molecules [7].

2. Experimental

2.1. Materials

DDS was purchased from Ria International LLC, East Hanover, USA, batch 20100128. The purchased DDS contains not less than 99.0 per cent and not more than the equivalent of 101.0 per cent of 4,4′-sulphonyldianiline. All solvents (DCM, DMSO and 2-propanol) used for recrystallisation were of analytical grade and were purchased from ACE Chemicals, South Africa.

2.2. Crystal preparation

A requisite amount of anhydrous DDS was added to each pure solvent and heated until boiling point. The hot, saturated solution were covered with Parafilm® (Pechiney, USA) and placed in a dark cupboard where it was left to spontaneously recrystallise while slowly cooling down to room temperature (~25°C). The glass container containing the recrystallised products and also the purchased DDS was protected from light by covering it with foil whenever it was removed from the dark cupboard for analysis.

2.3. Thermal microscopy (TM)

Single crystals from each product were submerged in silicon oil and heated on a thermo microscope equipped with a hot stage (Leitz Wetzlar hotstage with a Goertz Metrawatt BBC Metratherm 1200d thermometer). Any changes in the solid sample in relation to the temperature change were observed through a Nikon Eclipse E400 (Nikon, Japan) microscope at a ten time magnification with crossed polarised light. Images were captured using a Nikon DS-Fil camera with NIS-Elements F 2.30 (Nikon, Japan) image capturing software.

2.4. Scanning Electron Microscopy (SEM)

Samples were analysed by covering the carbon tape on the SEM pin with sample, and it was then covered with a gold-palladium film (Eiko engineering ion coater IB-2, Japan) in a vacuum. The samples were placed in the microscope sample holder and analysed using a FEI Quanta 200 ESEM & Oxford INCA 400 EDS microscope system (FEI Corporation, USA) which operated at 10 kV under high vacuum modes while heating the sample at 10°C.min^{-1}. DDS was crystallised in 2-propanol to provide us with a well-defined recrystallised crystal of DDS since the original powder form was composed of pieces of various shapes and sizes.

2.5. Differential Scanning Calorimetry (DSC)

Temperature and enthalpy values were measured with a Shimadzu DSC-60A instrument (Shimadzu, Japan) and the data generated using TA60 version 2.11 software. Approximately 4-8 mg of each sample was weighed and heated in an aluminium crucible with a pierced lid. Samples were heated at 10°C.min^{-1} in an inert nitrogen atmosphere flowing at 35 mL.min^{-1}. The instrument was calibrated with high purity indium and tin standards according to first principles.

2.6. Modulated Temperature DSC (MTDSC)

MTDSC work was done on a TA Q200 MDSC™ and analysis of the results was done using TA Universal Analysis software. The aluminium TZero™ reference and sample pans were

all weighed to ensure that no difference in weight greater than 0.1 mg existed. The sample weight was meticulously controlled (1 ± 0.07 mg) to ensure reproducibility. The parameters for the MTDSC were chosen after great consideration and experimentation. All samples were heated after being held isothermally at 25°C for one minute at an underlying heating rate of 2°C.min^{-1} to 200°C. Amplitude of 0.7°C was added to produce proper heating-and-cooling modulation to the underlying heating rate and the period of such a full modulation lasted 40 seconds.

2.7. Variable temperature XRD (VTXRD)

VTXRD data were generated using a PANaytical EMPYREAN (PANalytical, Netherland) with CuKα-radiation at a minimum step size of 0.0001 °θ, using a PIXcel3D detector. Generator settings were at 45 mA, 40 kV. An Anton Paar Cryo and humidity chamber (Anton Paar, Germany) was used for the heating of the samples. The samples were heated at 10°C.min^{-1} to a predetermined temperature where a 5 minute scan was done; longer scans could improve resolution but would cause unnecessary temperature exposure leading to desolvation.

3. Results and discussion

3.1. The solid-solid phase transition of DDS as observed on the TM and SEM

A solid-solid phase transition was easily observed at ± 82°C upon heating a toluene recrystallised DDS sample (figure 3) on the TM. Using polarised light the phase transition was seen as a front moving from one side of the crystal to the other. This moving front can also be seen during solid-solid phase transitions for other API's such as ethambutol [8].

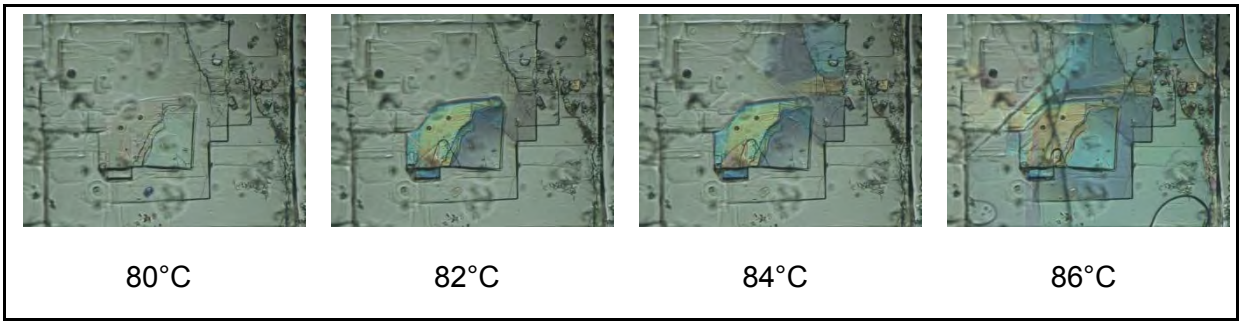

Figure 3. TM micrographs of DDS recrystallised from DMSO. The solid-solid phase transition can be seen as a front moving from one side of the crystal to the other.

The phase transition can also be seen as a wave moving through the crystal when observing a recrystallised crystal using SEM (figure 4). This event takes place at 63°C; this temperature is lower than the normal ~82°C that was observed using different thermal analysis techniques, but it should be taken into account that this event took place under vacuum. [Please see the file "Phase transition SEM" on the included picture CD which will be submitted as supplementary information for submission for more detailed images]. This might have been caused by an anisotropic change in unit cell volume due to a conformational change in the molecule. The anticholinergic agent oxitropium bromide was able to jump because of an anisotropic expansion in its cell volume [9]. Upon heating of a prismatic single-crystal of oxitropium bromide the crystal undergoes a highly anisotropic change in the cell-unit volume which causes it to jump a couple of centimetres high from the heating stage resulting in disaggregation of the crystal. This phase transformation takes place at 45°C and appears to be reversible under slower heating rates of 5°C.min^{-1}.

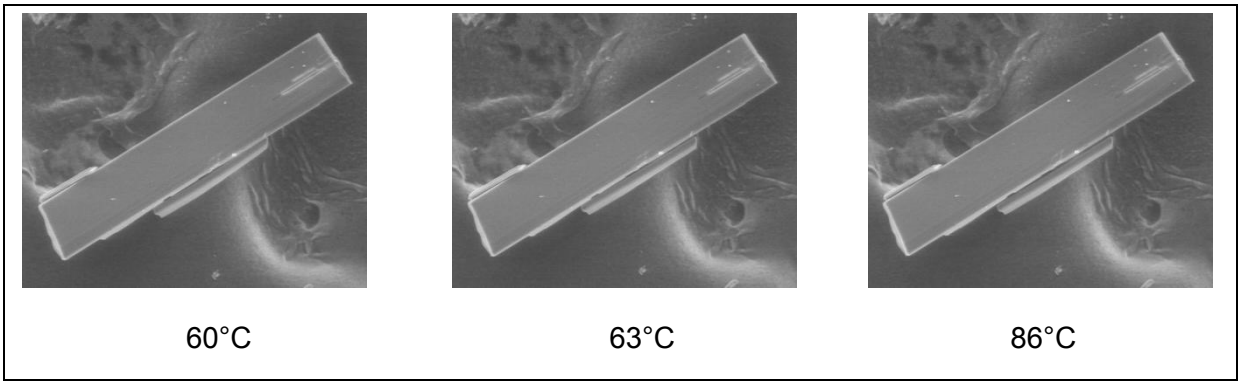

Figure 4. SEM micrographs of DDS recrystallised from 2-propranol.

3.2. Thermal behaviour of DDS according to DSC

Two distinct endotherms can be seen upon heating of DDS over the heating range (25 – 200°C) at 82 and 177°C respectively (figure 5a).

Analysis was also done on the DDS•0.5(DCM) solvate which yielded three additional endotherms in the temperature range of melting (figure 5b). This analysis was repeated for different DDS•0.5(DCM) batches also using different heating rates; all produced these multiple endotherms. These endotherms were respectively observed at 173°C, 177°C and 180.2°C. Further investigation had to be done to identify these endothermic peaks.

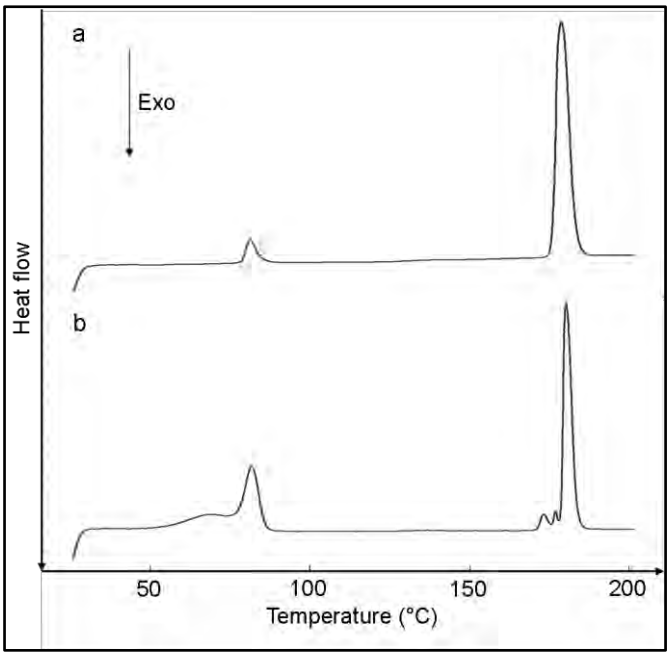

Figure 5. DSC thermograms of DDS (a) and DDS•(0.5)DCM (b). The solid-solid phase transition can be seen as an endothermic peak at ~82°C while with DDS•(0.5)DCM this peak is obscured during desolvation. DDS showed a melting endotherm at 177°C while DDS•(0.5)DCM had three endotherms around the temperatures of melting.

3.2.1. VTPXRD for DDS

From the VTPXRD data in figure 6; it can be seen that the internal structure of DDS changes somewhere between 60-90°C (~82°C as measured using DSC analysis) to DDS form II. Upon cooling of the samples from 120°C to ambient temperature it enantiotropically converted back to DDS form III. This process is reversible and can be repeated many times.

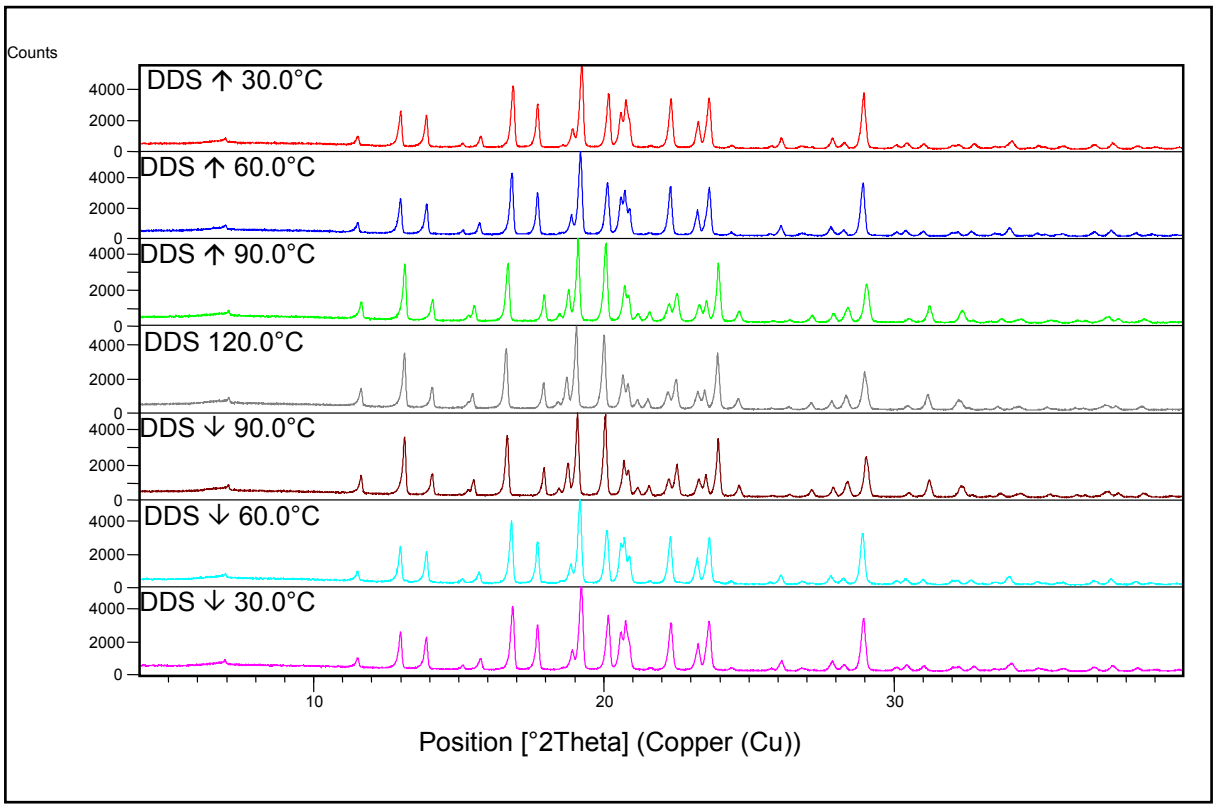

Figure 6. VTPXRD of DDS raw-materials when heated to 120 ± 5°C and cooled down to 30 ± 5°C.

Decomposition of DDS after melting was not seen using conventional DSC, but was illustrated by MTDSC and VTPXRD data. This would mean that the sample is not completely pure after melting; complete conversion back to form II and III was not possible as seen in figure 7.

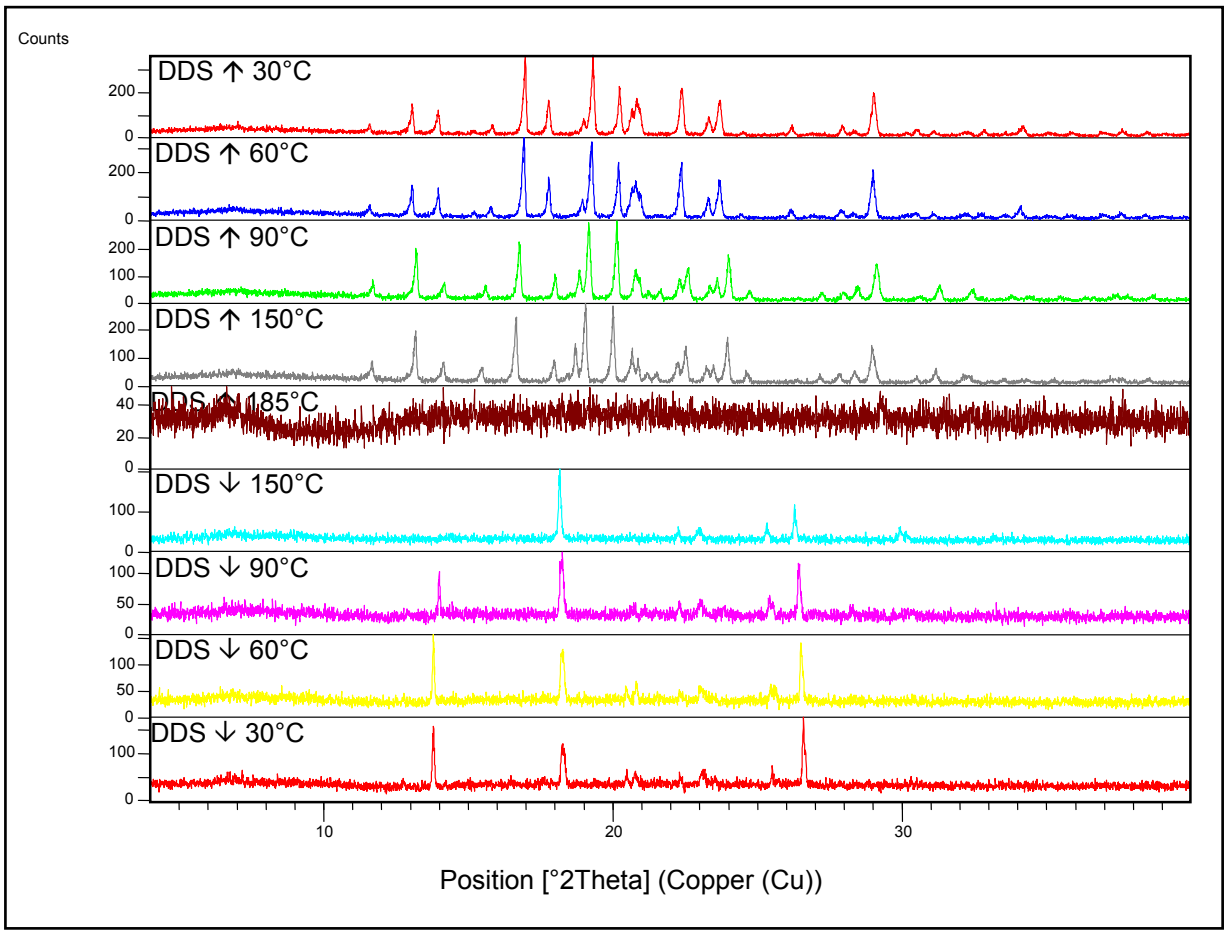

Figure 7. VTPXRD of DDS raw-materials when heated to 185 ± 5°C and cooled back down to 30 ± 5°C.

3.3. Thermal behaviour of DDS•0.5(DCM) solvate

DDS•0.5(DCM) did not follow the same trend as that of DDS upon heating. At 170 ± 5°C the internal structure of the desolvated DDS•0.5(DCM) still presents the same as that of DDS. However, at 175 ± 5°C the VTXRD pattern of the solvate differs significantly from that of DDS. This indicates that the new phase did not exist in the desolvated DDS•0.5(DCM) structure at 170 ± 5°C, but it did exist at 175 ± 5°C (figure 8). These results possibly explain the three endotherms that was seen in the DSC trace of DDS•0.5(DCM). A possible explanation would be that a solid-solid phase transition took place at 173°C where DDS form II converted to form I. The endotherm at 177°C might have been caused by the melting of a small amount of DDS form II that did not convert to DDS form I. DDS form I melts at ~180°C as was previously reported.

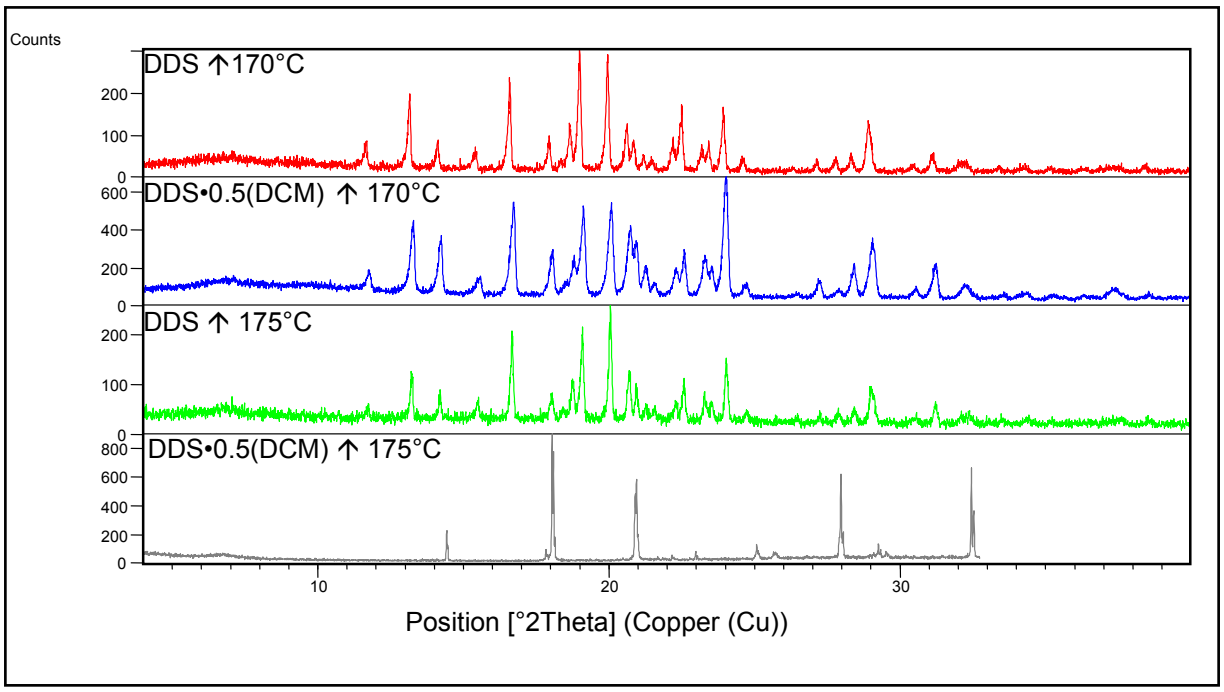

Figure 8. VTPXRD patterns of DDS and DDS•0.5(DCM) when heated to their melting points. At 170°C the VTPXRD patters are basically identical, but at 175°C the difference was significant.

MTDSC has the advantage of separating the total heat flow into reversing and non-reversing heat signals. Melting endotherms can generally be seen in the reversing and non-reversing heat signals. The solid-solid phase transition at ~82°C was also observed in both the reversing and non-reversing heat signals for DDS in figure 8.

The desolvation and phase transition peaks were clearly resolved in the non-reversing heat signals for DDS•0.5(DCM) (figure 10). The solid-solid phase transition can also be seen in the reversing heat signal at 84.6°C which is slightly higher than that of DDS in figure 9. The endotherms closer to the end was also resolved providing us with two signals in the non-reversing heat signal and three in the reversing heat signal. The endotherms seen at 172°C in both the reversing and non-reversing heat signals may be the solid-solid phase transition of DDS form II converting to form I, coinciding with the change in unit cell dimensions observed for DDS•0.5(DCM) at 175°C in figure 8. The small endotherm at 177°C was seen in the reversing heat signal which might be the melting of a small amount of DDS II that did not convert to form I. Form I was described by Kuhnert-Brandstätter and Moser [1] to melt at 179°C and that it is recrystallised from the melt of form II (which melts at 177°C); according to them there exists an enantiotropic relationship between form I and form II and also between form I and form III. The endothermic peak at ~180°C seen in the reversing and non-reversing heat signals was caused by the melting of DDS form I. This disagrees

with the statement of Kuhnert-Brandstätter and Moser but does coincide with their provided vapour pressure versus temperature plot (figure 2a).

Evaluation of TM micrographs of other recrystallised crystals with a higher melting point did not show any crystallisation taking place within the melt of these crystals (not shown here). This also verifies that the transition took place before melting of DDS form II.

An exothermic peak can be seen for all the samples from MTDSC traces after the melting endotherm; this was caused by decomposition of the melting sample. The DSC and MTDSC were both purged with nitrogen gas and pierced pans were used in the DSC while non-pierced, crimped pans were used in the MTDSC. Decomposition was observed on the MTDSC traces due to its greater sensitivity and its ability to separate different simultaneous thermal events from another. Samples were purged with compressed air in the VTXRD which would have a higher oxygen concentration and possibly lead to more oxidative decomposition.

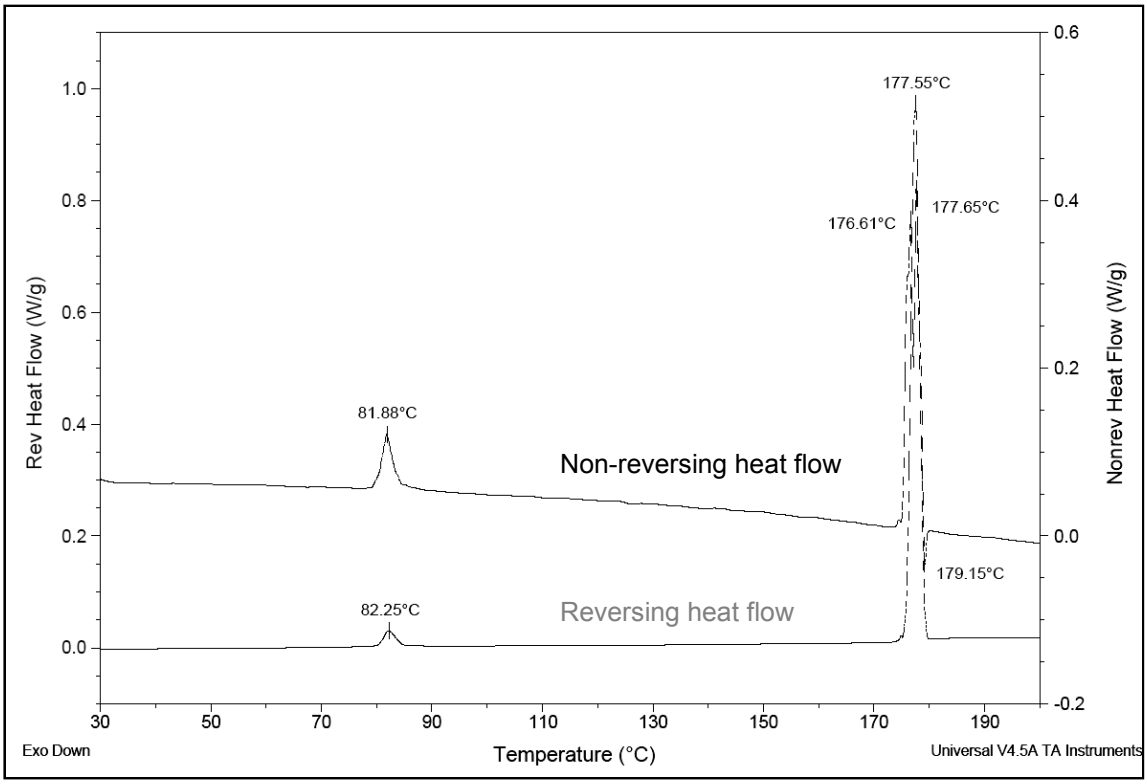

Figure 9. MTDSC traces for DDS over the heating range 25 -200°C.

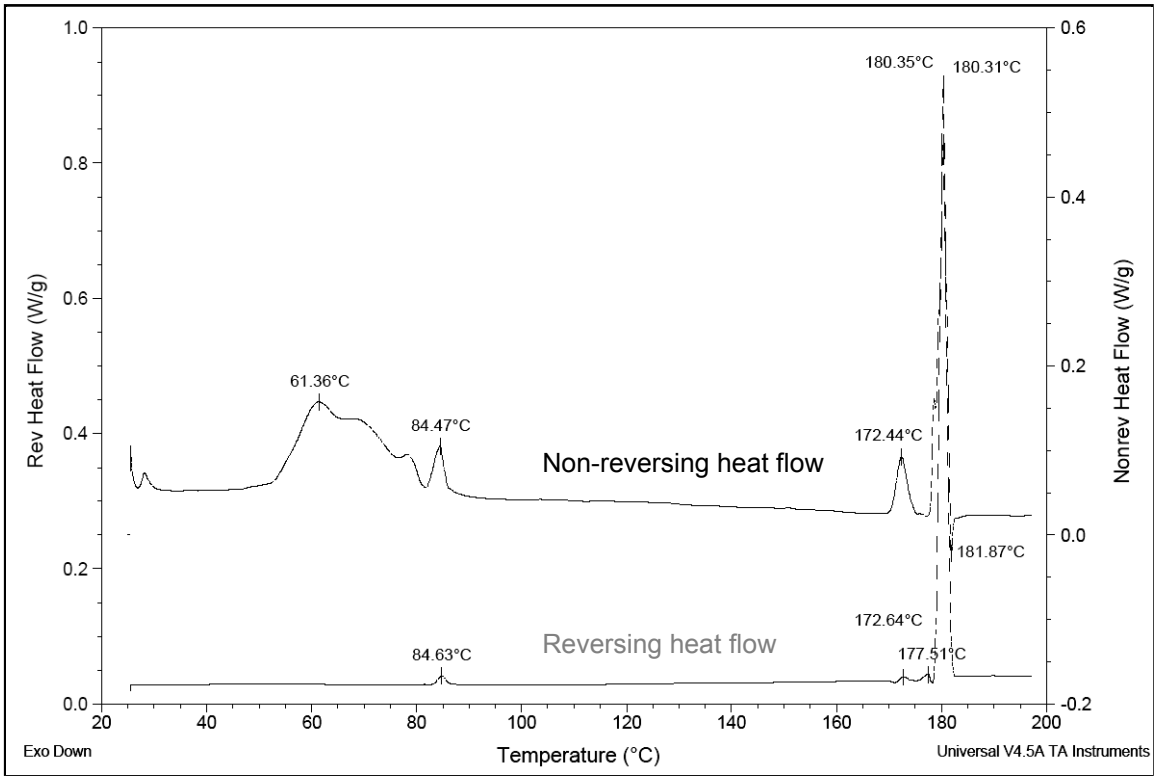

Figure 10. MTDSC traces for DDS•0.5(DCM) over the heating range 25 -200°C.

3.3.1. DSC heating/cooling cycle

Since the phase transition of DDS form II to form I took place below the melting point of DDS form II this could mean that the conversion took place *via* an enantiotropic mechanism. By analysing the stack of DDS and DDS•0.5(DCM) when exposed to a heating/cooling cycle it is possible to see that the melting of the desolvated DDS•0.5(DCM) initially took place at 180.5°C and then after going through a full cooling/heating cycle it melted at 177°C. This is in accordance with the results published by Butt [3], since he also did not find it possible to reproduce the higher melting point form again from the same sample.

The recrystallisation exotherms for DDS and the desolvated DDS•0.5(DCM) from the melt can be seen at **c**. Both recrystallised products from exotherm **c** converted back to the basic form III (70°C) at exotherm **d**. Although some decomposition was seen on MTDSC and VTPXRD, the commonality between the phase transitions and melting points suggests the extent of decomposition was not sufficient to influence this analytical method.

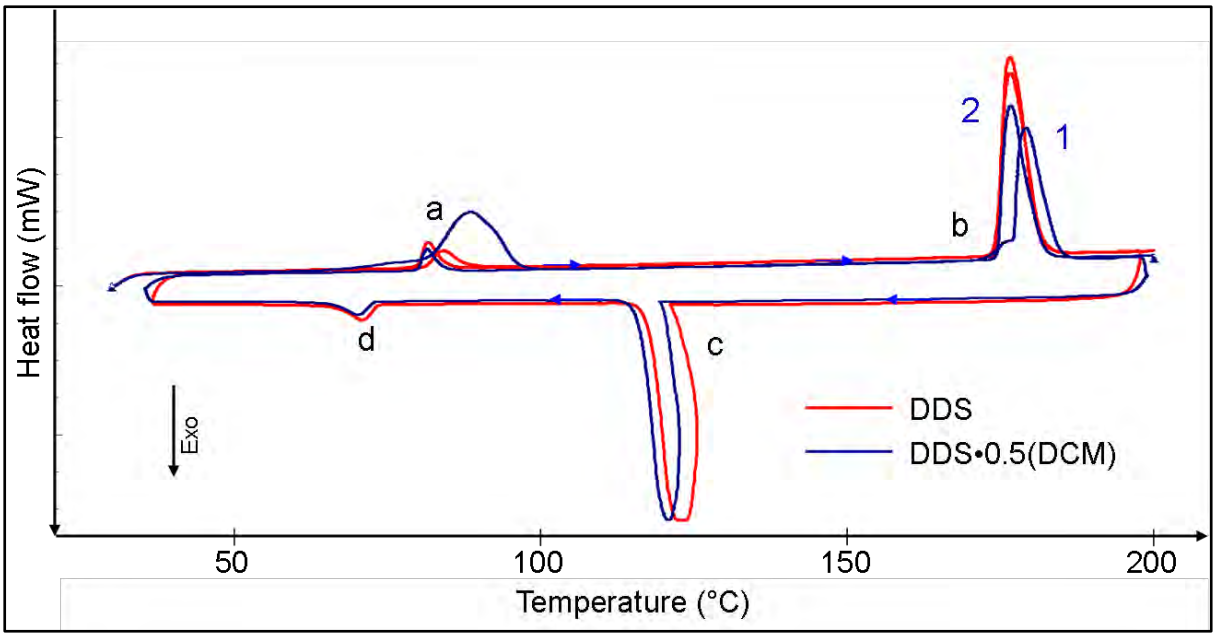

Figure 11. DSC thermogram stack of DDS (a) and DDS•(0.5)DCM. Initial desolvation and the solid-solid phase transition (at 82°C for DDS) can be seen for both products at point **a**; during the second heating run this phase transition was found at 80.5°C for both samples. DDS showed melting endotherms at 177°C during the first and second heating cycle (**b**). The first heating run of the desolvated DDS•(0.5)DCM produced multiple endotherms around the temperatures for melting (**b1**) with its peak at ~180°C. Only one melting endotherm can be seen at 177°C for the second heating-run of this sample (**b2**). Recrystallisation upon cooling of the melts from both products can be seen as point **c**; this took place at ~122°C. The solid-solid phase transition at **d** took place at the same temperature (80.5°C) for both samples.

The general assumption is that the polymorph with the higher melting point would be more stable and therefore more prevalent. Why then would the lower melting point be more prevalent during analysis of DDS? The answer may be given by Ostwald's Rule: "When leaving a given state and in transforming to another state, the state which is sought out is not the thermodynamically stable one, but the state nearest in stability to the original state" [10].

4. Conclusions

Investigation of DDS and its recrystallised products was absolutely necessary to evaluate the facts provided in previous publications since not much was known about the interrelationships of DDS's polymorphs.

This detailed characterisation of DDS leads to an understanding of the structural and thermodynamic relationship that exists between the polymorphic forms of DDS. Exposing a DDS sample to heating cycle; leads to recurring and reproducible peaks which is an indication for an enantiomeric relationship between DDS forms III and II. Heating the sample to melting point and subsequently cooling it to ambient temperature did not produce the same X-ray diffraction results as heating it to just below melting point. This is because the sample decomposes after melting. This point is particularly important during manufacturing and storage.

Exposing APIs to solvents may lead to solvate/hydrate formation which may negatively alter the pharmaceutical product's properties. The solid-solid phase transition seen before the melting of DDS•0.5(DCM) may possibly also be caused by pressure, light and moisture/solvents during manufacturing and storage. DDS form I has a higher melting point which might also lead to an even further decreased water solubility of DDS. The reproduction of DDS form I from a sample initially melting at ~180°C was not possible. It was also not possible to capture or maintain DDS form II or I at temperatures below 70°C; not by grinding; quench cooling a heated sample or melt using liquid nitrogen or any other way. This does not mean that it will not be possible in the future, but only that we were not able to create the right conditions for this to happen.

Acknowledgements

We are grateful to the North-West University, the University of Cape Town and the National Research Foundation of South Africa for financial support.

References

[1] M. Kuhnert-Brandstätter, I. Moser, Microchim. Acta. (1979) 125-136.

[2] C.E. Orzech, N.G. Nash, R.D. Daley, Dapsone, Academic Press, New York, 1976.

[3] L.T. Butt, J. Pharm. Pharmacol. 5 (1953) 568.

[4] J. Bernstein, Polymorphism in Molecular Crystals, Claredon press, Oxford, 2002.

[5] K.R. Morris, U.J. Griesser, G.J. Eckhardt, J.G. Stowell, Adv. Drug Deliver. Rev. 48 (2001) 91-114.

[6] D. Giron, Thermochim. Acta. 248 (1995) 1-59.

[7] H. Lemmer, N. Stieger, W. Liebenberg, M.R. Caira, Cryst. Growth Des. 12 (2012) 1683-1692.

[8] J.M. Rubin-Preminger, J. Bernstein, R.K. Harris, I.R. Evans, P.Y. Ghi, Cryst. Growth Des. 4 (2004) 431-439.

[9] Z. Skoko, S. Zamir, P. Naumov, J. Bernstein, J. Am. Chem. Soc. 132 (2010) 14191-14202.

[10] Threlfall T, Org. Process Res. Dev. 7 (2003) 1017-1027.